# Treating Acid Mine Drainage with Pervious Concrete and Quantifying the Impacts of Urban Stormwater N:P Ratio on Harmful Algal Blooms

Thesis

Presented in Partial Fulfillment of the Requirements for the Degree Master of Science in the Graduate School of The Ohio State University

By

Samuel Mark Riekert, B.S.

Graduate Program in Food, Agricultural and Biological Engineering

The Ohio State University

2022

Thesis Committee

Dr. Ryan J. Winston, Advisor

Dr. Lisa E. Burris, Co-Advisor

Jay F. Martin, Committee Member

## Abstract

Polluted water is a pressing burden for civilization. Management and treatment of polluted water is a costly but necessary process for the health of the environment and the humans that live in it. Demand for novel, inexpensive, and effective treatment options is constant, and further insight on their use and impacts are as important as ever for our changing world. Two such sources of polluted water are analyzed in this document: acid mine drainage and urban stormwater runoff.

Acid mine drainage (AMD), a negative consequence of the mining industry resulting from interaction between water, oxygen, and exposed bedrock, is prevalent worldwide and requires expensive and perpetual treatment. The Wilds, an animal reserve in southeastern Ohio situated on a retired strip mine site, has partnered with OSU to address AMD discharging into streams and ponds on its property. Pervious concrete has shown potential in neutralizing AMD, and this study was developed to determine the effectiveness of pervious concrete at removing heavy metals and neutralizing acid from an AMD source. Using various mix designs of pervious concrete, the individual removal behavior of aluminum, manganese, iron, and copper from natural and synthetic AMD sources was tracked. Pervious concrete cylinders were also used to model the length of a permeable reactive barrier to treat field-scale AMD. Furthermore, acid neutralization ability and durability of six concrete mixes were tested when exposed to a year of acidic

conditions. Experimentation revealed the concrete removes >95% of aluminum, iron and copper, and ~30% of manganese in natural AMD over 24 hours. Column testing indicated permeable reactive barriers of 4-8 meters in length are recommended to treat Al, Fe, and Cu. Pervious concrete compressive strength withstood a year of acid attack without significant decline, and results show a promising argument for the use of porous concrete in acid mine drainage treatment at field scale.

Lakes and rivers represent tremendous assets in the state of Ohio, as they are used for recreation, tourism, drinking water sources, commerce, and to support fisheries. Upland areas, including agricultural and urban lands, result in substantial pollution discharge to surface waters during runoff events, including nutrients from fertilizer, manure, and other sources. One negative consequence of nutrients in runoff is harmful algal blooms (HABs), which may contain various toxins and utilize dissolved oxygen in the water, causing fish kills to occur. The strength and scope of HABs is related to the nitrogen to phosphorus (N:P) ratio in runoff. Little is known about how urban land use and the presence or absence of stormwater control measures (SCMs) impacts the N:P ratio in stormwater. Two data sets were utilized to unpack these questions: (1) a land use and stormwater quality data set developed through field monitoring in the Dayton metropolitan area, and (2) the Blueprint Columbus data set which focused on green infrastructure in several watersheds in the Clintonville neighborhood of Columbus, Ohio. Multi-family residential, commercial, and light industrial land uses had the largest (>25) TN:TP ratios, suggesting their runoff contributes to more toxic variations of algal blooms and that SCM retrofits in these watersheds should focus on N removal. Single-family

residential, low-density residential, and heavy industrial had the most balanced TN:TP ratios, so runoff reduction to reduce overall nutrient load should be the focus of SCM retrofits in these watersheds. No significant changes to TN:TP ratio were observed after green infrastructure implementation or other infrastructure improvements (e.g., sanitary sewer lateral lining, downspout disconnection, and sump pump installation) in Columbus watersheds. As watersheds that received infrastructure retrofits were all single-family residential, no significant impact on N:P is not a negative result, suggesting retrofitted infrastructure removes N and P in a balanced manner.

# Dedication

I dedicate this thesis to my family, Mark, Jenna, Jeb, and Ellie Riekert, without whom I would be half the person I am today.

# Acknowledgments

To begin, I have to thank Dr. Ryan Winston for his help in completing this paper and this degree. He has helped me jump through many hoops to get here, from scheduling to experimentation to general academic guidance. He has been my help and guide from my last year of undergraduate into this last month of rapid thesis turnaround, and I would be in a lot of trouble if not for his patience and mentorship, as well as excellent editing skills!

Dr. Lisa Burris has been extraordinarily helpful and patient this past year and a half. Although I am a student outside her department, she has been greatly involved with meeting time, writing, and guidance on how this thesis has developed. She also built my concrete knowledge up in a year, and has greatly helped sharpen my experimental design process. She makes an effort to turn mistakes into learning opportunities and is an excellent mentor.

Ravi Patel deserves the sole credit for helping me build my concrete laboratory skills, and was a foundational contributor to all data collected for my pervious chapter. He designed or inspired most of the experiments I conducted and cast most of the concrete I ended up testing. Even after his work had ceased, he was always available to answer questions I had, months into the experimental process. I can’t thank him enough for the work he put into the experiment and me personally.

Yuija Min was also a crucial help in conducting my experimentation. He, alongside Dr. Zhe Liu, taught me how to operate the ICP-OES and obtain all concentration data I had needed. Dr. Liu was also extremely helpful to me through many ICP difficulties. In Dr. Burris's lab, many other students (particularly Cansu Acarturk, Erin Stewartson, and Jarron Mihoci) were great associates and friends throughout the year.

Dr. Winston's lab group contained some of the most helpful people I've ever met, and they were essential to completing my second chapter. Dr. Ian Simpson generously provided all of his data in the Dayton region, and was very helpful in providing me information throughout the entire year. Kay Bernard was instrumental in providing and managing data from Blueprint Columbus, alongside answering questions and even helping me with field data collection. Joey Smith and Kathryn Boening-Ulman jumped at the opportunity to teach me statistics, as well as providing me code and guiding me through a large amount of my statistical analysis.

I would also like to thank my third committee member Dr. Jay Martin, who (with 3 days of reading time) volunteered his time to help my graduation process.

Candy McBride, although we seemingly have not met in person, has been the most important keystone in completing this degree. She has helped me through countless problems (some of my own making) and has been incredibly helpful and patient for the last 3+ years of planning the graduate process.

# Vita

May 2017…….....……Pickerington North High School

May 2021.....B.S. Food, Agricultural, and Biological Engineering,
The Ohio State University

August 2018 to present.....Graduate Research Associate,
The Ohio State University

Fields of Study

Major Field: Food, Agricultural, and Biological Engineering

Table of Contents

Abstract ..... i

Dedication ..... iv

Acknowledgments ..... v

Vita ..... vii

Table of Contents ..... viii

List of Tables ..... xii

List of Figures ..... xv

Chapter 1. Pervious Concrete for Treatment of Acid Mine Drainage: Heavy Metal Sequestration and Acid Attack Impacts on Concrete Durability ..... 1

1.0 Abstract ..... 1

1.1 Introduction ..... 2

1.1.1 Acid Mine Drainage ..... 2

1.1.2 Traditional AMD Treatment ..... 6

1.1.3 Pervious Concrete ..... 9

1.1.4: Treatment Through Precipitation and Adsorption ..... 10

1.1.5: Fillers ..... 13

1.1.6: Study Objectives ..... 15

1.2 Materials and Methods ..... 16
1.2.1 Experimental Materials ..... 16
1.2.2 Concrete Sample Casting ..... 18
1.2.3 Acid Durability Testing ..... 19
1.2.4 Natural and Synthetic AMD Solution Preparation ..... 20
1.2.5. Metal Removal Tests ..... 21
1.2.6 Flow-Through Column Testing ..... 23
1.2.7 Sample Analysis ..... 24
1.2.8 Data Analysis ..... 24
1.3 Results ..... 25
1.3.1 OPC Removal of Metals in Single-Ion Solutions ..... 25
1.3.2 Impact of pH on Metal Removal ..... 30
1.3.3: Treatment of a Multi-Ion Solution ..... 36
1.3.4 Treatment of Natural AMD ..... 41
1.3.5 Column Tests ..... 44
1.3.6 Comparison of Treatment by Pervious Concrete Mixtures Utilizing Various Filler Materials ..... 48
1.3.7 Chronic Acid Impact on Neutralization ..... 52
1.3.8 Acid Durability ..... 54

1.4 Discussion ..... 57

1.5 Conclusion ..... 61

References ..... 63

Chapter 2. Unraveling Drivers of Harmful Algal Blooms: The Effects of Land Use and Green Infrastructure Implementation on Urban Runoff Nitrogen:Phosphorus Ratio ..... 69

2.0 Abstract ..... 69

2.1 Introduction ..... 70

2.2 Methods ..... 77

2.2.1 Watershed Descriptions and SCM Implementation ..... 77

2.2.2 Instrumentation and Data Collection ..... 81

2.2.3 Laboratory Analysis ..... 82

2.2.4 Data Analysis ..... 83

2.2.5 N:P ratio considerations ..... 85

2.3 Results and Discussion ..... 86

2.3.1 Effects of Urban Land Use on TN:TP ratio of stormwater runoff ..... 86

2.3.2 Effects of GSI implementation on urban runoff TN:TP ratio from single family residential watersheds ..... 95

2.4 Conclusions ..... 104

References ..... 106

Bibliography .....111

Appendix A .....121

List of Tables

Table 1: Acid mine drainage quality from mines worldwide. Included are United States EPA recommendations for water quality for human consumption, as well as aquatic life health given chronic exposure. ..... 4

Table 2: Metal concentrations used in this experimentation. Included is natural AMD as collected, and the designed mix concentrations of synthetic AMD and single-ion solutions of Al, Mn, Fe, and Cu. ..... 21

Table 3: Metal concentrations of OPC cubes during the contact time experiment. Data presented are the average of three cubes, with both concentration in mg/L and percent removal of metal in relation to the initial concentration. Negative values caused by regression line error in ICP analysis are represented by the lowest standard (0.01 mg/L at 50x dilution). ..... 27

Table 4: Slope of trendlines for stress at break data for all 6 concrete mixes, alongside average stress at break (psi) over the year of experimentation, initial, 6-month, and 12-month strength values. Estimate of months to reach 100 psi using initial (0-month) strength and acid slope of trendline is included. ..... 55

Table 5: Characteristics of Dayton (top) and Columbus (bottom) watersheds. Monitoring periods did not include winter months to avoid damage to monitoring equipment caused

by freezing. Some sampled events were excluded from this study if N or P data were incomplete. ..... 80
Table 6: Sample analysis methodology, sample preservation (if applicable), and method detection limits (MDL; mg/L for nutrients and total suspended solids or µg/L for heavy metals) for all pollutants analyzed by the National Center for Water Quality Research (NCWQR) and the City of Columbus laboratories. ..... 83
Table 7: Storm events used in Columbus TN:TP analysis, sorted into phases ..... 85
Table 8: Representation of Dunn test comparisons between urban land uses. Land uses that were proven to be significantly different ($p<0.05$) are colored in yellow to represent dissimilar TN:TP ratios between them. Land uses that were not proven to have different runoff TN:TP ratios are colored green ($p>0.05$). Only Dayton data is included for SFR comparisons. ..... 90
Table 9: TN, TP, and TN:TP summary statistics for pre-GSI, post-GSI, and post-$AI^2$ for the three treatment watersheds and the control watershed. ..... 97
Table 10: Normality tests for data sets used in ANCOVA analysis ..... 99
Table 11: ANCOVA tests conducted on TN:TP ratio between Pre-GSI and Post-GSI, as well as Pre-GSI and Post-$AI^2$ phases for each watershed. Significant ($p<0.05$) differences were not observed between phases in any watershed. ..... 99
Table 12: Comparison of TN and TP watershed-scale load for studies of single-family residential watersheds without GSI, single family residential watersheds with GSI, and undeveloped watersheds. ..... 103

Table 13: Comparison of concrete cube weights when soaked in water for 1 minute or 30 minutes. ..... 121

List of Figures

Figure 1: Satellite imagery of AMD sampling site in the Wilds near Zanesville, Ohio: (a) alongside Watson Road. (b). Sample site on the Wilds property, and (c) photograph of AMD sampling site. Satellite imagery credit of Google Earth ..... 6

Figure 2: MINTEQ model of metal hydroxide formation at an initial metal concentration of 1mmol (de Repentigny et. al., 2018) ..... 11

Figure 3: Al and Fe behavior in relation to pH. Source: Figure 9-11 (Crittenden, 2012) 12

Figure 4: Experimental setup for metal removal testing. ..... 22

Figure 5: OPC cubes from single ion runs, including unused OPC cube alongside Al, Mn, Fe, and Cu. ..... 26

Figure 6: Average metal percent removal by OPC cubes for runs 2 and 3 over time. ..... 29

Figure 7: Average solution pH for OPC cubes for runs 2 and 3 over time. ..... 31

Figure 8: Average metal percent removal versus solution pH for OPC cubes for runs 2 and 3. ..... 31

Figure 9: Percent removal of titrated metal pH-controlled solutions (i.e., no pervious concrete cube). ..... 33

Figure 10: Theoretical metal hydroxide formation over pH ranges. Initial concentrations of single-ion metals is represented by a dashed horizontal line, and each metal studied is colored with the associated color in previous graphs (Monhemius, 1977). ..... 34

Figure 11: Average solution pH via OPC cubes for runs 2 and 3 and run 3 of synthetic AMD over time. ..... 37
Figure 12: Average metal percent removal by OPC cubes for runs 2 and 3 and by synthetic AMD for run 3 over time. Colored portions correspond to precipitation ranges of pH-control. ..... 38
Figure 13: pH-control of synthetic AMD mix, with colored boxes mirroring pH ranges where a majority (>55%) of removal occurred. ..... 38
Figure 14: Average metal percent removal by OPC cubes for runs 2 and 3 of natural AMD and run 3 of synthetic AMD over time for synthetic vs. natural AMD. Colored portions of the figure correspond to precipitation ranges of pH-control ..... 42
Figure 15: pH-control of synthetic vs. natural AMD, with correspondingly colored boxes mirroring pH ranges where a majority (>55%) of removal took place. ..... 42
Figure 16: Metal removal as a percentage of initial concentration and pH of natural AMD poured through columns of OPC pervious concrete. Pore volume is a function of pass-throughs of the same 1L of AMD, and meters of column models sequential column length. ..... 45
Figure 17: Metal removal percentage relative to solution pH for natural AMD in concrete exposure testing and column testing ..... 46
Figure 18: Graph of single-ion solutions, assuming a relationship between exposure time and permeable reactive barrier (PRB) length. Length of PRB in meters, equivalent to 47.24 minutes of exposure time, is compared to percent removal. ..... 47

Figure 19: Percent removal of four single-ion solutions with OPC, FAF, FAC, and LP fillers over runs 2 and 3. Highlighted regions are pH ranges where a majority of metal removal took place in respective pH-controlled solutions..... 49
Figure 20: Percent removal of Al and Mn in multi-ion solutions with OPC, FAF, FAC, and LP fillers. Highlighted regions are pH ranges where a majority of metal removal took place in respective pH-controlled solutions..... 50
Figure 21: Average pH across a year of testing of treated acid for the 6 fillers in terms of days after acid replacement..... 52
Figure 22: Time to raise pH of the same cubes from 2.0 to 7.0, with acid changed on a weekly basis for each concrete mixture. ..... 53
Figure 23: Stress at break (psi) of all six concrete mixes tested each month. Acid-soaked cubes are presented alongside their limewater-control counterparts. ..... 55
Figure 24: Watersheds monitored by Simpson (2022) in the Dayton metropolitan area and in Battelle-Darby Creek Metropark. ..... 78
Figure 25: Watersheds monitored as part of the Blueprint Columbus project in the Clintonville neighborhood of Columbus, OH. All watersheds are primarily single-family residential land use (i.e., non-shaded areas). Stormwater control measures and monitoring locations are shown as points. Existing storm sewers are in red with watershed boundaries in yellow. Beechwold served as an experimental control while the other three watersheds were monitored before and after GSI retrofits as well as a third monitoring period where additional infrastructure implementation ($AI^2$) occurred in the watersheds. Image from Bernard et al. (2022). ..... 79

Figure 26: Comparison of seasonal TN:TP ratios for all land uses, with data points colored to match the originating land use ..... 87
Figure 27: Comparison of TN:TP ratios for all land uses, with datapoints colored to match the season of each storm event. ..... 89
Figure 28: Comparison of TN:TP ratio of all single-family residential (SFR) neighborhoods analyzed. Red signifies watersheds in the Columbus area (Pre-GSI only) and blue represents Dayton-area SFR watersheds. ..... 92
Figure 29: Exceedance probability of TN:TP ratio by land use relative to that to surpass N-replete growth conditions. Included is an inset table showing the value at which each land use crosses the 31.58 TN:TP threshold. ..... 93
Figure 30: Comparisons of median pollutant concentration for each watershed for (a) total nitrogen (mg/L), (b) total phosphorus (mg/L), and (c) presents TN:TP ratios (mol/mol). Median absolute deviation among storm events is represented in positive and negative error bars ..... 96
Figure 31: ANCOVA models for TN:TP ratios in watersheds with GSI and $AI^2$ implementation. No significant differences ($p>0.05$) were observed in TN:TP ratios from treatment watersheds relative to the control. ..... 100
Figure 32: Synthetic AMD pH-controlled solutions, one with 0.4 mmol of Ca added and one without. Percent removal of Al and Mn is compared over pH. ..... 122

# Chapter 1. Pervious Concrete for Treatment of Acid Mine Drainage: Heavy Metal Sequestration and Acid Attack Impacts on Concrete Durability

## 1.0 Abstract

Acid mine drainage (AMD), a negative consequence of the mining industry resulting from interaction between water, oxygen, and exposed bedrock, is prevalent worldwide and requires expensive and perpetual treatment. The Wilds, an animal reserve in southeastern Ohio situated on a retired strip mine site, has partnered with OSU to address AMD discharging into streams and ponds on its property. Pervious concrete has shown potential in neutralizing AMD, and this study was developed to determine the effectiveness of pervious concrete at removing heavy metals and neutralizing acid from an AMD source. Using various mix designs of pervious concrete, the individual removal behavior of aluminum, manganese, iron, and copper from natural and synthetic AMD sources was tracked. Pervious concrete cylinders were also used to model length of a permeable reactive barrier to treat field-scale AMD. Furthermore, acid neutralization ability and durability of six concrete mixes were tested when exposed to a year of acidic conditions. Experimentation revealed the concrete removes >95% of aluminum, iron and copper, and ~30% of manganese in natural AMD over 24 hours. Column testing indicated permeable reactive barriers of 4-8 meters in length are recommended to treat Al, Fe, and Cu.

Pervious concrete compressive strength withstood a year of acid attack without significant decline, and results show a promising argument for the use of porous concrete in acid mine drainage treatment at field scale.

## 1.1 Introduction

### 1.1.1 Acid Mine Drainage

Coal and metal mining has provided humankind with the critical natural resources to build the modern world. However, the extraction of rocks and minerals has not come without its drawbacks, including public safety concerns, erosion, habitat loss, and air and water pollution (Thornton, 1996). One of the major ecological impacts of large-scale mining operations is the inadvertent generation and subsequent release of acid mine drainage (AMD) to nearby streams and lakes. AMD is created when exposed bedrock containing sulfides such as $FeS_2$ dissolves in water, releasing excess $H^+$ ions through interaction with $H_2O$ and $O_2$ (Naidu et. al., 2019, Larsson et. al., 2017, Shabalala and Ekolu, 2019). The resulting acidic water promotes further dissolution of surrounding rock, releasing metals such as lead (Pb), iron (Fe), aluminum (Al), manganese (Mn), cadmium (Cd), zinc (Zn), and copper (Cu) into solution. If not treated prior to discharge, acid mine drainage causes substantial ecological damage in receiving waters, including increased toxicity, biological disturbance, infrastructure damage, and increased water treatment costs for human consumption (Skousen et. al., 2017).

AMD characteristics vary substantially based on location, and worldwide AMD compositions are summarized in terms of metal concentrations and pH in Table 1. This includes the water quality of the AMD source used in this study (The Wilds, Cumberland, Ohio, USA)

and the US EPA's aquatic life criteria and human health criteria (USEPA, 2009). These mines emit highly acidic drainage (pH 1.5 – 5.8) with metals concentrations often well in excess of the US EPA aquatic life and human health recommendations (USEPA, 2009). As both active and retired mining sites can release AMD for decades, prevention and treatment can be a costly and onerous process.

Table 1: Acid mine drainage quality from mines worldwide. Included are United States EPA recommendations for water quality for human consumption, as well as aquatic life health given chronic exposure.

| Study | Location | Source | Pollutant Concentration (in mg/L) | | | | | | | | |
|---|---|---|---|---|---|---|---|---|---|---|---|
| | | | Fe | Al | Mn | Cu | Ni | Zn | Pb | As | $SO_4$ |
| Valente & Gomes, 2008 | Northern Portugal | Valdarcas metal mine | 2100 | 3700 | 200 | 17 | - | 8.7 | - | 9.6 | 5900 |
| MacIngova & Luptakova, 2012 | Slovakia | Smolnik sulphidic deposit | 410 | 110 | 36 | 8.4 | - | 12 | - | - | 2900 |
| Shabalala et. al., 2017 | Gauteng, Souh Africa | gold mine | 12 | 3.0 | 130 | 0.10 | 1.30 | 1.4 | 0.03 | - | 1100 |
| Shabalala et. al., 2017 | Gauteng, South Africa | coal mine | 9.0 | 6.0 | 20 | 0.10 | 0.60 | 2.8 | 0.03 | - | 2900 |
| Thisani et. al., 2021 | KwaZulu-Natal, South Africa | abandoned coal mine | 44 | 77 | 11 | 0 | 0.05 | 0.08 | 0 | 0 | 2200 |
| Ekolu et. al., 2014 | South Africa | gold mine | 220 | - | 17 | | - | - | - | - | 3100 |
| Liu et. al., 2020 | Duyun City, China | abandoned coal mines | 590 | - | 1.3 | 0.27 | - | 0.43 | 0.01 | 0.01 | 3000 |
| Liu et. al., 2020 | Duliu Town, China | coal mine | 1000 | - | 260 | 4.9 | - | 9.4 | 0.01 | 0.25 | 5000 |
| da Silveira et. al., 2009 | Brazil | abandoned coal mine | 3.0 | 34 | 2.1 | - | - | - | - | - | 800 |
| Periera et. al., 2020 | Figueria, Brazil | active coal company | 610 | 270 | 38 | - | - | 63 | 0.41 | 0.85 | 7400 |
| Daubert & Brennan, 2007 | Altoona, Pennsylvania | coal mine | 21 | 14 | 12 | | - | - | - | - | 490 |
| Wei et. al., 2005 | Virginia | coal mine | 160 | 81 | 2.0 | 0.01 | 1.0 | 2.7 | - | - | 1500 |
| Matlock et. al., 2002 | Pikeville, KY | abandoned coal mine | 190 | 0.50 | 4.7 | 0.01 | - | - | 0.02 | 0.02 | - |
| AMD, Wilds (Current Study) | Zanesville, Ohio | reclaimed coal strip mine | 0.00 | 31 | 13 | 0.00 | 0.01 | 0.01 | 0.01 | - | - |
| US EPA Recommended Water Quality | Aquatic Life Criteria-Chronic | - | 1.0 | varies | - | - | 0.05 | 0.12 | 2.5e-3 | 0.15 | - |
| US EPA Recommended Water Quality | Human Health Criteria | - | - | - | 0.05 | 1.30 | 0.61 | 7.4 | - | 1.8e-6 | - |

The Wilds is a conservation and zoological reserve on land formerly used as a surface mining operation run by American Electric Power (AEP), which strip-mined for coal from the 1940s to the 1980s (Watters et. al., 2005). The site was remediated in two phases as regulations changed, resulting in a northern, reforested portion and a southern grassland portion. This difference is a result of changing regulations, eventually requiring more extensive reforestation efforts as AEP ceased operations. However, even with the reclamation effort, exposed rock continues to cause AMD contamination of streams and lakes on the northern ("Tree Law") portion of the property (Stanley, 2020, O'Reilly, 2020). In partnership with the Wilds, AMD sourced from the property (with the sample site location pictured in Figure 1) has been used in laboratory testing to develop a novel, inexpensive, and reliable method of AMD treatment.

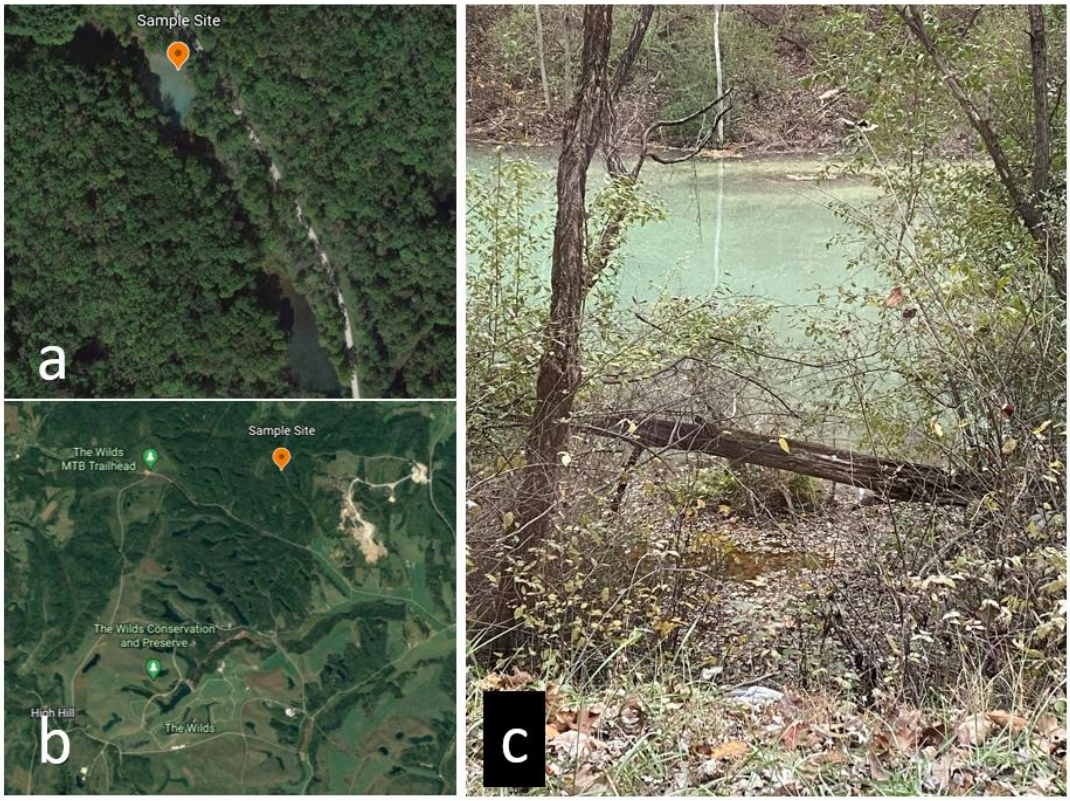


Figure 1: Satellite imagery of AMD sampling site in the Wilds near Zanesville, Ohio: (a) alongside Watson Road. (b). Sample site on the Wilds property, and (c) photograph of AMD sampling site. Satellite imagery credit of Google Earth

### 1.1.2 Traditional AMD Treatment

Treatment of AMD can be a costly and onerous process, with operation and maintenance efforts needed decades after mining operations cease (Johnson and Hallberg, 2005, Naidu et. al., 2019, Skousen et al., 2017, Skousen et. al., 2019). The estimated worldwide total liability to remediate contaminated runoff from abandoned mines is in excess of $100 billion (Tremblay and Hogan, 2001). While active mines require AMD treatment, retired mining sites are often more expensive

to remediate on a yearly basis (Naidu et. al., 2019). To maintain watershed health or regional water quality standards, AMD prevention or treatment must be considered for each at-risk mine site. AMD prevention is accomplished through site construction or remediation that eliminates contact between water and rock, but AMD must be treated using either passive or active systems if prevention fails (Skousen et. al., 2019, Johnson and Hallberg, 2005).

To prevent leaching of AMD, multiple steps can be taken before passive or active treatment is necessary. Prevention methods are meant to protect exposed sulfide materials from forming AMD when in contact with water, air, or microbes (Naidu et. al., 2019, Skousen et. al., 2019). Deep mines may be flooded and sealed to prevent oxygen and microbe infiltration, or sulfide-producing materials may be placed in a body of water to prevent contact with oxygen (Skousen et. al., 2019, Johnson and Hallberg, 2005). Backfilling, in combination with vegetation establishment, can also prevent contaminant transport (Skousen et. al., 2019, Naidu et. al., 2019). Acidic wastes may be combined with alkaline amendments or alkaline wastes to efficiently counteract AMD formation. Although favored due to lower costs and reliable upkeep, complete prevention of AMD formation is often impractical and many sites require AMD treatment.

Depending on site conditions, AMD may be better suited to remediation through either a passive or active treatment system. Active systems require continual maintenance and upkeep but are more reliable and flexible depending on the AMD makeup and site requirements. The most common form of active treatment is chemical neutralization (Johnson and Hallberg, 2005), which raises the pH of the AMD, allowing for simultaneous metal removal through precipitation. Active dosing into the AMD is performed using limestone ($CaCO_3$), hydrated lime ($Ca(OH)_2$), sodium carbonate, sodium hydroxide, or ammonia (Johnson and Hallberg, 2005, Skousen et. al.,

2019). The ideal chemical varies depending on AMD chemistry, flow rate, site characteristics, and monetary constraints (Skousen et. al., 2019). Active systems often produce high-water content sludge that can be costly to treat and dispose of. Steps can be taken to refine sludge formation and removal (Johnson and Hallberg, 2005), and metals can be reharnessed from the sludge at a limited scale (Naidu et. al., 2019).

Passive treatment systems are classified by their relatively limited maintenance and lack of a continuous chemical input. They take advantage of biological and chemical processes to treat AMD at relatively low flow rates (Skousen et. al., 2017, Skousen et. al., 2019, Naidu et. al., 2019). Anaerobic/aerobic wetlands, anoxic limestone drains, open limestone channels, bioreactors, and permeable reactive barriers can all be used to passively treat AMD. Once construction is complete, costs of passive treatment systems are generally low, with maintenance including occasional sludge or associated metal precipitate removal. However, passive treatment systems require sufficient land and a consistent, low-volume flow of AMD.

Permeable reactive barriers (PRBs) are intended to passively intercept flowing AMD with an alkaline or biological material (Shabalala et. al., 2014, Johnson and Hallberg, 2005, Naidu et. al., 2019, Gavaskar, 1999). They are generally installed as a pit or trench filled with limestone and organic waste. The mix is designed to have high enough porosity to not disrupt flow and enough specific surface area to sufficiently treat wastewater. The organic matter is intended to be a carbon source for sulfide-reducing bacteria, and the barrier therefore provides chemical and biological treatment (Shabalala et. al., 2014).

### 1.1.3 Pervious Concrete

Pervious concrete may provide a suitable alternative method of AMD remediation. Hardened concrete has a high pH of 11-13, primarily due to the portland cement paste and the calcium hydroxide formed during the hydration process (Tennis and Jennings, 2000, Scrivener et. al., 2019, Ekolu and Bitandi, 2018) and so may neutralize the low pH AMD system. Equation (1) details the hydration of cement using "x" and "n" to denote the variable stoichiometry of C[1] and H in many C-S-H products (Marchon and Flatt, 2016). Note Equation 1 utilizes 'cement chemistry notation' in lieu of stochiometric equations. During the cement hydration process moisture combines with cement phases ($C_3S$, $C_2S$) to create hydration products like calcium silicate hydrate (C-S-H) and calcium hydroxide (Li et. al., 2019, Tennis and Jennings, 2000, Scrivener et. al., 2019, Ekolu and Bitandi, 2018). Hydration of cement compounds like $C_3S$ creates long chain-like products including C-S-H. which causes the surface area of the concrete to greatly increase (Marchon and Flatt, 2016, Tennis and Jennings, 2000).

$$C_3S + (3 - x - n)H_2O \rightarrow C_x - S - H_n + (3 - x)CH \quad (1)$$

The hydration product lime ($Ca(OH_2)$ or CH) neutralizes acid, and when it is present it prevents other products in the concrete from dissolving under acid attack (Gutberlet et. al., 2015). C-S-H and other phases in the hydrated cement paste will begin to break down following chronic exposure to acid, resulting in further hydration of unhydrated cement particles (Shively et. al., 1986, Beulah and Prahallada, 2012, Ekolu and Bitandi, 2018). Products like C-S-H are reduced into weak silica solids, as well as iron and alumina products (Shively et. al., 1986). This

[1] Cement chemistry notations: C = CaO, S = $SiO_2$, H = $H_2O$

breakdown takes time, and Ekolu and Bitandi (2018) modeled that a PRB of pervious concrete under acid attack with a pH of ~3 can last 10 years without contaminant breakthrough.

Pervious concrete filters are designed to capitalize on the strength and alkalinity of traditional concrete while maximizing water flow and permeability. Pervious concrete contains coarse aggregates (>4.8 mm) and cement but omits fine particles like sand, creating pore space within the concrete structure that allows for substantial hydraulic conductivity (Holmes et. al., 2018, Thisani et. al., 2021). The porosity typically ranges from 15-25% (e.g., depending on aggregate size) to prevent precipitates and organics from clogging pores while maximizing water flow rate and exposed surface area (Knox et. al., 2012, Holmes et. al., 2017).

Pervious concrete has demonstrated efficacy in treating stormwater runoff and wastewater (Haselbach et. al., 2014, Holmes et. al., 2017, Teymouri et. al., 2020, Knox et. al., 2012, Ekolu and Bitandi, 2018). It has high porosity, alkaline chemistry, and extensive internal surface area, making it a potential method for PRB-style treatment of AMD. Recent studies propose using pervious concrete as a method of AMD treatment, due to its ability to neutralize acidity and remove metals through mechanisms including precipitation and adsorption (Shabalala and Ekolu, 2019, Holmes et. al., 2018, Shabalala, 2020, Knox et. al., 2012, Thisani et. al., 2021, Shabalala et. al., 2017, Ekolu et. al., 2014).

### 1.1.4: Treatment Through Precipitation and Adsorption

Since pervious concrete increases the pH of solutions it interacts with (Knox et. al., 2012), precipitation is a primary contributor to its heavy metal removal capabilities. Precipitation in alkaline solutions commonly results from metal hydroxide and metal carbonate formation

(Muthu et. al., 2019, Sdiri et. al., 2012, Li et. al., 2019). The ability of pervious concrete to raise pH and its concurrent release of calcium ions is crucial to the formation of these precipitates, especially if high concentrations of cations lead to competition over available surface sites for adsorption (Holmes et. al., 2017).

The sequestration of heavy metals in aqueous solutions is affected by pH, but each element precipitates in different pH ranges. Figure 2 (de Repentigny et. al., 2018) details metal hydroxide formation in 1 mmol solutions using the modeling software MINTEQ (Gustafsson 2011). A more detailed precipitation graph of Al(III) can be found in Figure 3. Varying pH ranges in AMD underscore the importance of understanding precipitation for elements like Fe and Al. The low pH ranges at which hydroxides form suggest the primary removal mechanism will be precipitation, and any interaction with pervious concrete is likely to quickly raise pH and lead to metal-hydroxide formation before adsorption occurs.

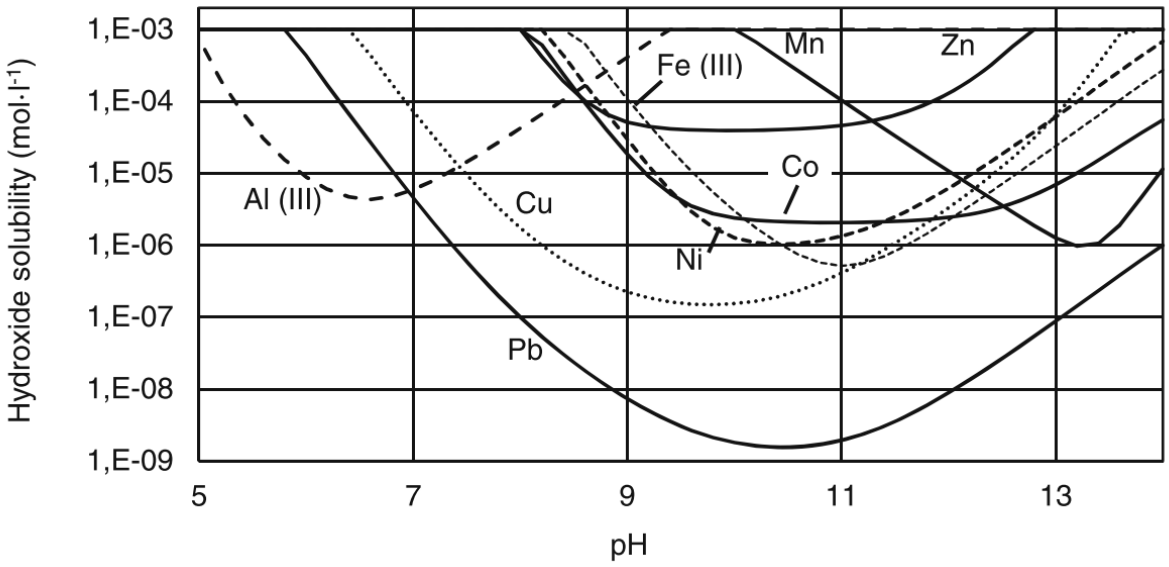


Figure 2: MINTEQ model of metal hydroxide formation at an initial metal concentration of 1mmol (de Repentigny et. al., 2018)

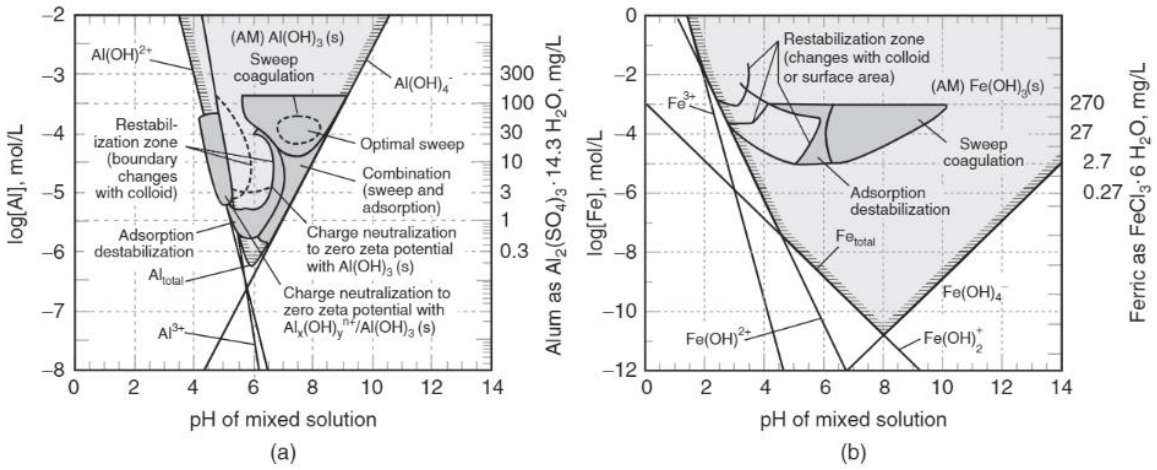


Figure 3: Al and Fe behavior in relation to pH. Source: Figure 9-11 (Crittenden, 2012)

Adsorption is an important part of the metal removal process, and the aggregate and cement in the concrete play distinct roles therein (Holmes et. al., 2017). High pH favors both sorption and precipitation of metals, but at low pH adsorption is especially favored as a removal mechanism (Hale et. al., 2012). Portland cement has multiple important components for adsorption of heavy metals. Portlandite, calcium aluminates, and C-S-H are all surface components that can physiosorb metals and remove them from solution (Holmes et. al., 2017, Li et. al., 2019). Limestone is primarily composed of calcite ($CaCO_3$), which forms a crystalline structure in pure limestones and can sorb metals (Knox et. al., 2012). Adsorption to the crystal surface and absorption into the structure warps the crystal face, leading to even greater contaminant sorption. It has been established that impure limestone generally has better sorption properties than pure calcite (Sdiri et. al., 2012). Silanols, iron and aluminum oxides, and other groups may have greater adsorption potential than pure limestone and lead to different and unpredictable chemical phenomena (Sdiri and Bouaziz, 2014, Sdiri et. al., 2012). Impure

limestone also has greater surface area and may contain finer particles, leading to more reactive sites to adsorb metals.

Zinc, copper, and manganese all follow similar removal mechanisms and have high likelihood to adsorb to materials in concrete. Zinc is commonly removed by adsorption to cement surface complexes, and less commonly removed through precipitation (Muthu et. al., 2019, Hale et. al., 2012). However, Pickering (1983) found that calcite alone was not sufficient to remove Zn until a pH of 7.6 was reached to produce $Zn(OH)_2$, a precipitate. Manganese and copper are less effective at adsorbing to calcite than Zn and begin to precipitate when surface sites are saturated and pH has reached a sufficiently high level (Pickering, 1983). Both are aided by C-S-H formation in cement, which is used to physiosorb metals to prevent leaching (Li et. al., 2019). Because of the high pH required to precipitate Mn and Cu, the complex surfaces present in pervious concrete are important in adsorbing these metals.

### 1.1.5: Fillers

As of 2019, combustion of coal made up approximately 40% of the global energy supply (Czuma et. al., 2019). A common unburned byproduct of this process is fly ash, making up 75-80% of the total coal ash created worldwide, and the $5^{th}$ most prolific raw material on earth (Ahmaruzzaman, 2009, Saboo et. al., 2019). Using fly ash waste as a filler in concrete to replace a portion of the portland cement is therefore a sustainable and economical option. Fly ash is primarily composed of aluminosilicate glass particles, which are spherical in shape and fine-grained (Ahmaruzzaman, 2009, Saboo et. al., 2019, Czuma et. al., 2019). It has pozzolanic properties, in which reactions with calcium hydroxide form additional C-S-H and strengthen and

densify the OPC hydrated matrix. Fly ash has been utilized in pervious concrete in multiple studies (Uma Maguesvari and Sundararajan, 2017, Saboo et. al., 2019), with results indicating slightly lower strength than a 100% cement mix as well as reduced porosity and permeability.

Natural zeolite is a compound consisting of tetrahedral structures of aluminosilicates and oxygen atoms. This structure allows for void formation due to the internal space resulting in high surface area of these $SiO_4$ tetrahedrals (Knox et. al., 2012, Ok et. al., 2007, Liu and Li, 2020). Resulting voids create more permeability and contaminant adsorption, and as a result zeolites are commonly used as low-cost adsorbents for wastewater treatment (Tasic et. al., 2019). Zeolites have also been shown to have pozzolanic reactivity and can increase the strength of a concrete when used as a filler in small amounts (Liu and Li, 2020, Burris and Juenger, 2016). Natural zeolite is therefore theorized to provide beneficial effects when used in a pervious concrete system.

Limestone has proven adsorption qualities and is often used in passive treatment systems due to its ability to raise pH. Besides these treatment properties, limestone powder has also been studied as a cost-effective filler for concrete (Senhadji et. al., 2014, Ong et. al., 2016), and as of 2022 many U.S. cement producers have transitioned to producing only portland cements with greater than 10% limestone addition (i.e., portland limestone cement – PLC). Incorporation of limestone into the cement can have different outcomes on concrete strength, depending on the particle size and percentage replacement. Wang et. al. (2018) found that finer and lower concentrations of limestone powder will increase concrete strength, while higher replacement rates with large particle size will decrease strength. They also determined that the nucleation effects of a fine limestone powder will increase hydration product formation. Ong et. al. (2016)

found that using limestone powder as a cement replacement in pervious concrete created similar void content and porosity to a 100% OPC paste, while treating an organic compound like naphthalene more effectively.

Similar in origin to fly ashes, flue-gas desulphurization (FGD) is a by-product of coal production, typically added to aid in removal of $SO_2$ emissions. FGD primarily consists of gypsum ($CaSO_4 \cdot H_2O$) and is generally regarded as a waste worldwide (Wright and Khatib, 2016, Stehouwer et. al., 1995). As it is unsorted waste, FGD generally contains a mix of the combustion ash, $SO_2$ reaction products like gypsum ($CaSO_4 \cdot H_2O$), and unspent sorbent like lime. This unspent sorbent adds a highly alkaline nature to the FGD waste, which in turn can treat metal pollution through precipitation (Stehouwer et. al., 1995). Due to the variety of FGD samples around the world, performance as a concrete filler is hard to quantify. Khatib et. al. (2015) created a synthetic mix of gypsum and fly ashes for greater consistency and found a mix of no more than 10-15% synthetic FGD could increase concrete strength.

### 1.1.6: Study Objectives

Acid mine drainage is a worldwide concern, and treatment is a costly but necessary process. Concrete has both the ability to neutralize pH and remove metals from solution, and pervious concrete has the added benefit of greater surface area and pore space to further accommodate this process. Different metals need different conditions for treatment, however, and varying concrete fillers have different availability and treatment impacts. In this study, five filler materials were compared with an OPC pervious concrete mixture and tested for durability and pH neutralization efficiency under chronic acid attack. Pervious concrete cubes of OPC and

three of the fillers were tested for their ability to remove individual solutions of dissolved Al, Mn, Fe, and Cu. These same concrete mixes were used to treat natural AMD alongside synthetic AMD mixtures with similar metal proportions as the natural AMD source. The ability of the concrete to remove metals from the single and multi-ion systems was assessed and compared and the removal mechanism were investigated. AMD was also treated using a more realistic flow column setup of pervious concrete to establish a link between contact time, concrete surface exposure, pH neutralization, and metals removal. Finally, long term exposure of the pervious concrete to acidic solutions and changes in porosity and compressive strength were investigated in order to estimate total system life.

## 1.2 Materials and Methods

### 1.2.1 Experimental Materials

The aggregate used in the pervious concrete was #8 limestone obtained from a local Columbus area aggregate supplier, and cement was an ASTM Type 1 Ordinary Portland Cement (OPC) from Fairborn Cement. Five supplementary cementitious materials (SCMs) or fillers were explored in this experiment, replacing 25% of the OPC. Two types of fly ashes were utilized, specifically class C and F (FAF and FAC). Clinoptilolite zeolite (Zeo) was sourced from Bear River Zeolite Company (Preston, ID), and flue-gas desulfurization (FGD) was sourced from an Ohio coal combustion product landfill site. Limestone powder (LP) was also used and was shown to be primarily calcite through x-ray diffraction testing.

Pervious concrete mix characteristics were based off previous Burris lab research. Mix designs of varying aggregate size, water to cement (w/c) ratio, cement to aggregate ratio (c/agg), and percentage of fines were tested for compressive strength, density, porosity, and permeability. The following trends were established by Finn Haughn in the Burris lab:

- C/agg ratios above 0.15 restrict permeability and lead to infiltration rates slower than feasible for use in AMD stream applications.
- Smaller aggregate results in greater compressive strength than larger aggregate but slows water flow through the pervious concrete.
- Higher w/c ratios lead to higher strength but lower permeability. A ratio of 0.35 was optimal to balance these two considerations.
- Little variation in permeability and strength was observed between 0 and 5% fines.

Given these observations, a mix design utilizing #8 limestone, c/agg ratio of 0.2, w/c ratio of 0.3, and 0% fines was selected for all concrete used in this experimentation. SCM or filler mixes utilized a 25% substitution of OPC. Concrete batch proportions were 1502.9 $kg/m^3$ of aggregate, 142.6 $kg/m^3$ of water, and 300.6 $kg/m^3$ of OPC. For concrete with fillers (FAF, FAC, LP, Zeo, FGD), only 225.4 $kg/m^3$ of OPC was used and 75.1 $kg/m^3$ of each filler was added.

Water used throughout this experiment, including to cast concrete, was 15.0 MΩcm DI water. Varying metal sulfides, acids, and bases were used to create and titrate metal solutions, including technical grade sulfuric acid (Fischer Chemical, UN1830), lab grade nitric acid (Fischer Scientific) and extra pure sodium hydroxide (Acros Organics). The metal salts used were aluminum sulfate hydrate ($Al_2SO_4 \cdot 18H_2O$), manganese sulfate monohydrate ($MnSO_4 \cdot H_2O$), cupric sulfate ($CuSO_4 \cdot 5H_2O$), and ferrous sulfate heptahydrate ($FeSO_4 \cdot 7H_2O$), all

certified ACS grade. The aluminum, manganese, and copper sulfates were manufactured by Fischer Scientific while the iron sulfate was from Sigma-Aldrich. Argon gas was supplied from the Ohio State University gas store, pre-purified at 99.998%.

### 1.2.2 Concrete Sample Casting

To cast concrete cubes, 2-inch cubic molds were cleaned and coated lightly with concrete form oil from Copper State Petroleum. Following ASTM C109, each mold was filled halfway with the mortar and tamped 16 times; then, the remainder of the mold was filled and tamped another 16 times. If space remained between the top of the mold and the concrete, the cube was hand-filled and tamped 16 times again until the mold was filled to the top and level. Molds were then wrapped in plastic wrap and placed in a curing room maintained at 72 °C and 100% relative humidity (RH) for 24 hours. After 24 hours samples were carefully demolded and placed back into the curing room for at minimum 28 days.

Similarly, to cast 3-inch diameter, 6-inch height pervious concrete cylinders, the cylinders were filled halfway with fresh concrete and tamped 25 times with a 3/8” metal rod with a hemispherical tip. The mold was filled and tamped 25 times again, repeating until the concrete filled the mold to the top and was level. Molds were wrapped in plastic wrap, cured in the curing room for 24 hours, demolded, then cured a minimum of 28 days or until the time of testing.

### 1.2.3 Acid Durability Testing

After curing for 28 days, cubes were soaked in either 0.01M, pH 2 sulfuric acid or saturated limewater (e.g., experimental control). Cubes were exposed to the acid at a rate of 1.14 volumes of solution per bulk volume of concrete, and were stored in sealed containers at room temperature. The acid solution was replaced weekly for 12 months. One box containing 6 cubes of each pervious concrete mix was monitored for pH change over time to analyze the effectiveness of acid treatment over an extended period. The solution pH in the designated containers was measured on day 1, 2, and 7 post-acid replacement on a weekly or bi-weekly basis. Each box was shaken for 3-5 seconds and then pH was measured to the nearest tenth.

Every 4 weeks a set of cubes cured in limewater and acid were tested in triplicate to determine the strength and porosity of each pervious concrete mix. As cement hydration continues for months or years following initial mixing, the limewater cube strength was tracked to identify acid damage relative to expected strength development. Porosity was determined using the procedure from Haselbach et al. (2005), except cubes were conditioned for 1 minute prior to recording wet mass instead of the 30 minutes as recommend by the authors. Congruence of the methods was verified (see Table 13 in the appendix) and results did not differ by more than 1% between soaking times. In order to determine porosity, triplicates of acid and limewater-soaked cubes were removed from their curing solutions and air-dried for at least 24 hours. Using a scale (Adam Equipment, CBK 100a) with a weigh-below hook to measure tension, a wire-mesh basket was connected and suspended in water. After taring the scale, the dry mass of each cube was measured. A cube was then submerged in the water, shaken back and forth by hand to

eliminate air bubbles, and set on the basket. After a period of at least a minute, the mass of the submerged cube was recorded. Porosity was calculated using Haselbach's formula:

$$Porosity\ \% = \left[1 - \frac{\frac{Dry\ Mass - Submerged\ Mass}{Aggregate\ Density}}{Density\ of\ Water}\right] * 100 \quad (1)$$

Immediately following porosity calculations, these cubes were broken using a Forney Compression machine following ASTM C109. The compressive strength was measured using specifications of 75% break percentage, a ramp rate of 75 psi/s, and a 2-inch cube.

### 1.2.4 Natural and Synthetic AMD Solution Preparation

The natural AMD used in this experiment was sourced from a stream in the northeast portion of the Wilds in Cumberland, Ohio (location: 39.87243°N, -81.70616°W). Samples were taken directly below the outlet of a pipe containing an underground flow of AMD in the summer and fall of 2021. The sample site was in ~6 inches of water with red-orange solids lining the bottom of the pond. A pH of 4.5 was measured at this location using a Sper Scientific Basic pH Meter and matching pH probe.

Prior to use, each container was decanted to separate and remove the red-orange precipitate, mud, leaves, and settled organics. All AMD collected at the field site was intermixed to provide a homogenous solution and combined into several Nalgene containers with pH values ranging from 4.01 to 4.12. Metal ions measured in the AMD solutions were copper(II), iron(II), aluminum(III), and manganese(II); these were selected to model common ions in other natural AMD sources (Table 1). For each, the appropriate metal-sulfate was selected as in Larsson et. al. (2017), MacIngova and Luptakova (2012), and Li et. al. (2019).

To assess the ability of the pervious concrete to remove each metal from solution, 1 mmol metal ion solutions of aluminum, iron, manganese, and/or copper were made by combining metal sulfate solids and DI water in a beaker, adjusting the solution to a pH of 4.0 (±0.2) and stirring to dissolve all solids. A pH probe (Orion Dual Star from Thermo Scientific) with a compatible Epoxy-Body electrode was used to determine the pH of the batch before exposure to the concrete. Concentrations used for each mix and measured for the natural AMD are presented in mg/L in Table 2.

Table 2: Metal concentrations used in this experimentation. Included is natural AMD as collected, and the designed mix concentrations of synthetic AMD and single-ion solutions of Al, Mn, Fe, and Cu.

| Solution | Metal Concentration (mg/L) | | | |
|---|---|---|---|---|
| | Al | Mn | Fe | Cu |
| Natural AMD | 31.12 | 13.29 | 0.036 | 0.0016 |
| Synthetic AMD | 31.12 | 13.29 | - | - |
| Al | 26.98 | - | - | - |
| Mn | - | 54.94 | - | - |
| Fe | - | - | 55.85 | - |
| Cu | - | - | - | 63.55 |

1.2.5. Metal Removal Tests

To assess the metals removal capacity of the pervious concrete, small-scale tests measuring the impact of concrete on pH and metal concentration over time were conducted. Four mixes with different fillers (OPC, fly ash F, fly ash C, and limestone powder) were tested in triplicate on natural AMD, the synthetic AMD mix, and single-ion solutions containing 1 mmol of copper, iron, manganese, and aluminum. Cubes were suspended in cylindrical containers of

approximately 1 L (Figure 4) and sampled at 5, 10, 15, and 30 minutes as well as 1, 3, 6, and 24 hours. Each cube was re-exposed to the metal solution 3 times for each solution to assess changes in removal capacity and kinetics.

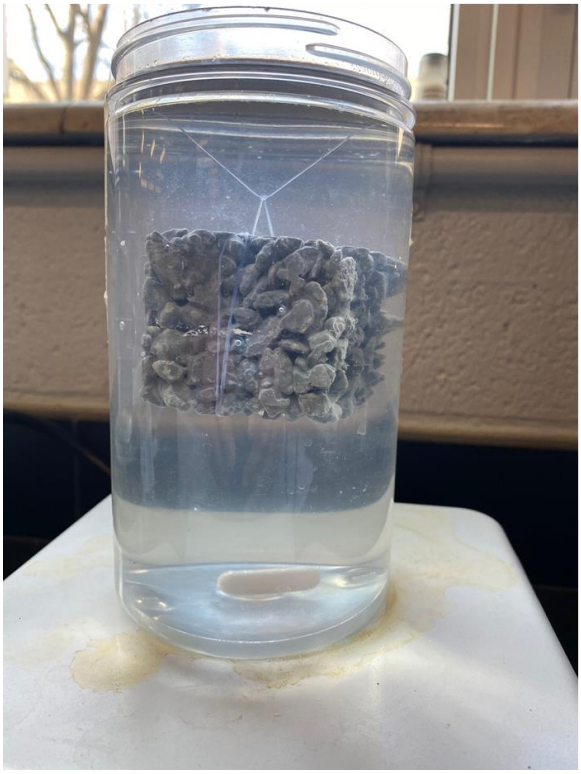

Figure 4: Experimental setup for metal removal testing.

To differentiate the impact concrete has on metal removal, pH-controlled solutions were analyzed for precipitation behavior of each metal solution tested. Using the same metal concentrations and testing procedure, these pH controls omitted pervious concrete cubes and pH was gradually increased from 4 to >10 using a concentrated stock of sodium hydroxide. Samples were taken at indeterminate intervals based on volume of sodium hydroxide added to capture behavior during precipitation as well as over the entire range tested.

### 1.2.6 Flow-Through Column Testing

Three cylinders of OPC pervious concrete were created to demonstrate the treatment of AMD in a bench-scale setup. Following methods in Haselbach et. al. (2005), the average porosity of three cylinders was determined and pore volume was approximated at 100mL. A volume of 1L of natural AMD was selected for each cylinder to represent 10 pore-volumes of AMD to be treated over many pass-throughs.

Two halves of a 7.5 cm diameter PVC pipe were lined with rubber to prevent piping along the outside of the pervious concrete cylinder. The pervious concrete cylinder was placed inside the PVC and the halves were secured together using two hose clamps and suspended above an empty 2L beaker. After measurement of initial pH and sample collection for later metals analysis, a liter of AMD was slowly poured into the top of the concrete cylinder. After the solution had finished flowing through, the beakers were swapped and the process was repeated using the same solution. When samples were taken, the solution pH was measured and 2mL of AMD was filtered for metal analysis.

Average pore volume of the cylinders was 0.144 mL/L of concrete volume or approximately 100 mL per cylinder. One liter of natural AMD was repeatedly applied through each cylinder, and each pass-through of the 1L of AMD is referred to as 10 pore volumes. The cumulative length of pervious concrete treatment was calculated as the depth of the core (15.2 cm) multiplied by the number of pass-throughs conducted. This can be used to model how long a permeable reactive barrier would have to be to treat field-scale AMD. Data from pass-throughs 0-10 were averaged from columns 1, 2, and 3, and data from up to 70 pass-throughs were then averaged from columns 2 and 3 as column 1 testing was halted after 10 pass-throughs.

### 1.2.7 Sample Analysis

Samples of either AMD or individual metal solutions were filtered and stored in individual tubes prior to analysis using an Inductively Coupled Plasma – Optical Emission Spectrometer (Agilent Technologies 5100 ICP-OES, used in tandem with an Agilent SPS 4 Autosampler). Approximately 2 mL subsamples were filtered using a 0.2 μm syringe filter into a clean test tube. Before processing, samples were first diluted 50x using a 2% nitric acid solution, and accompanying metal standards were created in a similar concentration range (0.01, 0.1, 1, 10 mg/L). Standards were created using ICP multi-element standard solution VIII from Supelco.

### 1.2.8 Data Analysis

At least two optical wavelengths for each metal were analyzed, and data were processed using Microsoft Excel. Linear trendlines between the four standards were created over each optical wavelength for each metal of interest. The trendline equation was used to determine concentration in mg/L of each wavelength; these values were averaged to determine metal concentration in the analyzed sample. Measured concentrations were multiplied by 50 to calculate the undiluted concentration of each sample.

In most cases, runs 2 and 3 for each metal solution were treated as equivalent and data were combined for final graphic creation. Both triplicates for runs 2 and 3 were averaged, and standard deviation between the six cubes was calculated for pH and concentration in mg/L. All

graphics were created in Microsoft Excel, with standard deviation above and below each data point expressed as positive and negative error bars.

To determine concrete mix effectiveness for acid neutralization over time, linear interpolation was conducted using pH values between 1 day and 2 days post-change. Interpolation was used to determine the time of solution neutralization (i.e., pH of 7.0) between the two nearest measured timepoints. Exact time of acid replacement and measurement on days 1 and 2 was recorded to account for variation between acid replacement and time tested the following days. Trendlines, as calculated by Microsoft Excel, are included for each series in the consistent colors.

## 1.3 Results

### 1.3.1 OPC Removal of Metals in Single-Ion Solutions

Aluminum, manganese, iron, and copper sulfate solutions were treated by a concrete mix containing 100% ordinary Portland cement (OPC). Individual metal solutions were tested to determine treatment trends of metals over time while exposed to pervious concrete. Three runs of each metal were done using the same concrete to analyze treatment differences as exposure increased and surface sites became occupied.

Notable differences were seen between run 1 when compared to runs 2 and 3. Runs 2 and 3 exhibited initial leaching of Al, Fe, and Cu, while run 1 did not. Trends in metals concentrations with time for runs 2 and 3 were very similar in all metal solutions, with run 1 having large deviation from the other two. This phenomenon is likely due to efflorescence of calcium hydroxide (CH) on the unused cubes impacting the chemistry of run 1 (Pernicová,

2014). Runs 2 and 3 also had precipitate remaining from previous runs causing leaching and creating similar chemistry. Cubes from each metal solution after 3 runs are shown in Figure 5, demonstrating the efflorescence of an unused cube and the precipitation of metals on the four used cubes.

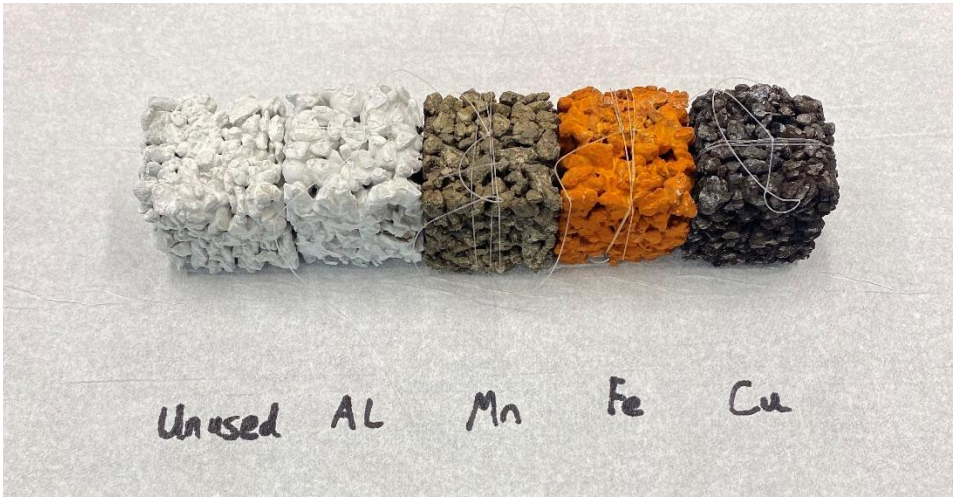


Figure 5: OPC cubes from single ion runs, including unused OPC cube alongside Al, Mn, Fe, and Cu.

Heavy metal concentration data from all three runs is presented in Table 3. Average concentration in mg/L is shown, as well as percent removal in relation to initial concentration (T=0). Initial leaching behavior can be seen as negative percent removal in runs 2 and 3 of aluminum, iron, and copper until 30 minutes of contact time had elapsed.

Table 3: Metal concentrations of OPC cubes during the contact time experiment. Data presented are the average of three cubes, with both concentration in mg/L and percent removal of metal in relation to the initial concentration. Negative values caused by regression line error in ICP analysis are represented by the lowest standard (0.01 mg/L at 50x dilution).

| | | | Contact Time | | | | | | | | | EPA Quality Recommendations |
|---|---|---|---|---|---|---|---|---|---|---|---|---|
| | | | 0 | 5 | 10 | 15 | 30 | 1 | 3 | 6 | 24 | |
| Metal | Run | Units | Minutes | | | | | Hours | | | | |
| Al | Run 1 | mg/L | 27.30 | 24.53 | 22.76 | 22.10 | 15.04 | 8.25 | 0.27 | 0.21 | 1.20 | Varies for Al depending on water chemistry |
| | | % removal | 0.0 | 10.2 | 16.6 | 19.1 | 44.9 | 69.8 | 99.0 | 99.2 | 95.6 | |
| | Run 2 | mg/L | 22.24 | 23.29 | 25.02 | 22.98 | 18.08 | 8.59 | 0.71 | 0.31 | 0.33 | |
| | | % removal | 0.0 | -4.7 | -12.5 | -3.3 | 18.7 | 61.4 | 96.8 | 98.6 | 98.5 | |
| | Run 3 | mg/L | 21.92 | 23.08 | 26.00 | 25.03 | 22.44 | 10.47 | 0.63 | 0.34 | 0.30 | |
| | | % removal | 0.0 | -5.3 | -18.6 | -14.2 | -2.3 | 52.3 | 97.1 | 98.4 | 98.6 | |
| Mn | Run 1 | mg/L | 68.52 | 63.38 | 66.38 | 63.18 | 64.36 | 63.56 | 61.72 | 63.48 | 56.09 | 0.05 mg/L from human health criteria table. Equivalent to ~99.92% removal |
| | | % removal | 0.0 | 7.5 | 3.1 | 7.8 | 6.1 | 7.2 | 9.9 | 7.3 | 18.1 | |
| | Run 2 | mg/L | 67.42 | 63.03 | 61.71 | 63.19 | 61.96 | 53.59 | 49.58 | 47.91 | 39.82 | |
| | | % removal | 0.0 | 6.5 | 8.5 | 6.3 | 8.1 | 20.5 | 26.5 | 28.9 | 40.9 | |
| | Run 3 | mg/L | 61.93 | 62.73 | 59.56 | 60.73 | 60.86 | 53.96 | 48.82 | 46.54 | 39.82 | |
| | | % removal | 0.0 | -1.3 | 3.8 | 1.9 | 1.7 | 12.9 | 21.2 | 24.9 | 35.7 | |
| Fe | Run 1 | mg/L | 55.98 | 51.58 | 45.68 | 40.15 | 28.22 | 10.89 | 0.23 | 0.12 | 0.22 | 1.0 mg/L from aquatic life criteria table. Equivalent to ~98% removal |
| | | % removal | 0.0 | 7.9 | 18.4 | 28.3 | 49.6 | 80.5 | 99.6 | 99.8 | 99.6 | |
| | Run 2 | mg/L | 43.28 | 44.05 | 50.37 | 46.73 | 33.10 | 17.95 | 0.74 | -0.33 | <0.5 | |
| | | % removal | 0.0 | -1.8 | -16.4 | -8.0 | 23.5 | 58.5 | 98.3 | 100.8 | 100 | |
| | Run 3 | mg/L | 45.21 | 45.89 | 50.71 | 48.38 | 40.12 | 19.50 | 1.26 | -0.30 | <0.5 | |
| | | % removal | 0.0 | -1.5 | -12.2 | -7.0 | 11.3 | 56.9 | 97.2 | 100.7 | 100 | |
| Cu | Run 1 | mg/L | 56.64 | 57.70 | 57.35 | 56.03 | 54.70 | 37.78 | 15.93 | 2.28 | 0.22 | 1.3 mg/L from aquatic life criteria table. Equivalent to ~97% removal |
| | | % removal | 0.0 | -1.9 | -1.3 | 1.1 | 3.4 | 33.3 | 71.9 | 96.0 | 99.6 | |
| | Run 2 | mg/L | 49.17 | 52.74 | 60.35 | 61.76 | 57.63 | 38.80 | 13.76 | 2.00 | <0.5 | |
| | | % removal | 0.0 | -7.3 | -22.7 | -25.6 | -17.2 | 21.1 | 72.0 | 95.9 | 100 | |
| | Run 3 | mg/L | 50.61 | 53.46 | 59.81 | 59.84 | 54.07 | 34.81 | 10.13 | 1.70 | <0.5 | |
| | | % removal | 0.0 | -5.6 | -18.2 | -18.2 | -6.8 | 31.2 | 80.0 | 96.6 | 100 | |

Metal data from runs 2 and 3 are combined in Figure 6. Standard deviations between all six tests (triplicates of runs 2 and 3) were calculated and added as positive and negative error bars. This combination of later runs is meant to model concrete with repeat exposure to elevated metal concentrations in a low pH solution, similar to that of AMD.

Al, Fe, and Cu experienced initial leaching in the first 30 minutes of runs 2 and 3, with residual metals from previous runs increasing concentration by nearly 20%. After 10 minutes (15 min for Cu), leaching slowed and dissolved metals began to decrease in concentration. As precipitation takes place in higher pH ranges, redissolution of previous precipitates in fresh 4.0 pH solution may be causing initial leaching seen in this experimentation. After 30 minutes (<60 min for Cu), metals concentrations in solution were less than at the start of experimentation, suggesting precipitation and adsorption processes were at play as pH increased. As the OPC continued to interact with the metal ions in solution, further treatment occurred until >95% of the Al and Fe were removed by 3 hours of contact time, with Cu needing 6 hours for similar removal. The trends for Mn did not follow those for the other three metals as Mn showed no initial leaching effect. Less than 10% of initial Mn was removed in the first 30 minutes of contact time, with only 36-41% of the Mn removed by the end of the 24-hr period. This suggests that if Mn is the target metal for removal at an AMD site, another AMD treatment technology may be better suited for use.

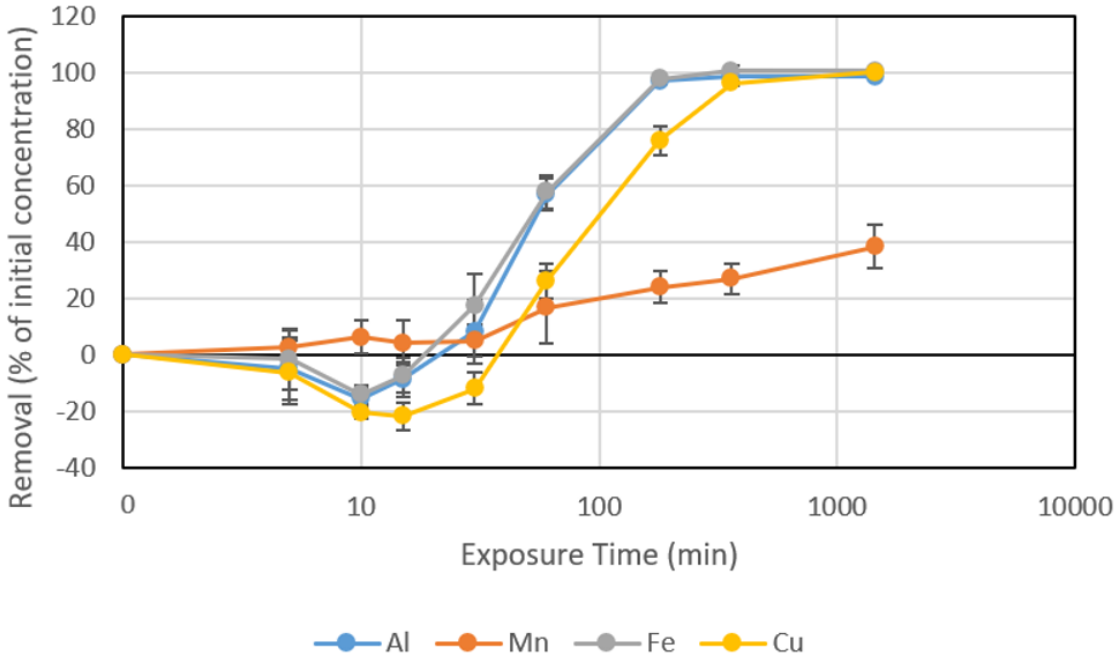


Figure 6: Average metal percent removal by OPC cubes for runs 2 and 3 over time.

This phase of experimentation suggests that pervious concrete is best utilized for AMD treatment under continuous flow conditions and at relatively low flow rates, where the contact time is on the order of hours and not minutes or seconds. Mn can be treated via concrete, but more than 24 hours of contact time may be required to see substantial removal. This suggests that another AMD treatment technology, such as absorbents or Mn-oxidizing microbes, may be more efficient at Mn removal than pervious concrete (Li et. al., 2019).

### 1.3.2 Impact of pH on Metal Removal

Alongside metal concentration, pH of the singular metal solutions treated by OPC was analyzed to determine the ability of pervious concrete to neutralize acid and the resulting effect of moderation in pH on metals removal. Presented in Figure 7 is the average of runs 2 and 3 of OPC as featured in Figure 6 previously. The exposure time is compared to pH.

While pH of Mn, Fe, and Cu solutions began to increase within 5 minutes, the dynamics of the Al solution were slower, taking approximately 1 hour for pH to exceed 4.5. The pH of Fe and Cu solutions remained between 5.5 and 6.5 from 10 minutes to 3 hours. The Mn solution pH did not continue to increase after 6 hours, when it reached 8.0. These periods where pH gain plateaued are exactly the times during which metals were experiencing the highest removal, as seen in Figure 8.

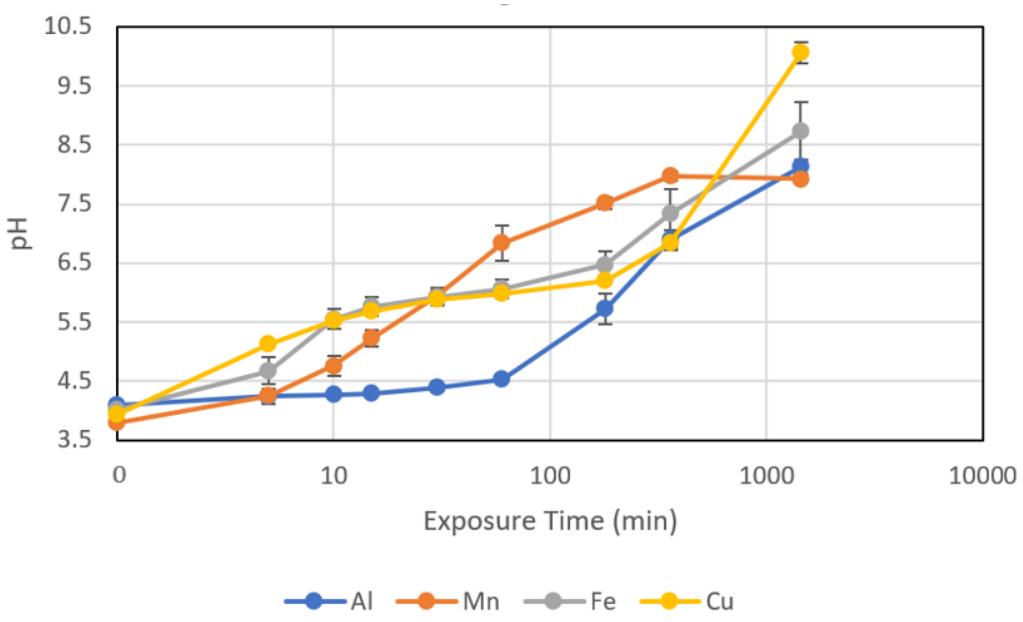


Figure 7: Average solution pH for OPC cubes for runs 2 and 3 over time.

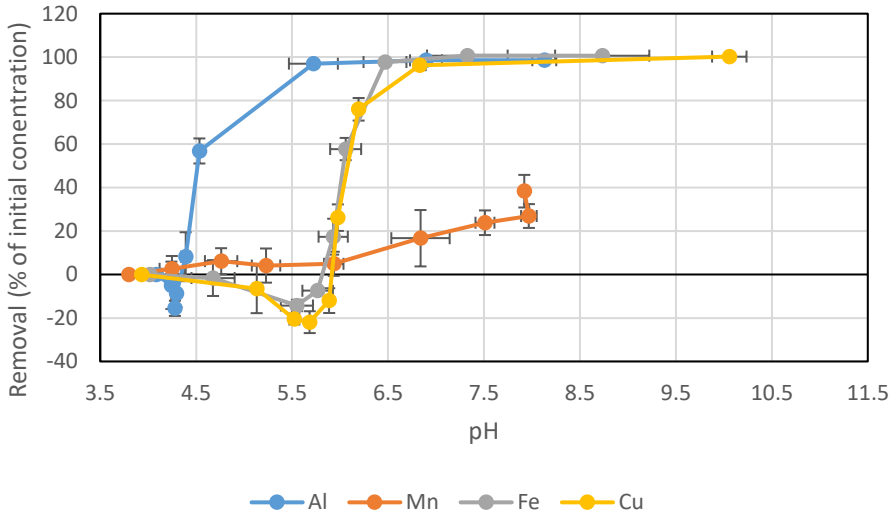


Figure 8: Average metal percent removal versus solution pH for OPC cubes for runs 2 and 3.

Figure 8 shows removal percentage of metals as a function of pH. Near vertical lines on Figure 8 represent small ranges of pH where large proportions of metals were removed. The greatest removal for Al took place immediately below a pH of 4.5, removing 60% of the Al from solution. Mn was not substantially removal until a pH of 8.0, and the experiment was concluded before greater than 40% removal was obtained. Both Fe and Cu followed similar trends, with greater than 80% removal at a pH less than 6.5.

To understand whether metals removal occurred through precipitation due to increased pH or as a result of physical adsorption to the concrete surface, changes in dissolved metals concentration across a similar range of pH but without pervious concrete exposure were tested to determine precipitation behavior. Figure 9 details all four individual metals and their percent removal relative to solution pH. Each metal has a range of pH values where an outsized portion of removal takes place: 4.0 to 5.0 for Al, 7.5 to 8.5 for Mn, 5.5 to 6.0 for Fe, and 5.5 to 6.5 for Cu. Redissolution of Al was also observed from a pH of 9 to 10.

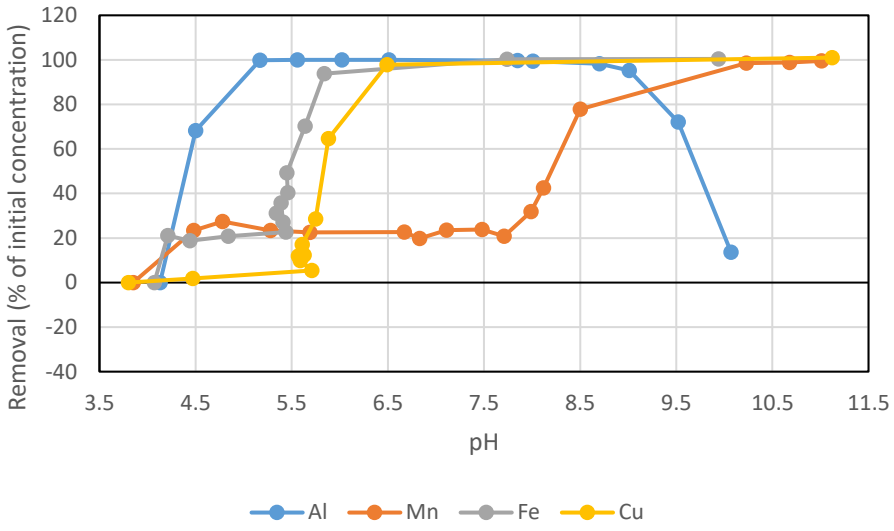


Figure 9: Percent removal of titrated metal pH-controlled solutions (i.e., no pervious concrete cube).

Theoretical pH ranges of metal hydroxide formation were calculated by Monhemius (1977; Figure 10) with metals relevant to this experiment highlighted. Al was shown to precipitate from pH 4.5 to 5.0, Mn from 9.0 to 10.0, Fe(II) from 7.5 to 8.5, and Cu from pH 5.5 to 6.5. These ranges generally aligned with the regions of maximum precipitation from single-ion solutions herein.

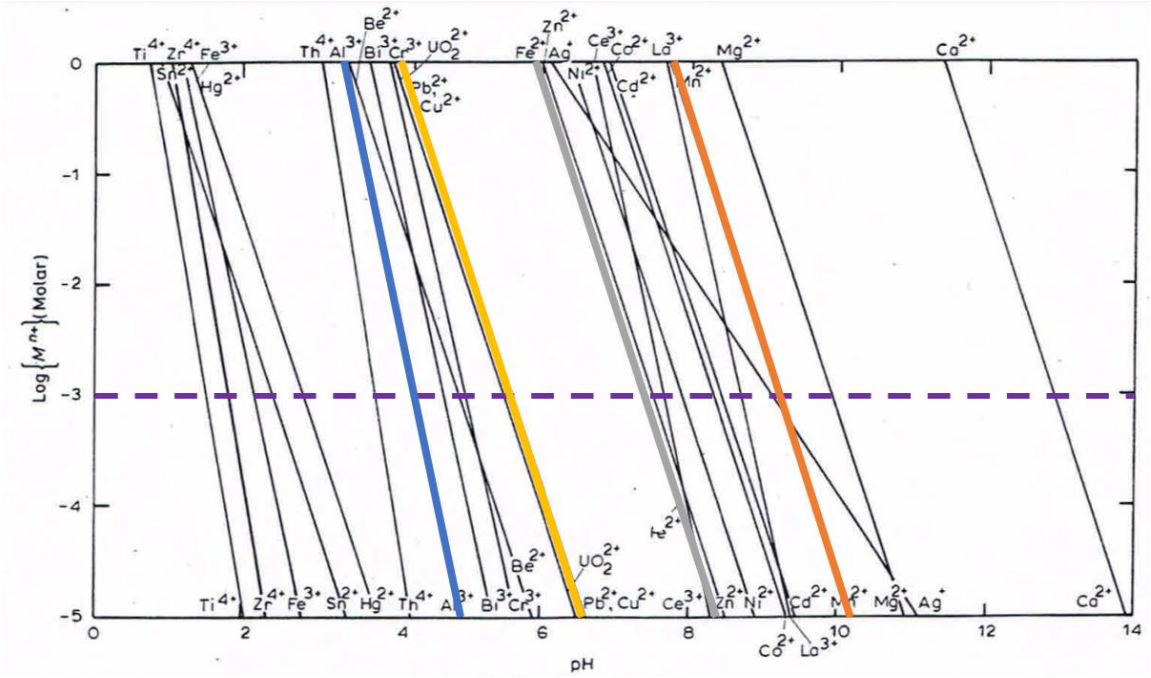


Figure 10: Theoretical metal hydroxide formation over pH ranges. Initial concentrations of single-ion metals is represented by a dashed horizontal line, and each metal studied is colored with the associated color in previous graphs (Monhemius, 1977).

Removal of each metal ion followed different trends. Aluminum precipitated out of solution with little pH increase and was >95% removed by pH 5.5. This removal correlates with a region in Figure 7 in which pH does not increase by more than 0.5 for the first hour of exposure. $Al(OH)_3$ dominates solutions at $10^{-3}$ mol/L [Al] starting at a pH of 5.0 (e.g., Figure 3), with a transition phase of $Al(OH)^{2+}$ beginning at 4.5. The pH hardly changed for the first hour of exposure time to pervious concrete, likely because excess hydroxide ions were used to form precipitates until most Al was removed. The pH-control in Figure 9 supports these conclusions given Al is >99% removed by a pH of 5.2, and both these ranges match theoretical Al precipitation ranges (Figure 10).

Manganese removal was sparing at lower pH, as <10% removal occurred before a pH of 6.0. It was not until a pH of 8 that significant precipitation occurred (Figure 8 and Figure 9), while precipitation theoretically occurs at pH 9 (Figure 10). Figure 7 further supports Mn precipitation as a removal mechanism at high pH, given pH remains consistent at 8.0 from 6 to 24 hours. Figure 9 shows that the largest proportion of Mn removal, from 20% to 80%, occurred within a pH range of 7.5 to 8.5. The concrete-exposed solution showed steady Mn removal up to a pH of 8.0 with 27% removal, beyond which precipitation appeared to dominate. This slow Mn removal in the concrete-exposed solution where little occurred in the pH-controlled solution may suggest removal of Mn due to adsorption and interaction with pervious concrete itself at <8.0 pH.

Fe has a higher pH of precipitation than Al, but both have similar treatment dynamics (Figure 6). Iron reached a pH of approximately 6 within 5-10 minutes and then probably began to form iron hydroxides (Figure 6). Fe precipitated from solution at a higher pH when treated by concrete versus the pH-control. 50% removal of Fe, for example, was observed at a pH of 6 in concrete but around 5.5 in the pH-controlled solution. Calcium ion concentrations in the solutions were not found to impact this behavior (Figure 32 in the appendix). Both solutions precipitated at lower ranges than theory for Fe(II) suggests at pH 7.5 to 8.5 (Figure 10). This may be partially explained by the formation of $FeCO_3$, which Fajardo et. al. (2013) found precipitation best occurred at initial conditions of pH 6.0.

Similar metal precipitation dynamics occurred in the Cu samples. A majority of Cu ion removal occurred between pH values of 5.9-6.2 when in contact with the concrete

sample, but the precipitation occurred in the pH-controlled sample at a slightly lower pH range of 5.6-5.9. The theoretical precipitation ranges of 5.5 to 6.5 closely matches the behavior of the pH-controlled solutions, and the concrete-exposure tests started precipitation at lower ranges but still matched the theoretical ranges.

These experiments suggest that the >95% removal of metals from the single-ion metal solutions is largely due to solution pH increases and resultant precipitation. In order to observe substantial metal removal from AMD, pH should be increased to >5.0 for Al, >6.5 for Fe and Cu, and >9.0 for Mn. Redissolution of Al begins around pH 9.0 and excessive increases in solution pH may result in recontamination of the water if precipitates are known to redissolve at higher pH values, as is the case with Al (Figure 3). These singular solution tests and controls suggest concurrently treating Al and Mn in solution via precipitation will not be ideal, as redissolution of Al begins when Mn precipitation begins.

### 1.3.3: Treatment of a Multi-Ion Solution

To account for interactions between varying heavy metal ions in AMD, a synthetic mix was made to model the metal concentrations found in natural samples taken at the Wilds. This mix included the most significant pollutants in the natural AMD, specifically 31.1 mg/L of Al and 13.3 mg/L of Mn. As Fe and Cu concentrations in natural AMD obtained at the Wilds were several orders of magnitude smaller (0.036 and 0.016 mg/L, respectively), they were not included in the synthetic AMD mix.

The dynamics of pH change of the synthetic AMD mix is compared in Figure 11 to the Al and Mn dynamics discussed in previous sections. Figure 12 features Al and Mn percent removal in regard to pH as along with removal of Al and Mn in the synthetic AMD mix to assess multi-ion removal. The colored boxes in Figure 12 identify the pH ranges where substantial removal (>55%) of dissolved ions occurred in the synthetic AMD pH-control solution (Figure 13).

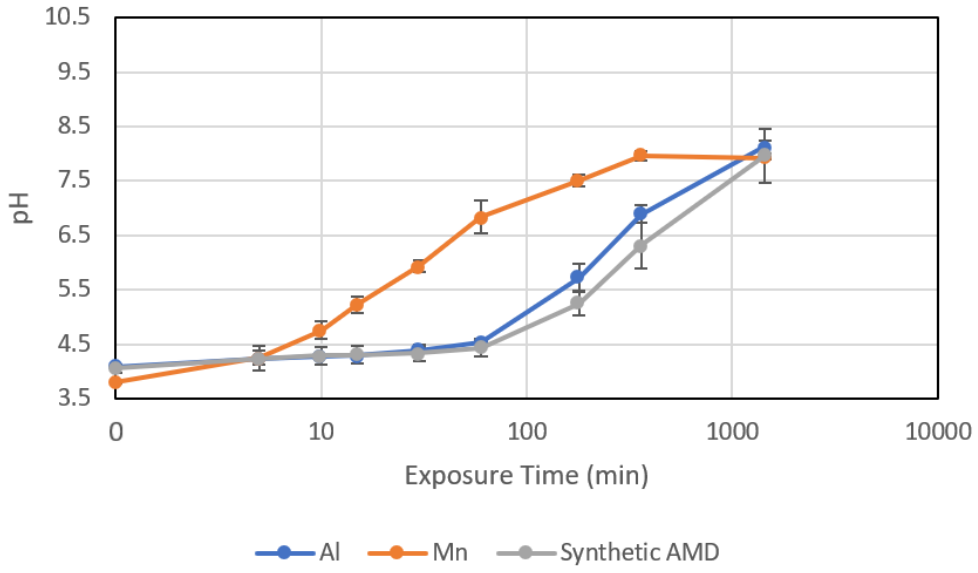


Figure 11: Average solution pH via OPC cubes for runs 2 and 3 and run 3 of synthetic AMD over time.

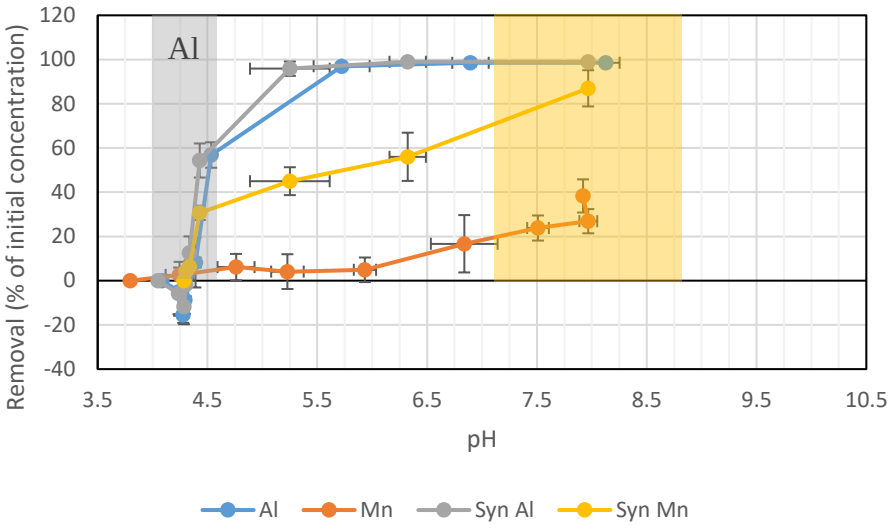


Figure 12: Average metal percent removal by OPC cubes for runs 2 and 3 and by synthetic AMD for run 3 over time. Colored portions correspond to precipitation ranges of pH-control.

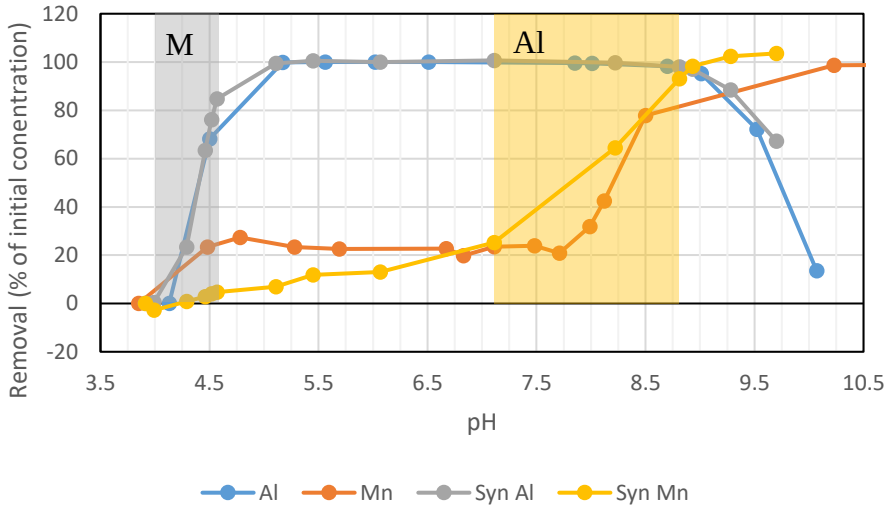


Figure 13: pH-control of synthetic AMD mix, with colored boxes mirroring pH ranges where a majority (>55%) of removal occurred.

Change of pH in the synthetic AMD closely followed the behavior of Al, as seen in Figure 11. The single-ion Mn solution reached a pH of 7 in the first 60 minutes, while both Al and synthetic AMD only reached a pH of 4.5 in that time. However, after 1 hour, Al had higher pH than synthetic AMD, likely due to interference between Al and Mn in the multi-ion system. At 24 hours of exposure time, each solution had a near equivalent pH of ~8.0.

Al removal was similar between the single-ion solution and synthetic AMD (Figure 12). Mn in the synthetic AMD was removed at a higher proportion (87%) at 24 hours than Mn in the single ion solution (38%). However, it is important to note that synthetic AMD had a lower concentration of Mn at 13.3 mg/L compared to 54.9 mg/L for the single-ion Mn. The single-ion solution removed more overall Mn (20.9 mg/L removed compared to 11.6 mg/L). Mn was also removed (30.7%) from the synthetic AMD mix in the first 60 minutes with little pH change. Precipitation is unlikely to account for removal in this range (expected precipitation at pH 8.0+); this is also true for Mn removal up to 6 hours, where 56% was removed at a pH of 6.3.

Figure 13 presents the removal percentage of pH-controls for Al, Mn, and each metal in the synthetic AMD mix. For Al, >99% removal was observed from a pH of 4.0 to 5.1. Both single-ion Al and synthetic Al exposed to concrete surpassed 50% removal and likely would have reached similar removal to pH-controls with additional data collected in the first hour.

Mn removal between the two pH-controls in Figure 13 varied more than for the Al samples. While a 20% initial removal of Mn was observed in the single-ion solution,

this was not observed in the synthetic AMD, but 25% removal of dissolved Mn did occur by pH 7.1. In the single-ion Mn pH-controlled solution, there was no concentration change from pH 4.5 to 7.7. Comparing Mn removal in the pH range of 7.0 to 9.0 is difficult due to a lack of overlapping data, but ~80% removal occurred before pH 9.0 in both solutions. Most synthetic AMD Mn removal did not occur in this range, as 56.0% was removed as the pH increased to 6.3 due to interactions with pervious concrete. This further supports adsorption, rather than pH-controlled precipitation, as being the primary removal mechanism for Mn in synthetic AMD.

One potential difficulty in utilizing pH to control metal ion precipitation results from simultaneous presence of multiple ions in solution that do not precipitate until high pH and others that redissolve at high pH. In the pH-controlled single-ion solutions, Al began to redissolve at a pH of 9.0, while Mn did not reach >80% removal until above pH 8.5 (with pH 9.0 recommended as a target for >99% Mn removal). With this overlap in effects only one ion can be removed from the system – either Al will precipitate from solution at pH < 9.0 or Mn will precipitate from solution at pH > 9.0. However, incorporation of pervious concrete and adsorption of Mn at lower concentration than the single-ion solution may partially address this issue. In a multi-ion solution mimicking natural AMD exposed to pervious concrete, 99% of Al and 87% of Mn was removed over the 24-hour exposure period. When Mn concentration matched natural AMD, adsorption to concrete acted as a primary removal mechanism and redissolution of Al was not observed. Pervious concrete, therefore, was shown to be an effective treatment of a

synthetic AMD mix with >85% treatment of both metals given 24 hours of exposure time.

### 1.3.4 Treatment of Natural AMD

Treatment of a natural AMD was compared to the synthetic AMD mix (Figure 13). The synthetic AMD was designed to utilize similar concentrations of metals present at the highest concentrations (Al and Mn) but did not include trace amounts of other metals and elements (Ni, Zn, Pb, etc.) nor natural organic matter (NOM) (Tables 1 and 2).

The dynamics of neutralization of pH over exposure time was similar between synthetic and natural AMD for the first 6 hours of treatment. At 24 hours, however, synthetic AMD reached a pH of 8.0 while natural AMD reached a pH of 8.9. This is the second highest pH value observed after 24 hours behind the single ion solution of Cu (10.1 pH).

Figure 14 details metal removal as a function of pH when synthetic and natural AMD are exposed to OPC pervious concrete. Figure 15 shows Al and Mn from both synthetic and natural AMD solutions. Highlighted regions of the Figure 13 correspond to precipitation ranges of pH-controlled solutions. Two data points with <25% to >80% removal were selected as the boundaries for precipitation in these pH-controlled solutions.

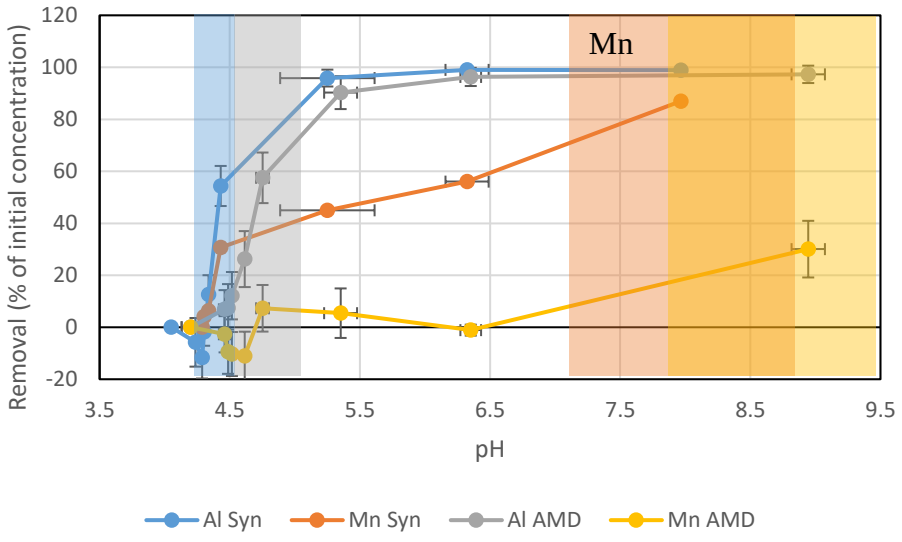


Figure 14: Average metal percent removal by OPC cubes for runs 2 and 3 of natural AMD and run 3 of synthetic AMD over time for synthetic vs. natural AMD. Colored portions of the figure correspond to precipitation ranges of pH-control

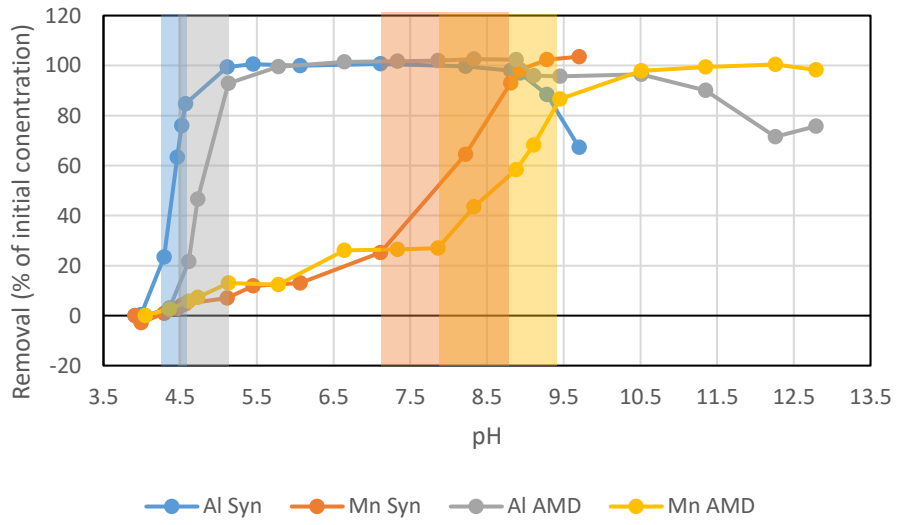


Figure 15: pH-control of synthetic vs. natural AMD, with correspondingly colored boxes mirroring pH ranges where a majority (>55%) of removal took place.

Natural AMD required higher pH values for Al and Mn removal compared to the synthetic AMD. Greater than 50% removal of Al in both solutions occurred after 1 hour of exposure to pervious concrete, but the resulting synthetic and natural AMD pHs were 4.4 and 4.8, respectively. Mn removal was highly variable, with 30% removal in natural AMD after 24 hours compared to 87% for synthetic AMD. At 6 hours, Mn in the natural AMD solution was still leaching from previous runs, with a -1.1% removal percentage. Al in Figure 15 closely follows its behavior in Figure 14 for both natural and synthetic AMD. Greater than 50% of Al is removed within the associated precipitation ranges on Figure 14. Redissolution of Al was observed in both synthetic and natural AMD pH-controlled solutions; while synthetic Al removal drops to 67% at pH 9.7, for natural AMD Al removal is >95% up to pH 10.5, with maximum redissolution reached at 71.5% removal and a pH of 12.9.

Mn removal in natural AMD varied greatly between exposure to concrete versus in a pH-controlled solution. In a pH-controlled solution, natural Mn removal followed the trends of synthetic AMD, but a majority of its removal (27% to 87%) occurred in a range ~0.7 pH higher than synthetic AMD. No substantial removal of Mn in natural AMD occurred when exposed to pervious concrete and when pH was below the Mn precipitation range, nor did it surpass 30% removal by pH 8.8 (58% removal of Mn in pH-controlled solution at pH 8.9).

For synthetic AMD (Figure 12 and Figure 13), pervious concrete aided removal of Mn compared to a pH-control, likely due to adsorption. However, concrete impeded natural AMD Mn removal compared to a pH-control, as evidenced by

Figure 14 and Figure 15. Presence of concrete had little impact on Al in synthetic and natural AMD, but Al in natural AMD consistently precipitated at higher pH than in the synthetic solution and also experienced less overall redissolution at higher pH (Figure 15).

### 1.3.5 Column Tests

3-in diameter by 6-in height (7.6 by 15.2 cm) pervious concrete cylinders were constructed for flow-through testing with natural AMD. Metals removal dynamics with exposure time to concrete has been discussed in preceding sections, and column tests were done to evaluate metal ion removal under more realistic flow conditions. Column tests can be used to link hydraulic retention time to water quality improvement and model a system with flowing AMD as opposed to stationary exposure. Figure 16 shows the treatment of Al/Mn and pH change in comparison to pore volume as well as the additive length of column in meters through which the solution would have had to flow to achieve the corresponding level of water treatment.

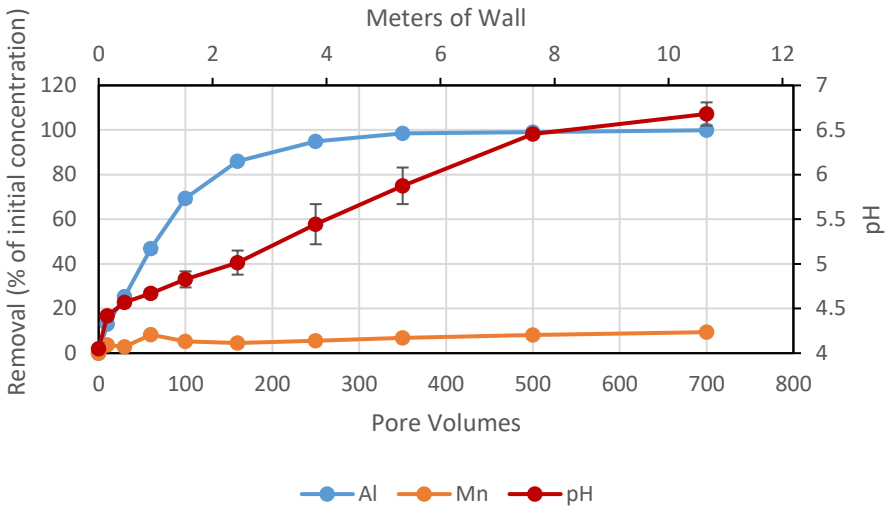


Figure 16: Metal removal as a percentage of initial concentration and pH of natural AMD poured through columns of OPC pervious concrete. Pore volume is a function of pass-throughs of the same 1L of AMD, and meters of column models sequential column length.

70 pass-throughs, equivalent to a cylinder 10.7 m in length, were conducted using columns 2 and 3; during these tests, pH increased from 4.0 to 6.8, Al removal was 99.9%, and Mn removal was 9.4%. With only 16 pass throughs (160 pore volumes), Al surpassed 86% removal at pH 5.0. Greater than 85% removal at pH 5.0 is consistent with Al in solutions discussed previously, as single-ion, synthetic AMD, and natural AMD all surpassed pH 5.0 and concurrently had >85% removal between 1 and 3 hours of exposure to OPC cubes. Comparison of pH and metal removal percentage is presented in Figure 17, which visualizes relative overlap in the removal characteristics of columns and cubes. Figure 17 shows that the suspended cube test method can accurately assess ion removal potential in more realistic flow-through conditions.

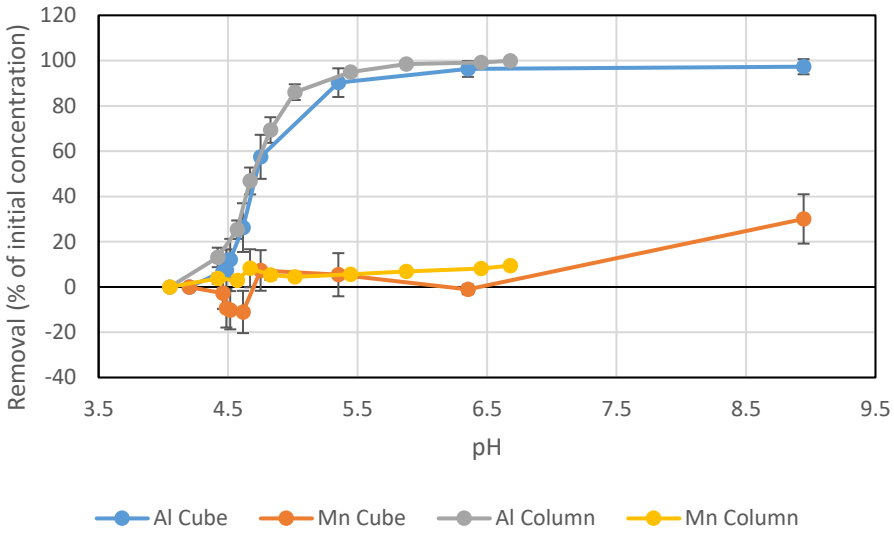


Figure 17: Metal removal percentage relative to solution pH for natural AMD in concrete exposure testing and column testing

Mn removal did not exceed 10% as pH ranges reached in experimentation were not high enough to reach Mn precipitation ranges as determined by pH-controlled solutions in Figure 9, Figure 13, and Figure 15. For natural AMD exposed to pervious concrete cubes over time, no removal of Mn occurred at pH 6.3 and 6 hours elapsed. After 24 hours, Mn reached 30% removal at pH 8.9, but more pore volume exposure and a longer PRB would have been necessary to reach that pH value in the column tests.

Since Al removal from natural AMD exposure tests closely overlapped Al removal from column tests (Figure 17), a relationship was inferred between PRB length and exposure time. This relationship was determined by linking a common endpoint between the column and cube with approximately >95% removal of natural AMD Al. Overlapping ranges of 0-360 minutes and 0-7.62 meters of PRB created the same removal and pH, and division creates a constant of 47.24 minutes of exposure per meter

of PRB. This constant represents that every meter of PRB length is equivalent to 47 minutes of contact time with the concrete cubes used in experimentation, suggesting PRBs will be effective in treating field-scale AMD without needing 3-6 hours of concrete exposure.

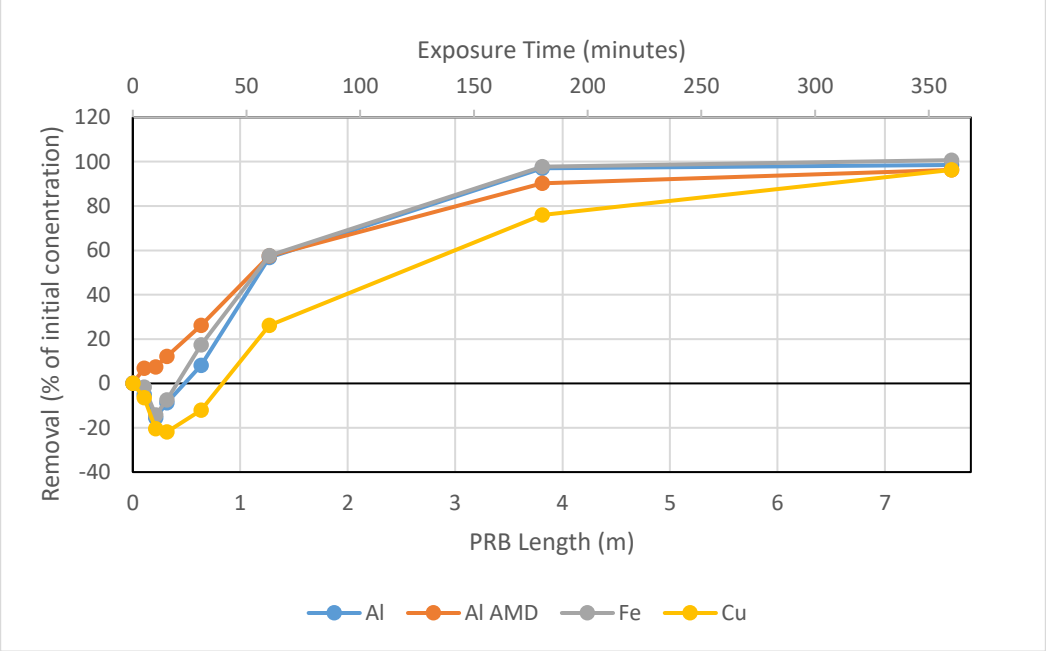


Figure 18: Graph of single-ion solutions, assuming a relationship between exposure time and permeable reactive barrier (PRB) length. Length of PRB in meters, equivalent to 47.24 minutes of exposure time, is compared to percent removal.

The single-ion solutions of Al, Fe, and Cu (Figure 18) give estimates of PRB length required to treat different proportions of dissolved metals. Natural AMD Al from concrete exposure testing was also included to compare to a natural system. 3.8 meters of PRB is akin to 3 hours of exposure, wherein Al and Fe removal was >95%. A much longer 7.6-meter PRB may be required if treating Cu is a concern. Mn showed varying

removal in natural systems and showed no change in the column test, so the data was not included since the PRB length needed to treat Mn may be prohibitively large.

### 1.3.6 Comparison of Treatment by Pervious Concrete Mixtures Utilizing Various Filler Materials

Alongside each metal solution tested with OPC pervious cubes, identical experiments were conducted using class F fly ash (FAF), class C fly ash (FAC), and limestone powder (LP) concrete. Each concrete mix and solution type was analyzed in triplicate over three runs, with average values of runs 2 and 3 being used to present data as in previous sections. In Figure 19 and Figure 20, OPC-exposed solutions (as discussed in sections 1.3.1-4) are compared to the three other concrete mixes in terms of pH and percent removal. Figure 19 details data from all single-ion solutions, and Figure 20 includes data from Al and Mn in synthetic and natural AMD. Highlighted regions in each graph correspond to pH-ranges where a majority of metal removal took place in the associated pH-controlled solutions.

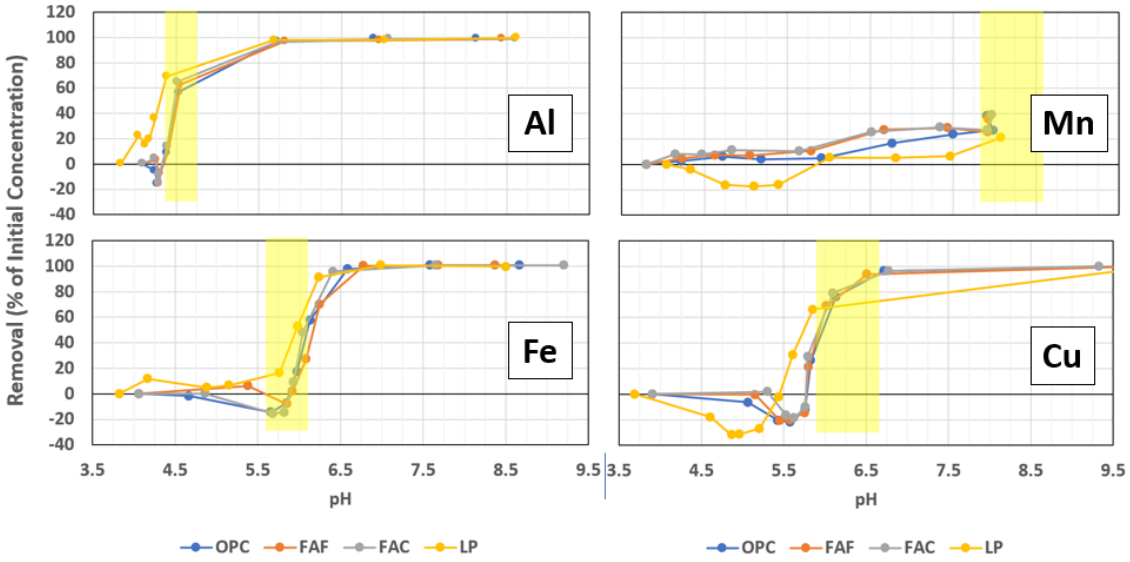


Figure 19: Percent removal of four single-ion solutions with OPC, FAF, FAC, and LP fillers over runs 2 and 3. Highlighted regions are pH ranges where a majority of metal removal took place in respective pH-controlled solutions

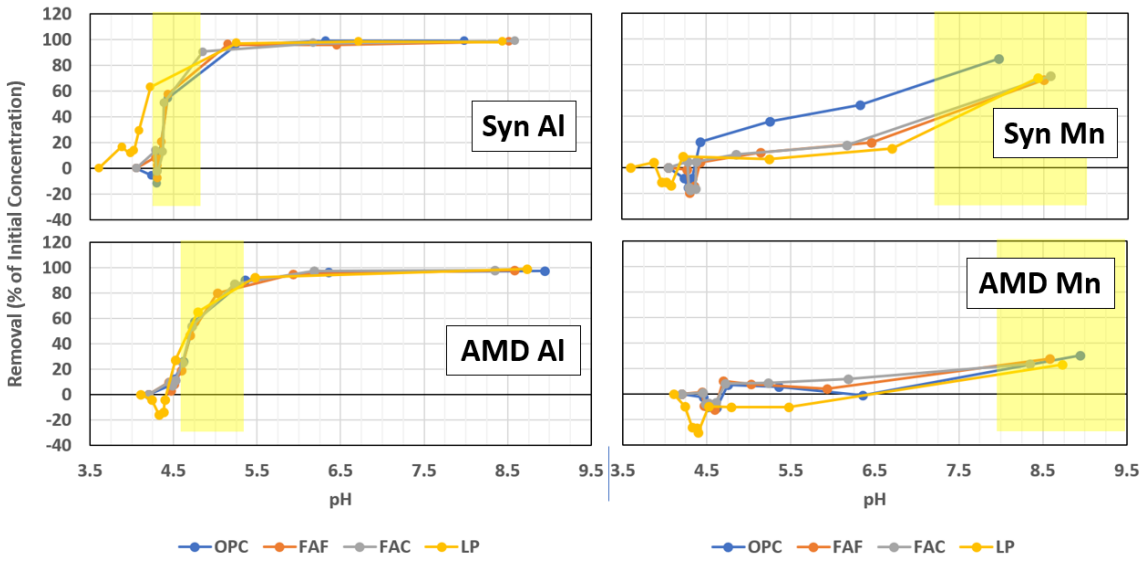


Figure 20: Percent removal of Al and Mn in multi-ion solutions with OPC, FAF, FAC, and LP fillers. Highlighted regions are pH ranges where a majority of metal removal took place in respective pH-controlled solutions

In a single-ion solution, Al was best treated through use of the LP concrete. The Al runs with LP had a lower initial pH, but showed little signs of leaching and most precipitation occurred ~0.25 pH lower than the other fillers. The most significant removal of metal ions for all fillers occurred in the range dictated by the pH-control. Similar behavior was observed with the synthetic AMD Al in Figure 20, but in natural AMD the LP concrete precipitated Al in the same range as other fillers and had slower removal based on exposure time.

Both FAF and FAC followed similar removal dynamics in the single-ion Mn runs. Both show ~10% more removal of Mn around pH 6.5 than OPC, with LP removal consistently lower and with some leaching observed. The behavior was not duplicated in the synthetic or natural AMD, both of which had lower initial concentrations of Mn. OPC

performed best in treatment of synthetic AMD, with all other fillers removing approximately 14% less Mn after 24 hours (yet reaching ~0.5 higher pH). Removal of Mn from natural AMD was similar between OPC, FAF, and FAC, with the fly ash concretes not leaching Mn at 6 hours as observed in OPC tests. Greater leaching and minimal removal of Mn occurred in the LP sample until 24 hours of contact time, at which time all fillers reached 22-30% removal.

Fe experienced similar precipitation behavior between OPC, FAF, and FAC, with the pH ranges of removal higher than that of the pH-controlled solution (Figure 17). LP precipitated Fe ~0.25 pH lower, with no leaching compared to the other fillers. Cu removal was similar across the OPC, FAF, and FAC concrete mixtures. LP leached Cu up to -31% (compared to -21% of the other fillers on average) and removed only 66% of Cu at 6 hours compared to 94-96% of the other fillers.

OPC exhibited the highest removal of Mn in synthetic AMD, but otherwise closely matched the fly ash mixtures tested (Figure 20). FAF and FAC performed better than OPC when treating single-ion Mn, but the difference between FAF and FAC was negligible throughout experimentation. LP was shown to be a favorable filler when treating single-ion Al and synthetic AMD Al, but had slower removal dynamics for Al in natural AMD. LP precipitated Fe and Cu at lower pH, but treatment of Cu was significantly slower than other fillers. LP is not recommended when treating Mn, as removal was slower (~20% less removal at most timepoints) and lower at similar pH to the other fillers. When treating natural AMD is intended, there is no clear distinction

between the performance of OPC. FAF, and FAC. Differentiation in field application may rely on factors like site conditions, budget, and filler availability.

### 1.3.7 Chronic Acid Impact on Neutralization

Pervious concrete cubes made with all 6 concrete mixes (OPC, FAF, FAC, LP, zeolite (Zeo), and flue gas desulfurization product (FGD)) were constructed for durability tests over the course of 12 months. The elapsed time required for each filler/mix to raise pH from 2.0 to 7.0 is plotted in Figure 20.

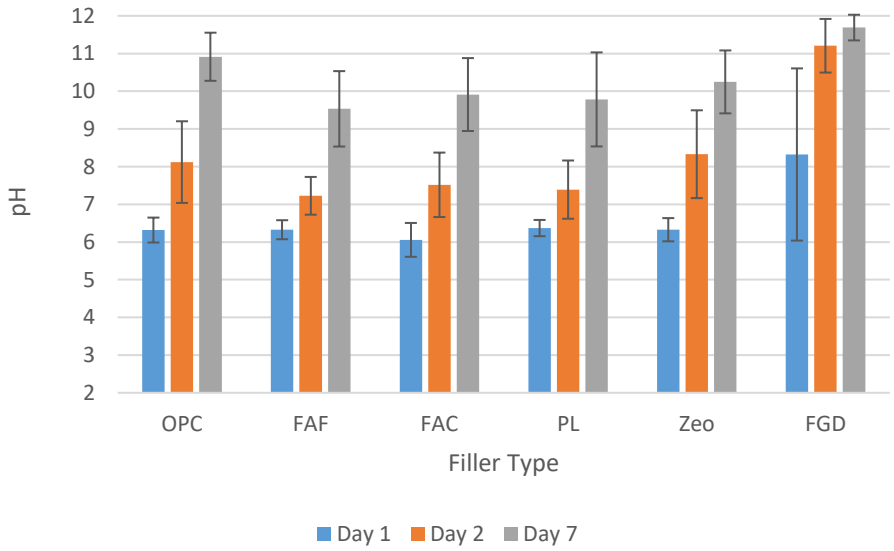


Figure 21: Average pH across a year of testing of treated acid for the 6 fillers in terms of days after acid replacement.

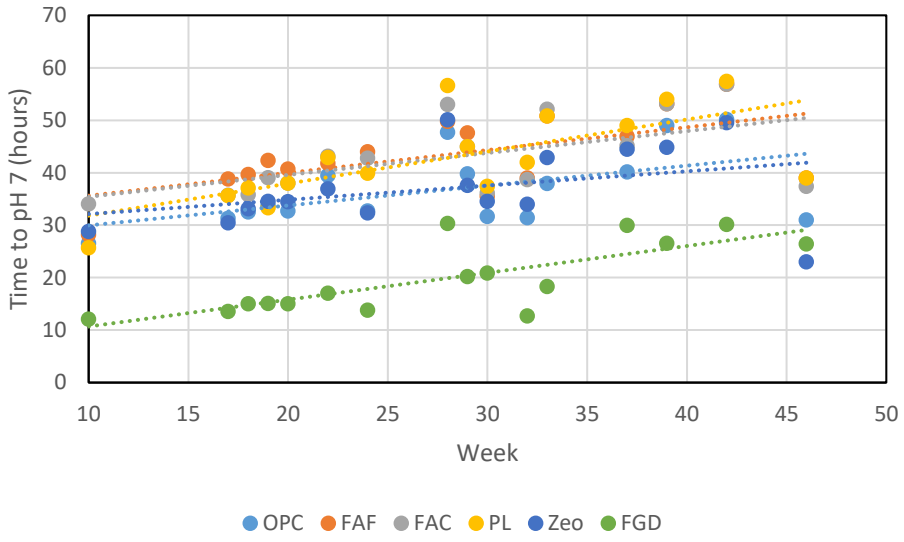


Figure 22: Time to raise pH of the same cubes from 2.0 to 7.0, with acid changed on a weekly basis for each concrete mixture.

OPC, FAF, FAC, LP, and Zeo mixes all raised pH from 2.0 to 6.0-6.4 in one day on average (Figure 21). Higher variability in the achieved pH was seen on day 2, with FAF, FAC and LP reaching pH levels of 7.2 to 7.5, OPC averaging pH 8.1, and Zeo reaching pH 8.3. On day 7, OPC caused the highest increase in pH of the mixes, reaching pH 10.9. FAF had the lowest final pH of 9.5. FGD behaved differently from the other mixes, with average pH on day 1 (pH 8.3) matching or exceeding all other fillers on day 2. FGD also reached an average of pH 11.2 on day 2, higher than the other fillers achieved in a week. As pH only increased to 11.7 for FGD on day 7, it had a much smaller increase in pH between day 2 and 7 than any other filler.

Figure 22 shows the disparate behavior of FGD compared to other fillers, as it reached pH 7 first in all weeks but the last. For example, FGD reached pH 7.0 in 12-15 hours from weeks 10 to 20, while all other fillers required 26-42 hours to reach pH 7.0.

However, the time for FGD to reach pH 7.0 increased at a faster rate than in other concrete mixtures, suggesting that it may be losing its neutralization abilities faster than the other mixes. The Zeo and OPC mixtures have closely overlapping trendlines and similar removal times, treating acid on average faster than FAF, FAC, and LP. FAF and FAC have closely overlapping trendlines, with little variation between their performance. LP has the steepest slope of the concrete mixtures, gaining 0.61 hours per week to reach pH 7.0, suggesting it is the least resilient mixture to long term acid attack.

### 1.3.8 Acid Durability

Alongside pH testing, compressive strength of the concrete mixtures (OPC, FAF, FAC, LP, Zeo, and FGD) were tracked each month for a year (Figure 23). Each mixture was tested in triplicate, with the max stress at break (in psi) recorded. Porosity and weight variations of each cube were also tracked but were not incorporated into the results shown below.

shows the slope of the linear regression relating strength to time for each concrete mix. Positive values indicate strength gain over the 12-month period; the inverse of this relationship is also true. Average stress at break in psi was also included and was calculated for each mix type in an acid or limewater soak. Initial stress at break for each mix was included, alongside 6- month data for acid and base-soaked concrete and 12-month data for acid-soaked concrete. Included in the table is concrete lifespan until 100 psi of strength is reached, calculated by using the linear regression trendline and initial concrete stress at break.

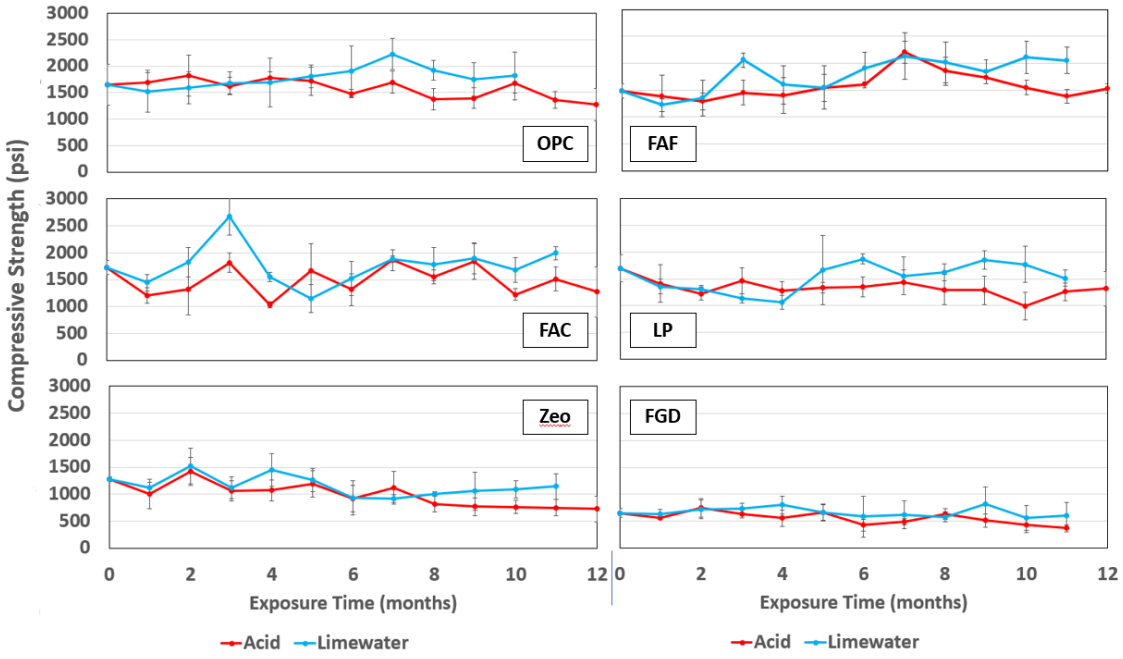


Figure 23: Stress at break (psi) of all six concrete mixes tested each month. Acid-soaked cubes are presented alongside their limewater-control counterparts.

Table 4: Slope of trendlines for stress at break data for all 6 concrete mixes, alongside average stress at break (psi) over the year of experimentation, initial, 6-month, and 12-month strength values. Estimate of months to reach 100 psi using initial (0-month) strength and acid slope of trendline is included.

| | | OPC | FAF | FAC | LP | Zeo | FGD |
|---|---|---|---|---|---|---|---|
| Slope of Trendline (psi/month) | Acid | -33.198 | 20.218 | -1.43 | -23.93 | -47.45 | -22.02 |
| | Base | 36.335 | 68.43 | 8.78 | 33.63 | -26 | -6.5 |
| Average Stress at Break (psi) | Acid | 1581 | 1570 | 1487 | 1334 | 990 | 550 |
| | Base | 1782 | 1777 | 1759 | 1535 | 1158 | 659 |
| Stress at Break, 0 months (psi) | Both | 1655 | 1483 | 1721 | 1701 | 1277 | 644 |
| Stress at Break, 6 months (psi) | Acid | 1483 | 1598 | 1315 | 1352 | 920 | 420 |
| | Base | 1907 | 1910 | 1517 | 1874 | 932 | 579 |
| Stress at Break, 12 months (psi) | Acid | 1276 | 1534 | 1272 | 1316 | 727 | 363 (11mo) |
| Time Until 100 psi (months) | Acid | 46 | ∞ | 1133 | 66 | 24 | 24 |

It is well known that OPC concrete will continue to hydrate and gain strength over time when sufficient moisture is available (Bullard et. al., 2011). As a result of continued hydration, it may not be possible to assess acid degradation from the strength change associated with acid-soaked cubes alone. Tracking changes in the limewater cured concrete, and differences between the limewater-cured and acid-solution-exposed samples provides better understanding of strength degradation.

OPC cubes were the strongest, with FAF and FAC generating similar compressive strengths. FGD was the weakest concrete tested, having 35% of the average strength of OPC when under acid attack and 37% the strength when both were cured in limewater.

Slope is useful to differentiate natural curing of concrete versus strength loss due to acid attack and predict potential behavior over more than a year of study. OPC, when cured in limewater, gained ~36 psi of strength each month. However, weekly acid attack caused the concrete to lose ~33 psi/month, for a total difference in sample strength of ~69 psi/month between expected strength and strength in the acid-degraded sample. LP followed similar trends, with a strength gain of ~33 psi/month in limewater and a loss of ~24 psi/month when in acid. No strength loss was observed for FAF in acid and it had the highest rate of strength gain of any concrete mix in limewater or acid (~68 psi/month in limewater and ~20 psi/month in acid). FAC, on the other hand, had a low magnitude of strength gain in limewater at ~9 psi/month and a strength loss in acid of ~1 psi/month. Instead of gaining strength in limewater, zeolite lost ~26 psi/month and lost ~47 psi/month in acid. FGD also lost strength in limewater and acid, but at smaller magnitudes of ~7 and ~22 psi/month, respectively.

All concrete mixes besides FGD showed increasing differences of strength between acid and limewater-soaked cubes in the latter part of testing. While no concrete failed under acid attack, these differences in strength suggest the time of experimentation was great enough to begin to show degradation. Under acid attack, fillers FAF, FAC, LP, and FGD did not lose strength as fast as OPC. However, OPC was the strongest concrete mix from 0 to 6 months, and if less than a 1-year service period is desired, OPC is likely to be the strongest concrete. Over longer periods fillers like FAF and FAC may retain strength more effectively. Estimates of concrete durability calculated that FAF would not lose strength due to its positive strength gain in acid, and FAC would last nearly a decade given its modest loss of strength over time. Concrete mixes with Zeo and FGD gained no significant strength even when soaked in limewater, and were the weakest fillers tested by a significant margin.

## 1.4 Discussion

Surface adsorption is a well-studied mechanism of metal removal, but results herein paint a nebulous picture of whether adsorption played a major role in removal of metals from solution. Precipitation due to pH increases appeared to control ion removal in most of the systems tracked in this study, and leaching of metals made it difficult to identify the occurrence of adsorption behavior in low pH ranges prior to known ion precipitation pH ranges. The exception occurred in the synthetic AMD solution where Mn removal was much higher when exposed to the OPC concrete than the control, suggesting adsorption played a role in removal. However, similar behavior was not

observed in the non-OPC concrete mixtures. More work on pervious concrete/AMD mixtures is needed to confirm adsorption as a Mn removal mechanism.

Al and Fe single-ion solutions had the same treatment times using OPC, but Fe required a higher pH range to precipitate. This disparity is attributed to the concrete's rapid ability to raise pH to a level to incite precipitation within the first 15 minutes of exposure. Cu precipitated in a similar pH range as Fe but underwent a much longer precipitation process (~6 hours as opposed to 3 hours for >95% removal). All filler concrete mixtures removed Fe consistently, and all mixtures should work similarly for field treatment of dissolved Fe. Copper, on the other hand, was treated at a lower pH using the LP concrete mixture, but at a significantly slower rate. As time may be the most important factor in treatment, LP may be not be preferable over other types of concrete mixtures.

Mn removal was impeded by the use of concrete in natural AMD compared to the pH-controlled solution. When compared to a synthetic mix, natural AMD had elevated pH ranges of precipitation for Al and Mn, but Al (like Fe) still had similar removal time during interaction with pervious concrete. Precipitation of Mn occurs in the range where Al will redissolve into solution, and can create a potential conflict in removal of both ions. However, Al in natural AMD was less likely to redissolve compared to synthetic Al solutions, indicating this may be less of a concern in natural systems.

Regarding the impact of filler materials on the performance of the pervious concrete filter systems, fly ash containing concrete mixtures (FAF and FAC) behaved similarly in metal treatment and pH neutralization. FAF was more durable than FAC and

was the only concrete mix to not only retain, but gain strength in acidic conditions, suggesting it may be durable in a long-term AMD treatment system. Little difference between OPC and fly ash was observed in metal removal testing, with fly ashes showing a slight advantage in single-ion Mn removal but having worse performance against Mn in synthetic AMD.

Limestone powder used in a 25% replacement of OPC cement lowered the precipitation ranges of single-ion Al, Fe, and Cu, as well as Al in a synthetic AMD solution. It is known that upon dissolution in acidic conditions, the carbonate ($CO_3^{2-}$) ions that make up the calcium carbonate (limestone) mineral are released into solution (Pickering, 1983). Natural dissolution of calcite may remove metals through formation of metal carbonates in place of hydroxide ions (which would result in increased pH), resulting in lower pH precipitation ranges associated with the use of the LP mixture (Chen et al., 2018). Al removal dynamics were faster compared to other filler mixtures, but delayed Cu removal. LP concrete was also the slowest and removed the least Al and Mn in natural AMD. The LP mixture concrete had lower strength than the OPC and fly ash mixes, but has been found in other studies to improve concrete strength when added in smaller dosages than the 25% replacement used herein (Wang et. al., 2018). Limestone powder showed potential if metal removal is desired at lower pH, but is otherwise not recommended to treat a natural AMD system when alternative mixture formulations are available.

Natural zeolite has been shown to add strength to concrete (Burris and Juenger, 2016, Liu and Li, 2020). However, the 25% replacement used in this experimentation

created the second weakest concrete, that lost strength when exposed to acid solutions. The Zeo concrete raised pH similarly to OPC, but strength and durability considerations suggest a lower proportion of Zeo in the mix design will benefit future use of the material in concrete.

FGD was the weakest filler tested in this experimentation. Previous research (Khatib et. al. 2015) recommends no more than 10-15% replacement of OPC with FGD, with higher ratios leading to significant strength loss. Unspent sorbent in FGD, such as lime, treated acid significantly faster than other ions. If concrete strength and longevity is not prioritized in a natural system, FGD may be an effective filler, capable of quickly raising solution pH and precipitating dissolved metals from solution.

A concern of determining longevity of PRBs is potential pore-space clogging due to metal precipitation. No conclusions could be drawn from this experimentation, as runs 2 and 3 of concrete exposure testing behaved similarly and only 1L of AMD was tested on each column.

Translating lab-scale results to predicted field requirements is important to understand practical aspects of PRB implementation. Based on the relationship between treatment time and length of a theoretical PRB made of OPC pervious concrete, if >95% removal is desired for highly concentrated Al or Fe, a PRB length of at least 4 meters long is recommended, with 8 meters desirable for Cu treatment. PRBs to treat ~50% of each ion and fully account for potential leaching should be at least 1 meter in length (2m for Cu). The length of PRB required to treat Mn was not determined through this experimentation, as pH ranges did not reach levels to precipitate Mn in exposure tests and column tests

experienced little removal. It seems field treatment of Mn using pervious concrete-based PRBs may be impractical.

## 1.5 Conclusion

This experiment focused on the removal of dissolved metals from single-ion as well as synthetic and natural multi-ion AMD mixtures by pervious concrete composed of four concrete mixes utilizing portland cement, class C and F fly ash, and limestone powder. Column tests were conducted to correlate exposure time and required PRB length with ion removal. Long-term acid neutralization and durability tests tracked changes in concrete strength over approximately a year of acid exposure. Major findings are as follows:

- Aluminum was treated by precipitation in all solutions and with all concrete mixes at pH ranges of 4.0-5.5.
- Mn was not able to be effectively treated in single-ion or natural AMD solutions using pervious concrete, suggesting different methods must be used to target Mn removal.
- Fe and Cu were treated by precipitation in pH ranges of 5.5 to 6.5 when exposed to the pervious concrete.
- 3 hours of contact time is recommended to treat Al and Fe, with 6 hours needed for Cu removal. Greater than 24 hours is required for Mn treatment, resulting in an unreasonably long PRB at field scale.

- Permeable reactive barriers made of pervious concrete should be 4-8 meters long to effectively remove dissolved Al, Fe, and Cu from solution. Reduced functionality will be observed in barriers less than 1 meter long.
- Fly ash concrete mixtures behaved similar to OPC concrete with regards to filtration and pH neutralization potential. Limestone powder lowered pH precipitation ranges compared to other fillers but also slowed reaction time in some metal systems.
- The ability to neutralize pH over year-long acid exposure was confirmed, although effectiveness decreased slightly with time.
- Strength of pervious concrete under a year of acid attack was generally maintained. The OPC concrete mixture generated the highest compressive strength. The FAF concrete mixture continued to gain strength throughout the 12-month testing period, even when exposed to acid, suggesting good long-term durability of this mixture.

References

Ahmaruzzaman, M. (2010). A review on the utilization of fly ash. Progress in Energy and Combustion Science, 36(3), 327–363.

Beulah, M., & Prahallada, M. C. (2012). Effect of replacement of cement by metakalion on the properties of high performance concrete subjected to hydrochloric acid attack. *International Journal of Engineering Research and Applications*, 2(6), 033-038.

Bullard, J. W., Jennings, H. M., Livingston, R. A., Nonat, A., Scherer, G. W., Schweitzer, J. S., Scrivener, K. L., & Thomas, J. J. (2011). Mechanisms of cement hydration. Cement and Concrete Research, 41(12), 1208–1223.

Burris, Lisa E., and Maria CG Juenger. "Milling as a pretreatment method for increasing the reactivity of natural zeolites for use as supplementary cementitious materials." Cement and Concrete Composites 65 (2016): 163-170.

Chen, Q., Yao, Y., Li, X., Lu, J., Zhou, J., & Huang, Z. (2018). Comparison of heavy metal removals from aqueous solutions by chemical precipitation and characteristics of precipitates. *Journal of Water Process Engineering*, 26 (October), 289–300.

Crittenden, J. C., Trussell, R. R., Hand, D. W., Howe, K. J., & Tchobanoglous, G. (2012). *MWH's water treatment: principles and design*. John Wiley & Sons.

Czuma, N., Baran, P., Franus, W., Zabierowski, P., & Zarębska, K. (2019). Synthesis of zeolites from fly ash with the use of modified two-step hydrothermal method and preliminary SO 2 sorption tests. *Adsorption Science and Technology*, 37(1–2), 61–76.

de Repentigny, C., Courcelles, B., & Zagury, G. J. (2018). Spent MgO-carbon refractory bricks as a material for permeable reactive barriers to treat a nickel- and cobalt-contaminated groundwater. *Environmental Science and Pollution Research*, 25(23), 23205–23214.

Ekolu, S. O., Azene, F. Z., & Diop, S. (2014, July). A concrete reactive barrier for acid mine drainage treatment. In *Proceedings of the Institution of Civil Engineers-Water Management* (Vol. 167, No. 7, pp. 373-380). Thomas Telford Ltd.

Ekolu, S. O., & Bitandi, L. K. (2018). Prediction of Longevities of ZVI and Pervious Concrete Reactive Barriers Using the Transport Simulation Model. *Journal of Environmental Engineering*, 144(9), 04018074.

Fajardo, V., Brown, B., Young, D., & Nešić, S. (2013). Study of the solubility of iron carbonate in the presence of acetic acid using an EQCM. *NACE - International Corrosion Conference Series*, 2452, 1–20.

Gavaskar, A. R. (1999). Design and construction techniques for permeable reactive barriers. *Journal of Hazardous Materials*, 68(1–2), 41–71.

Gustafsson J (2011) Visual MINTEQ ver. 3.0 KTH Department ofLand andWater Resources Engineering, Stockholm, Sweden Based on de Allison JD, Brown DS, Novo-Gradac KJ, MINTEQA2 ver 4, 1991

Gutberlet, T., Hilbig, H., & Beddoe, R. E. (2015). Acid attack on hydrated cement - Effect of mineral acids on the degradation process. *Cement and Concrete Research*, 74, 35–43.

Hale, B., Evans, L., & Lambert, R. (2012). Effects of cement or lime on Cd, Co, Cu, Ni, Pb, Sb and Zn mobility in field-contaminated and aged soils. *Journal of Hazardous Materials*, 199–200, 119–127.

Haselbach, L., Poor, C., & Tilson, J. (2014). Dissolved zinc and copper retention from stormwater runoff in ordinary portland cement pervious concrete. *Construction and Building Materials*, 53, 652–657.

Holmes, R. R., Hart, M. L., & Kevern, J. T. (2017). Enhancing the Ability of Pervious Concrete to Remove Heavy Metals from Stormwater. Journal of Sustainable Water in the Built Environment, 3(2), 04017004.

Holmes, R. R., Hart, M. L., & Kevern, J. T. (2017). Heavy metal removal capacity of individual components of permeable reactive concrete. Journal of Contaminant Hydrology, 196, 52–61.

Holmes, R. R., Hart, M. L., & Kevern, J. T. (2018). Removal and Breakthrough of Lead, Cadmium, and Zinc in Permeable Reactive Concrete. *Environmental Engineering Science*, 35(5), 408–419.

Johnson, D. B., & Hallberg, K. B. (2005). Acid mine drainage remediation options: A review. *Science of the Total Environment*, 338(1-2 SPEC. ISS.), 3–14.

Khatib, J. M., Mangat, P. S., & Wright, L. (2016). Mechanical and physical properties of concrete containing FGD waste. *Magazine of concrete Research*, 68(11), 550-560.

Knox, A. S., Paller, M. H., & Dixon, K. L. (2012). A Permeable Active Amendment Concrete (PAAC) for Contaminant Remediation and Erosion Control (ER-2134). June, 1–116.

Larsson, M., Nosrati, A., Kaur, S., Wagner, J., Baus, U., & Nydén, M. (2018). Copper removal from acid mine drainage-polluted water using glutaraldehyde-polyethyleneimine modified diatomaceous earth particles. *Heliyon*, 4(2), e00520.

Li, W., Ni, P., & Yi, Y. (2019). Comparison of reactive magnesia, quick lime, and ordinary Portland cement for stabilization/solidification of heavy metal-contaminated soils. *Science of the Total Environment*, 671, 741–753.

Li, Y., Xu, Z., Ma, H., & Hursthouse, A. S. (2019). Removal of Manganese(II) from Acid Mine Wastewater: A Review of the Challenges and Opportunities with Special Emphasis on Mn-Oxidizing Bacteria and Microalgae. *Water* **2019**, 11, 2493.

Liu, J., & Li, Y. (2020). Runoff purification effects of permeable concrete modified by diatomite and zeolite powder. *Advances in Materials Science and Engineering*, *2020*.

Marchon, D., & Flatt, R. J. (2016). Mechanisms of cement hydration. In *Science and Technology of Concrete Admixtures*. Elsevier Ltd.

Monhemius, A. J. (1977). Precipitation Diagrams for Metal Hydroxides, Sulphides, Arsenates and Phosphates. *Transactions of the Institution of Mining and Metallurgy, Section C: Mineral Processing and Extractive Metallurgy*, 86 (December 1977).

Muthu, M., Chandrasekharapuram Ramakrishnan, K., Santhanam, M., Rangarajan, M., & Kumar, M. (2019). Heavy Metal Removal and Leaching from Pervious Concrete Filter: Influence of Operating Water Head and Reduced Graphene Oxide Addition. *Journal of Environmental Engineering*, 145(9), 04019049.

Naidu, G., Ryu, S., Thiruvenkatachari, R., Choi, Y., Jeong, S., & Vigneswaran, S. (2019). A critical review on remediation, reuse, and resource recovery from acid mine drainage. *Environmental Pollution*, 247, 1110–1124.

Ok, Y. S., Yang, J. E., Zhang, Y. S., Kim, S. J., & Chung, D. Y. (2007). Heavy metal adsorption by a formulated zeolite-Portland cement mixture. *Journal of Hazardous Materials*, 147(1–2), 91–96.

Ong, S. K., Wang, K., Ling, Y., & Shi, G. (2016). Pervious Concrete Physical Characteristics and Effectiveness in Stormwater Pollution Reduction. April, 57.

O'Reilly, K. M. (2020). Investigating the Impacts of Acid Mine Drainage on Ecosystem Functioning Using a Leaf Litter Decomposition Analysis [Unpublished Undergraduate Thesis] The Ohio State University

Pernicová, R. (2014). Analysis of Formation and Testing of Efflorescence on Concrete Elements. Advanced Materials Research, 1025–1026, 641–644.

Pickering, W. F. (1983). Extraction of copper, lead, zinc or cadmium ions sorbed on calcium carbonate. *Water, Air, and Soil Pollution*, 20(3), 299-309.

Saboo, N., Shivhare, S., Kori, K. K., & Chandrappa, A. K. (2019). Effect of fly ash and metakaolin on pervious concrete properties. *Construction and Building Materials*, 223, 322–328.

Scrivener, K., Ouzia, A., Juilland, P., & Kunhi Mohamed, A. (2019). Advances in understanding cement hydration mechanisms. *Cement and Concrete Research*, 124(June), 105823.

Sdiri, A., & Bouaziz, S. (2014). Re-evaluation of several heavy metals removal by natural limestones. *Frontiers of Chemical Science and Engineering*, 8(4), 418–432.

Sdiri, A., Higashi, T., Jamoussi, F., & Bouaziz, S. (2012). Effects of impurities on the removal of heavy metals by natural limestones in aqueous systems. *Journal of Environmental Management*, 93(1), 245–253.

Senhadji, Y., Escadeillas, G., Mouli, M., Khelafi, H., & Benosman. (2014). Influence of natural pozzolan, silica fume and limestone fine on strength, acid resistance and microstructure of mortar. *Powder Technology*, 254, 314–323.

Shabalala, A. (2020). Efficacies of Pervious Concrete and Zero-Valent Iron as Reactive Media for Treating Acid Mine Drainage. *Mine Water Solutions, 14th IMWA Congress, Christchuch, New Zealand (9-13 November 2020)*, 83–87.

Shabalala, A. N., & Ekolu, S. O. (2019). Quality of water recovered by treating acid mine drainage using pervious concrete adsorbent. *Water SA*, 45(4), 638–647.

Shabalala, A. N., Ekolu, S. O., & Diop, S. (2014). Permeable reactive barriers for acid mine drainage treatment: a review. *Construction Materials and Structures*, 1416–1426.

Shively, W., Bishop, P., Gress, D., & Brown, T. (1986). Leaching tests of heavy metals stabilized with Portland cement. *Journal of the Water Pollution Control Federation*, 58(3), 234–241.

Skousen, G., Ziemkiewicz, P. F., & Mcdonald, L. M. (2019). The Extractive Industries and Society Acid mine drainage formation , control and treatment : Approaches and strategies. 6(October 2018), 241–249.

Skousen, J., Zipper, C. E., Rose, A., Ziemkiewicz, P. F., Nairn, R., McDonald, L. M., & Kleinmann, R. L. (2017). Review of Passive Systems for Acid Mine Drainage Treatment. In *Mine Water and the Environment* (Vol. 36, Issue 1, pp. 133–153). Springer Verlag.

Stanley, H. (2020). *The Role of Beaver Ponds in Aquatic Ecosystems Impacted by Acid Mine Drainage* [Unpublished Honors Undergraduate Thesis] The Ohio State University

Stehouwer, R. C., Sutton, P., Fowler, R. K., & Dick, W. A. (1995). *Minespoil amendment with dry flue gas desulfurization by-products: Element solubility and mobility* (Vol. 24, No. 1, pp. 165-174). American Society of Agronomy, Crop Science Society of America, and Soil Science Society of America.

Tasić, Ž. Z., Bogdanović, G. D., & Antonijević, M. M. (2019). Application of natural zeolite in wastewater treatment: A review. *Journal of Mining and Metallurgy A: Mining*, 55(1), 67–79.

Tennis, P. D., & Jennings, H. M. (2000). Model for two types of calcium silicate hydrate in the microstructure of Portland cement pastes. *Cement and Concrete Research*, 30(6), 855–863.

Teymouri, E., Mousavi, S. F., Karami, H., Farzin, S., & Hosseini Kheirabad, M. (2020). Municipal Wastewater pretreatment using porous concrete containing fine-grained mineral adsorbents. Journal of Water Process Engineering, 36(May), 101346.

Thisani, S. K., Kallon, D. V. Von, & Byrne, P. (2021). Effects of contact time and flow configuration on the acid mine drainage remediation capabilities of pervious concrete. *Sustainability (Switzerland)*, 13(19).

Thornton, I. (1996). Impacts of mining on the environment; some local, regional and global issues. *Applied Geochemistry*, 11(1–2), 355–361.

Tremblay, G.A., Hogan, C.M.: Mine Environment Neutral Drainage (MEND) Manual 5.4.2d: Prevention and Control. Canada Centre for Mineral and Energy Technology, Natural Resources Canada, Ottawa, 2001.

Uma Maguesvari, M., & Sundararajan, T. (2017). Influence of fly ash and fine aggregates on the characteristics of pervious concrete. *International Journal of Applied Engineering Research*, 12(8), 1598–1609.

USEPA. 2009. National Recommended water Quality Criteria, Office of Water, Office of Science and Technology (4304T), Washington, DC.

Wang, D., Shi, C., Farzadnia, N., Shi, Z., & Jia, H. (2018). A review on effects of limestone powder on the properties of concrete. *Construction and Building Materials*, 192, 153–166.

Watters, G. T., Menker, T., & O'Dee, S. H. (2005). A comparison of terrestrial snail faunas between strip-mined land and relatively undisturbed land in Ohio, USA - An evaluation of recovery potential and changing faunal assemblages. *Biological Conservation*, 126(2), 166–174.

Wright, L., & Khatib, J. M. (2016). Sustainability of desulphurised (FGD) waste in construction. In *Sustainability of Construction Materials* (Second Edi). Elsevier Ltd.

# Chapter 2. Unraveling Drivers of Harmful Algal Blooms: The Effects of Land Use and Green Infrastructure Implementation on Urban Runoff Nitrogen:Phosphorus Ratio

## 2.0 Abstract

Lakes and rivers represent tremendous assets in the state of Ohio, as they are used for recreation, tourism, drinking water sources, commerce, and to support fisheries. Upland areas, including agricultural and urban lands, result in substantial pollution discharge to surface waters during runoff events, including nutrients from fertilizer, manure, and other sources. One negative consequence of nutrients in runoff is harmful algal blooms (HABs), which may contain various toxins and utilize dissolved oxygen in the water, causing fish kills to occur. The strength and scope of HABs is related to the nitrogen to phosphorus (N:P) ratio in runoff. Little is known about how urban land use and the presence or absence of stormwater control measures (SCMs) impacts the N:P ratio in stormwater. Two data sets were utilized to unpack these questions: (1) a land use and stormwater quality data set developed through field monitoring in the Dayton metropolitan area, and (2) the Blueprint Columbus data set which focused on green infrastructure in several watersheds in the Clintonville neighborhood of Columbus, Ohio. Multi-family residential, commercial, and light industrial land uses had the largest (>25) TN:TP ratios, suggesting their runoff contributes to more toxic variations of algal blooms

and that SCM retrofits in these watersheds should focus on N removal. Single-family residential, low-density residential, and heavy industrial had the most balanced TN:TP ratios, so runoff reduction to reduce overall nutrient load should be the focus of SCM retrofits in these watersheds. No significant changes to TN:TP ratio were observed after green infrastructure implementation or other infrastructure improvements (e.g., sanitary sewer lateral lining, downspout disconnection, and sump pump installation) in Columbus watersheds. As watersheds that received infrastructure retrofits were all single-family residential, no significant impact on N:P is not a negative result, suggesting retrofitted infrastructure removes N and P in a balanced manner.

## 2.1 Introduction

Population growth and urbanization in recent decades have resulted in unintended consequences that must be carefully addressed. The water cycle is modified by increases in imperviousness and soil compaction in urban areas, leading to subsequent increases in stormwater runoff volume and peak flow rate. High frequency, flashy storm events cause accelerated erosion of the stream bed and banks and convey pollution to receiving waters (Finkenbine et. al., 2000). Sediments that result from increased erosion can harm wildlife, smother habitat, and reduce light penetration which prohibits growth of producers like plants (Marshall et. al., 2010, Correll 1998, Gobler et. al., 2016).

A further concern related to urbanization is the conveyance of more dissolved and sediment-bound pollutants from the watershed relative to pre-development. The transport of nitrogen, phosphorus, heavy metals, and various other organic and inorganic pollutants

is greatly exacerbated in runoff from developed lands (Fletcher et. al., 2013, Walsh et. al., 2005). This degradation in runoff quality can take place in any land use, as evidenced by the decades-long attention to nitrogen and phosphorus from agriculturally dominated watersheds (Reutter et al., 2011). Land use is a critical factor to consider when managing stormwater runoff as it drives runoff generation and determines inputs of pollutants with sources as varied as lawn fertilizers, galvanized materials, and hydrocarbons (Line et. al., 2002, Simpson et. al., 2022)

Since urban runoff is more polluted than undeveloped land (Tong et. al., 2018), pollutant treatment must be applied in urban areas to protect receiving waters. A widely accepted benchmark of stormwater management is the design philosophy of low impact development, with the goal of returning urban runoff quality and volume to predevelopment levels (Lee et. al., 2012). Most regions in the Midwestern and Eastern United States were once covered in deciduous forest. Modern forests and undeveloped land provide a comparison to historic conditions and are a model for attempting to design urban development to match natural conditions. Stormwater runoff quality and quantity from forests was compared to developed land use types in Simpson (2022) and further analyzed to quantify the impact urban land uses have compared to predevelopment conditions.

One direct method to address the growing problem of urban stormwater is known as green stormwater infrastructure (GSI). The role of GSI can vary from treatment of different contaminants, peak flow reduction, volume reduction/retention, etc. One common form of GSI is a bioretention cell, which captures runoff at its source and filters

it using highly permeable, engineered soil blends. These soils and an underdrain allow the design storm to be treated and slowly released at rates comparable to nonurban interflow (Debusk et al. 2011), preventing erosion and downstream infrastructure damage. Pollutant removal processes include adsorption, oxidation/reduction interactions, filtration, and biodegradation through microbial activity (Tirpak et. al., 2021). Bioretention systems include vegetation to enhance pollutant removal, as plants roots harbor microbes that encourage nutrient cycling and break down hydrocarbons (Diblasi et. al., 2008). Phytoremediation, the treatment of contamination through plant uptake, is also an important factor in bioretention cell function (Tirpak et. al., 2021).

Permeable pavement is another commonly utilized GSI technique which allows rainfall to infiltrate the pavement surface where it can be stored in an underlying open-graded aggregate reservoir. Although lacking plants, permeable pavement filters suspended solids and retains them in pore spaces, and metals are precipitated or adsorbed to concrete, asphalt, or underlying aggregate (Ong et. al., 2016, Holmes et. al., 2017). Organic pollutants such as nutrients and hydrocarbons can be captured long enough to biodegrade under biological activity (Ong et. al., 2016; Braswell et al. 2018). Through exfiltration and (relatively minor) evaporation of runoff, permeable pavement is part of the GSI toolbox to support low impact development goals (Kuruppu et. al., 2019).

While many pollutants are transported by stormwater, nutrient treatment by GSI is of particular interest in Ohio given regional algal bloom challenges. New bioretention cells have proven unreliable in reducing concentrations of nitrogen and phosphorus, likely due to leaching from media blends which are often amended with compost (Tirpak

et. al., 2021). Johnson and Hunt (2019) compared nitrogen and phosphorus treatment data from a bioretention cell after installation (2003-2004) to 17 years later (2017-2018) in the same cell. When the bioretention cell was new, total nitrogen (TN) and total phosphorus (TP) concentrations increased between the inlet and outlet of the cell, but overall load (or mass) of the nutrients was reduced due to the reduction of runoff volume. After 17 years of plant growth and soil evolution, the bioretention cell provided reductions of both TN and TP concentrations and load. Plant/microbial activity and the resulting organic carbon incorporated into the soil likely contributed to the removal and transformation of nitrogen, while phosphorus was treated by organismal uptake and sorption by the soils.

Nitrogen and phosphorus are crucial nutrients for life, but a side-effect of urban development is the excessive release of these nutrients through fertilizer use, pet waste, and atmospheric deposition (Hobbie et. al., 2017). Rural and agricultural sources include animal waste, agricultural fertilizers, confined animal feeding operations, and aquaculture wastewater (Glibert and Burkholder, 2011). Long linked with lake and ocean eutrophication, nitrogen and phosphorus management is necessary to decrease the prevalence and severity of harmful algal blooms (Bade et. al., 2009, Gobler et. al., 2016, Yindong et. al., 2021).

Harmful algal blooms (HABs) are a major economic and environmental concern for regions relying on large bodies of water for recreation, drinking water, or aesthetic appeal (Reutter et. al., 2011). Caused by increased eutrophication due to anthropogenic inputs of nutrients, HABs increase the biological oxygen demand (BOD) of the water, suffocating plant and animal life. HABs also produce odors and clog beaches with green,

red, or blue masses of scum. Of notable concern is the propensity of HABs such as microcystins to produce various toxins (Chaffin et. al., 2014). These toxins can endanger wildlife, poison swimmers or pets, or contaminate a local water supply (e.g., Toledo, Ohio in 2014; Barnard et. al., 2021).

Phosphorus retention is the focus of freshwater HAB reduction strategies (Reutter et. al., 2011). Phosphorus cannot be fixed or deposited from air as nitrogen can, and less overall phosphorus is utilized by algae. The lower phosphorus needs of HABs is supported by the Redfield ratio (Glibert and Burkholder, 2011), which is a widely accepted proportion of carbon, nitrogen, and phosphorus in marine phytoplankton biomass. Expressed as 106:16:1, this molar ratio of C:N:P is representative of the standard conditions of algal growth. Phosphorus was also shown to be the limiting nutrient for HAB growth in fresh waters in multiple early studies (Chiaundani and Vigh, 1974, Correll, 1998). HABs can still occur even in low-P environments due to the presence of cyanobacteria with adaptations to such environments (May et. al., 2010, Gobler et. al., 2016).

Nitrogen is credited as the limiting nutrient in marine HAB growth (Correll, 1998), but is often overlooked in watersheds draining to freshwaters. As nitrogen-fixing bacteria are historically credited as the species most likely to form HABs (Barnard et. al., 2021), it is often assumed reducing nitrogen load is a frivolous effort in freshwaters due to the utilization of atmospheric N. However, many species that produce acutely toxic blooms cannot fix atmospheric nitrogen, and rather require large inputs of N to produce toxins (Gobler et. al., 2016, Barnard et. al., 2021, Tong et. al., 2020). *Microcystis* and

other toxigenic cyanobacteria have multiple adaptations to protect against low P conditions, including vertical migration within the water column to access different nutrient content, rapid absorption of P as availability decreases, and the ability to digest and convert organic phosphate sources that are unavailable to most organisms (Gobler et. al., 2016). Studies have also confirmed the availability of nitrogen directly influences the amount of toxin produced by cyanobacteria (Gobler et. al., 2016). Thus, the traditional wisdom of limiting phosphorus in watersheds without concurrent nitrogen management strategies has the potential to exacerbate the presence and noxiousness of toxigenic blooms.

Seasonal fluctuations in nitrogen and phosphorus concentrations impact eutrophication of local waters, which can alter HAB timing and potency (Gobler et. al., 2016). Smith et. al. (2020) found that TN concentrations from urban watersheds in Columbus, Ohio, were significantly higher in spring and TP concentrations significantly higher in spring and fall. Yindong et. al. (2021) recommends a seasonal-specific nutrient management program, with N reductions in the spring and P reductions in summer. Nutrient loading to lakes is particularly important in late winter and spring as this tends to stoke summer algal blooms (Chaffin et. al., 2013).

The ratio of TN:TP in urban runoff is not widely considered in the larger context of HAB management or SCM design. Chaffin et. al. (2014) details the N:P ratio of waters in the Maumee Bay, a major nutrient contributor to western Lake Erie's HABs. Samples were taken at the mouth of the Maumee bay with N- and P-enriched bioassays conducted to determine N and P limited growth concentrations. While a statistically significant

value for P-replete growth was not found, the TN:TP value of 31.58 was determined as the threshold for N-replete growth. Above a TN:TP value of 31.58, no increase of nitrogen led to further algal growth relative to a control, while values below led to higher growth in a bioassay enriched by N.

Given the trends detailed above, recommendations can be deduced in managing ideal N:P for HAB growth. High P values encourage nitrogen-fixing cyanobacteria and a much greater potential for HAB biomass, as predicted by a low TN:TP ratio. High N values encourage cyanobacteria species of greater toxicity like *Microcystin*, as they have specific adaptations to low P environments and require high N inputs to produce toxins. At a TN:TP ratio of 31.58, HAB growth is no longer N-limited, and ratios should not approach this value to avoid more toxic blooms. A balanced TN:TP ratio, mirroring the Redfield ratio of 16:1, is hypothesized to cause more predictable and mild algal blooms (e.g., in concert with strategies that reduce overall nutrient load). However, TN:TP ratio cannot alone predict the potential for HAB growth as it does not consider overall pollutant mass.

It is critical to consider urban TN:TP ratio in stormwater runoff from different land uses to determine primary urban causes of nutrient imbalance which contribute to HABs. Furthermore, identifying 'hot spot' land uses can help to target management of nutrients in urban stormwater. In this study, data from the Dayton and Columbus, Ohio regions were utilized to determine N:P ratios in runoff from watersheds with distinct land uses. Furthermore, three of the watersheds in Columbus were retrofitted with GSI and additional infrastructure to control stormwater. The effects of neighborhood scale GSI

impacts on TN:TP ratio were analyzed in support of watershed-scale efforts to control algal blooms in freshwater systems.

## 2.2 Methods

### 2.2.1 Watershed Descriptions and SCM Implementation

For this study, pollutant concentration and load data were acquired from previous research located in the Dayton and Columbus regions to support the evaluation of TN:TP ratio as a function of land use. Thirteen urban watersheds in the Dayton metropolitan area and two forested watersheds in Battelle-Darby Creek Metropark (Franklin County, Ohio) were monitored for stormwater hydrology and water quality by Dr. Ian Simpson (Simpson 2022; Table 5). This monitoring occurred in phases, resulting in at least one year of data for each watershed (Figure 24). Eight different land uses were evaluated as part of this study: light industrial (2), heavy industrial (1), single-family residential (SFR; 3), multi-family residential (MFR; 1), low-density residential (LDR; 2), commercial (3), parking lot (1), and forest (2).

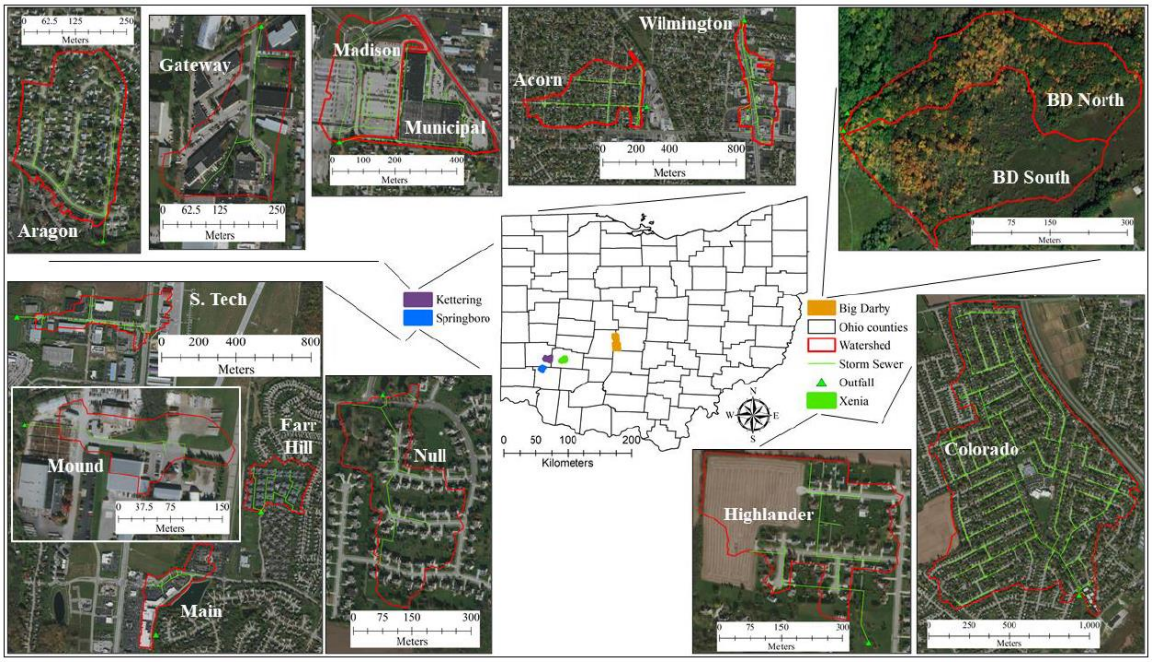


Figure 24: Watersheds monitored by Simpson (2022) in the Dayton metropolitan area and in Battelle-Darby Creek Metropark.

Six watersheds were monitored in the Clintonville neighborhood of Columbus, Ohio as part of the Blueprint Columbus project (Figure 25; Table 5). Wholistic monitoring began in 2016 to evaluate the impacts of GSI on stormwater runoff quantity and quality, ecosystem services, public health, property values, and neighborhood desirability. As described in Smith et. al. (in review), all six watersheds (Beechwold, Blenheim, Cooke-Glenmont, Indian Springs, Starett, and Whetstone) are primarily SFR land use and have been monitored since 2016 for runoff quantity and quality. For the evaluation of the effects of land use on TN:TP ratio herein, data for all six watersheds were utilized.

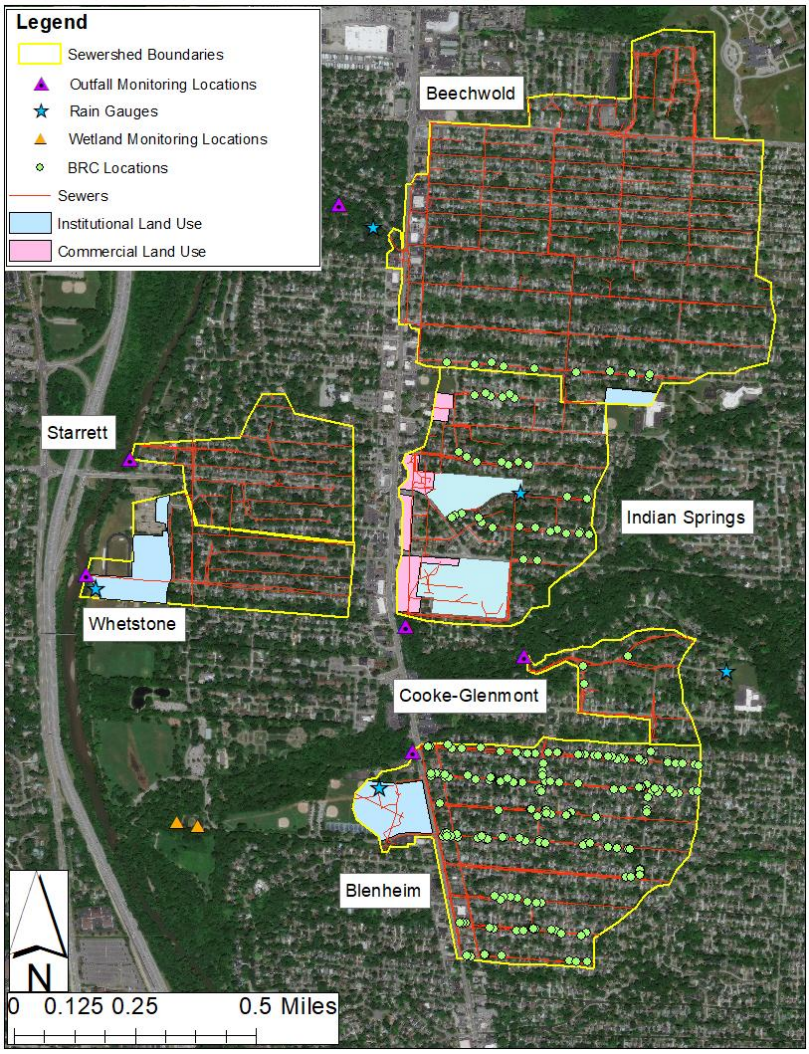


Figure 25: Watersheds monitored as part of the Blueprint Columbus project in the Clintonville neighborhood of Columbus, OH. All watersheds are primarily single-family residential land use (i.e., non-shaded areas). Stormwater control measures and monitoring locations are shown as points. Existing storm sewers are in red with watershed boundaries in yellow. Beechwold served as an experimental control while the other three watersheds were monitored before and after GSI retrofits as well as a third monitoring period where additional infrastructure implementation ($AI^2$) occurred in the watersheds. Image from Bernard et al. (2022).

Table 5: Characteristics of Dayton (top) and Columbus (bottom) watersheds. Monitoring periods did not include winter months to avoid damage to monitoring equipment caused by freezing. Some sampled events were excluded from this study if N or P data were incomplete.

| Watershed | Land Use | Area (ha) | % Impervious | Monitoring Start | Monitoring End | Sampled Events |
|---|---|---|---|---|---|---|
| Acorn | SFR | 19 | 45 | Oct 2018 | Dec 2019 | 19 |
| Aragon | SFR | 9 | 45 | Mar 2019 | Dec 2019 | 16 |
| Gateway | Light Industrial | 5 | 71 | Oct 2018 | Dec 2019 | 19 |
| Madison | Parking Lot | 9 | 70 | Mar 2019 | Dec 2019 | 18 |
| Municipal | Commercial | 7 | 78 | Mar 2019 | Dec 2019 | 16 |
| Wilmington | Commercial | 10 | 80 | Oct 2018 | Dec 2019 | 18 |
| Farr Hill | MFR | 7 | 53 | Mar 2020 | June 2021 | 24 |
| Main | Commercial | 7 | 81 | Mar 2020 | June 2021 | 16 |
| Mound | Heavy Industrial | 2 | 68 | Mar 2020 | June 2021 | 22 |
| Null | LDR | 11 | 20 | Mar 2020 | June 2021 | 15 |
| S. Tech | Light Industrial | 12 | 48 | Mar 2020 | June 2021 | 21 |
| Colorado | SFR | 154 | 38 | Mar 2020 | June 2021 | 23 |
| Highlander | LDR | 12 | 18 | Mar 2020 | June 2021 | 19 |
| BD North | Forest | 7 | 0 | May 2020 | May 2021 | 4 |
| BD South | Forest | 8 | 0.2 | May 2020 | May 2021 | 7 |
| Beechwold | SFR | 111 | 38 | June 2016 | Dec 2021 | 102 |
| Blenheim | SFR | 61 | 45 | June 2016 | Dec 2021 | 28 |
| Cooke-Glenmont | SFR | 12 | 31 | June 2016 | Dec 2021 | 65 |
| Indian Springs | SFR | 48 | 40 | June 2016 | Dec 2021 | 53 |
| Starrett | SFR | 22 | 35 | Aug 2019 | Dec 2021 | 66 |
| Whetstone | SFR | 19 | 35 | Aug 2019 | Dec 2021 | 38 |

Within the Columbus watersheds, four of the watersheds (Beechwold, Blenheim, Cooke-Glenmont, and Indian Springs) were utilized in a paired watershed analysis (Clausen and Spooner, 1993) to understand how infrastructure retrofits affected TN:TP ratio and nutrient generation in stormwater runoff. Beechwold served as an experimental

control, while the other three watersheds received first GSI retrofits (Figure 25) and subsequently sanitary sewer lateral lining, downspout disconnection, and sump pump installation (Bernard et al. 2022). Watershed monitoring followed 3 distinct phases: Pre-GSI, Post-GSI, and Post-AI$^2$. All watersheds were monitored for a period before any construction or installation of GSI occurred (i.e., the Pre-GSI phase). After construction of bioretention cells and permeable pavement was completed, data were collected during a Post-GSI period. More recently, additional infrastructure, including downspout redirection, sanitary sewer lateral linings, and sump pump installation, has been retrofitted into the treatment watersheds and the period thereafter has been designated post-all infrastructure implemented (Post-AI$^2$).

### 2.2.2 Instrumentation and Data Collection

Hydrologic and water quality data collection is described in detail in Simpson (2022), Smith et al. (in review), and Boening-Ulman et al. (2022). Briefly, manual and tipping bucket rain gauges were located within each watershed to collect hyetographs. Runoff hydrology and water quality monitoring was focused at storm sewer outfalls. Teledyne ISCO 750 area velocity sensors measured flow depth and velocity based upon the Doppler Effect. These transmitted data to ISCO 6712 autosamplers which obtained sample aliquots during wet weather on a runoff volume proportional basis. Aliquots were composited into a single sample for each monitoring location and storm event. Storm events were distinguished by a minimum 6-hour antecedent dry period and a 2.5 mm rainfall depth. Data collection procedures were the same for the watersheds in the Dayton and Columbus regions.

### 2.2.3 Laboratory Analysis

Within 24 hours of the cessation of rainfall, the monitoring sites were visited to retrieve samples. The composite bottle in the bottom of the autosampler was shaken vigorously and subsamples were immediately dispensed into laboratory bottles. These were preserved as appropriate (US EPA, 1993, US EPA, 1994, APHA et. al., 2012, Eaton et. al., 2005) and placed on ice to chill to <4°C. Dayton samples were taken to either the National Center for Water Quality Research at Heidelberg University or the City of Columbus water quality laboratory for analysis, while all Columbus samples went to the City of Columbus water quality laboratory. Samples were analyzed for various pollutants (Table 6), including nitrite ($NO_2$), nitrate ($NO_3$), total Kjeldahl nitrogen (TKN), total nitrogen (TN), orthophosphate (OP), soluble reactive phosphorus (SRP), and total phosphorus (TP).

Table 6: Sample analysis methodology, sample preservation (if applicable), and method detection limits (MDL; mg/L for nutrients and total suspended solids or µg/L for heavy metals) for all pollutants analyzed by the National Center for Water Quality Research (NCWQR) and the City of Columbus laboratories.

| | NCWQR | | City of Columbus | | |
|---|---|---|---|---|---|
| Pollutant | Laboratory Method | MDL | Laboratory Method | Preservation | MDL |
| $NO_2$ | EPA 300.1[b] | 0.012 | EPA 353.2[b] | $H_2SO_4$ | 0.018 |
| $NO_3$ | EPA 300.1[b] | 0.012 | EPA 353.2[b] | - | 0.043 |
| TKN | EPA 351.2[b] | 0.042 | EPA 351.2[b] | $H_2SO_4$ | 0.078 |
| TN | TKN + $NO_2$ + $NO_3$ | - | TKN + $NO_2$ + $NO_3$ | - | - |
| OP | EPA 365.1[b] | 0.001 | EPA 365.2[b] | - | 0.01 |
| TP | EPA 365.1[b] | 0.001 | EPA 365.2[b] | - | 0.1 |
| TSS | Standard Methods 2540D[a] | 3 | Standard Methods 2540D[a] | - | 2 |
| Cd | EPA 200.8[c] | 1 | EPA 200.8[c] | $HNO_3$ | 0.013 |
| Cr | EPA 200.8[c] | 1 | EPA 200.8[c] | $HNO_3$ | 0.36 |
| Cu | EPA 200.8[c] | 1 | EPA 200.8[c] | $HNO_3$ | 0.26 |
| Ni | EPA 200.8[c] | 1 | EPA 200.8[c] | $HNO_3$ | 0.025 |
| Pb | EPA 200.8[c] | 1 | EPA 200.8[c] | $HNO_3$ | 0.0086 |
| Zn | EPA 200.8[c] | 1 | EPA 200.8[c] | $HNO_3$ | 0.7 |

Eaton et al. (2005)[a]; USEPA (1993)[b]; USEPA (1994)[c]

### 2.2.4 Data Analysis

To calculate TN, $NO_2$, $NO_3$, and TKN concentrations were summed for each storm event. TN and TP concentrations were presented in mg/L herein to allow for comparison to other relevant studies. TN:TP ratio was calculated by direct division of both TN and TP. This value was reported as mol/mol to match most discussion of TN:TP

ratio in the literature, as well as common benchmarks like the Redfield ratio (16 moles N to 1 mole P).

Statistical analysis was either conducted using R (R Core Team, 2021) or the Real Statistics Resource Pack software (Zaiontz, 2021) in Microsoft Excel. Box and whisker plots were developed for TN:TP ratios by land use and season. Season was determined by equinoxes and solstices, with little collection of winter data resulting from freezing temperatures preventing data collection. SFR watersheds were then isolated and plotted individually to evaluate differences in TN:TP within a single land use. An exceedance probability plot comparing for TN:TP was constructed, with linear interpolation conducted to estimate what percent of storms crossed the TN:TP threshold of N-replete growth. Normality of TN:TP ratio for each land use was tested using the Shapiro-Wilk test and TN:TP ratios by land use were subsequently tested to compare TN:TP ratios of each urban land use with the Dunn test. These two statistical tests were only conducted with the Dayton watersheds. Only data from the Pre-GSI phase for the Columbus treatment watersheds was included in the resulting figures and graphs, along with all data from Columbus control, and Dayton watersheds.

Plots comparing TN, TP, and TN:TP were constructed for each phase of relevant Columbus watersheds. Median absolute differences (MAD) were calculated in lieu of standard deviation since data sets were non-parametric and these were subsequently used to inform error bars in plots. A paired-watershed approach was utilized to test for differences between watershed phases (Clausen and Spooner, 1993). Control/covariate TN:TP ratios were compared with TN:TP ratios for treatment watersheds to determine

significant differences using an analysis of covariance (ANCOVA). Pre-GSI was compared with Post-GSI and Post-$AI^2$ for each treatment watershed. Regression lines were plotted for each phase, with control and treatment values being compared for each phase and watershed. ANCOVA required matching storm events in the control (Beechwold) watershed to those in the treatment watersheds (Table 7), and as a result the table features both the number of overall events sampled and the number of events used in the ANCOVA.

Table 7: Storm events used in Columbus TN:TP analysis, sorted into phases

| | Beechwold | Blenheim | | | Cooke-Glenmont | | | Indian Springs | | |
|---|---|---|---|---|---|---|---|---|---|---|
| | Control | Pre-GSI | Post-GSI | Post-$AI^2$ | Pre-GSI | Post-GSI | Post-$AI^2$ | Pre-GSI | Post-GSI | Post-$AI^2$ |
| Overall events | 102 | 22 | 3 | 3 | 14 | 41 | 10 | 17 | 9 | 27 |
| Used in ANCOVA | - | 17 | 3 | 2 | 10 | 29 | 8 | 14 | 8 | 21 |

### 2.2.5 N:P ratio considerations

The ratio of TN:TP utilized in the analysis that follows is a useful metric insofar as general ecological health and runoff quality is concerned, but it is not all encompassing. Primarily, this metric does not consider whether TN and TP concentrations and loads are large or small in magnitude. Gobler et. al. (2016) found that low concentrations of both N and P favor non-N-fixing, low toxicity algal blooms. As eutrophication is firmly linked to HABs, very low concentrations of both N and P will reduce blooms (Barnard et. al., 2021). High concentrations of both N and P will result in

the same TN:TP ratio if both increase proportionally, but resulting HABs will be more biodiverse and potentially more toxic (Gobler et. al., 2016). The use of TN:TP ratio also does not consider the bioavailability of specific N and P forms (e.g., sediment-bound vs. aqueous phase; Glibert and Burkholder, 2011).

## 2.3 Results and Discussion

### 2.3.1 Effects of Urban Land Use on TN:TP ratio of stormwater runoff

The seasonal fluctuation of TN:TP ratio in urban runoff is presented in Figure 26, with the blue-dotted line from Chaffin et. al. (2014) representing the boundary of N-replete growth of 31.58:1 and the red-dotted line the Redfield ratio of 16:1. N-replete growth is an experimentally determined TN:TP ratio where additional N has no impact on algal growth, signifying conditions are highly favorable to toxic HAB varieties. The Redfield ratio is the canonical molar comparison of N and P in marine algal growth, benchmarking a balanced nutrient ratio that will not favor N-fixing (high P) or toxic (high N) algal blooms. Median TN:TP ratios of all storms are 19.3, 23.6, 16.9, and 20.6 for spring, summer, fall, and winter, respectively. Smith et. al. (2020) found that the Columbus watersheds analyzed had higher N and P in spring and higher P in fall. The lowest TN:TP ratios were observed in fall, matching proportionally higher seasonal P loading. Summer had the highest median TN:TP ratio among the urban watersheds. From a focus on TN:TP, N-specific removal should be prioritized in the summer to prevent more toxic blooms in that season. Across all land uses, the winter and spring (e.g., critical seasons for HAB nutrient load build-up) TN:TP ratios were modestly above the Redfield

ratio, suggesting the need to provide primarily runoff reduction but secondarily N treatment in SCMs. These medians, however, vary within specific land uses, and further management strategies must be tailored to specific land use runoff characteristics.

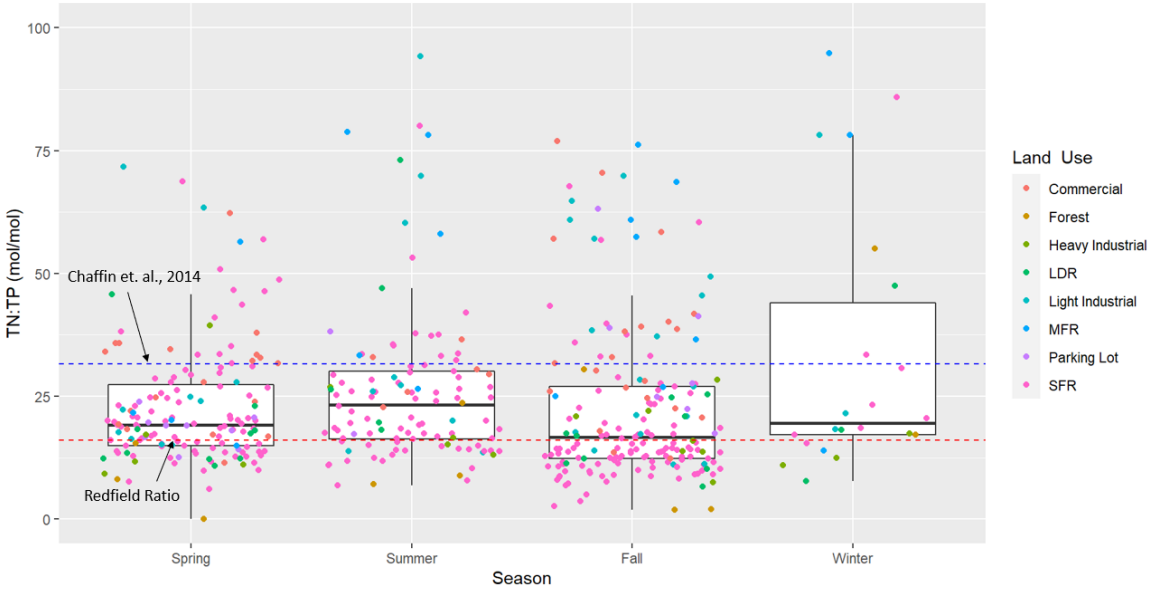


Figure 26: Comparison of seasonal TN:TP ratios for all land uses, with data points colored to match the originating land use

The comparison of TN:TP from all monitored land uses is presented in Figure 27. Several land uses presented had median values above the N-replete cut-off of 31.58, including MFR watersheds with median TN:TP ratios of 57.0, 3.5 times the Redfield ratio of 16. Commercial and light industrial land uses had high median TN:TP ratios of 31.7 and 26.0, respectively. Runoff from these land uses presents an elevated risk of developing toxic HABs compared to other urban land uses (Table 8). The forested

watersheds resulted in lower TN:TP ratios than in all urban land use types. Few runoff events were recorded from the forested watersheds due to their natural ability to abstract runoff. Runoff from the forested watersheds only occurred during 4 (BD North) and 7 (BD South) storm events due to the greater initial abstraction provided by the vegetation, soil, and lack of imperviousness (Simpson 2022). Therefore, only 4 and 7 storm events were sampled for water quality (Simpson 2022), resulting in substantially fewer data points for this land use than the other urban watersheds. Within this smaller data set, the forested watersheds typically produced runoff with elevated concentrations of TP vis-à-vis TN, which may be due to larger amounts of leaf detritus and woody vegetation contributing OP from this land use (Smith et. al., 2020). The percentage of TP as OP in runoff from the forested watersheds was 70%, compared to 29% in the urban watersheds.

Normality tests were done on TN:TP from each land use, and all but MFR were non-normal ($p<0.05$). Table 8 is a representation of Dunn tests comparing each land use in the Dayton watersheds. Land uses proven to not be similar in TN:TP runoff are colored yellow, and similar land uses are green. TN:TP ratios in SFR and heavy industrial runoff were not significantly different ($p>0.05$) than surrogates for pre-development runoff conditions (i.e., forest). These two land uses had the lowest urban median TN:TP ratios (14.82 for Dayton only SFR and 15.16 for heavy industrial), with forested watersheds producing the lowest median TN:TP ratio of 8.89. All other land uses produced runoff with significantly higher TN:TP ratios than forested conditions, suggesting nitrogen treatment should be the focus of SCM retrofit strategies for HAB control. The land use with the highest median TN:TP ratio, MFR, was significantly different from all other

land uses analyzed, suggesting special attention to management of TN:TP ratio in this land use.

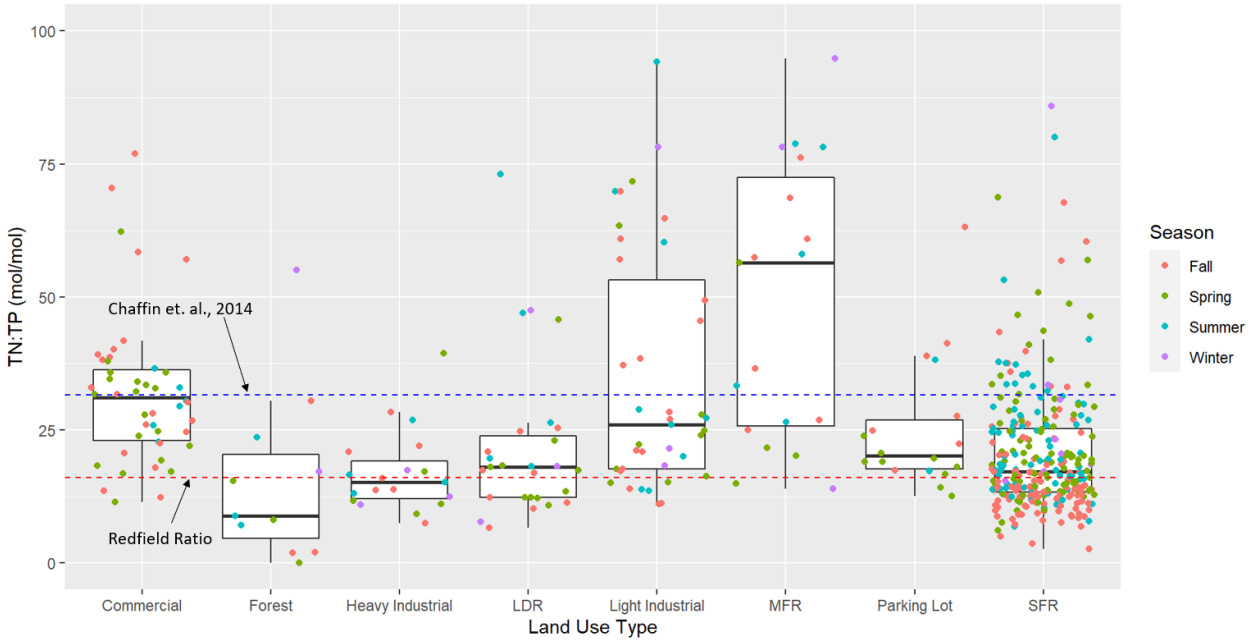


Figure 27: Comparison of TN:TP ratios for all land uses, with datapoints colored to match the season of each storm event.

Table 8: Representation of Dunn test comparisons between urban land uses. Land uses that were proven to be significantly different ($p<0.05$) are colored in yellow to represent dissimilar TN:TP ratios between them. Land uses that were not proven to have different runoff TN:TP ratios are colored green ($p>0.05$). Only Dayton data is included for SFR comparisons.

| | Commercial | Forest | Heavy Industrial | LDR | Light Industrial | MFR | Parking Lot | SFR |
|---|---|---|---|---|---|---|---|---|
| Commercial | - | - | - | - | - | - | - | - |
| Forest | 4.4E-04 | - | - | - | - | - | - | - |
| Heavy Industrial | 4.1E-06 | 0.24 | - | - | - | - | - | - |
| LDR | 7.1E-03 | 3.1E-02 | 0.11 | - | - | - | - | - |
| Light Industrial | 0.30 | 2.6E-03 | 3.0E-04 | 8.3E-02 | - | - | - | - |
| MFR | 5.3E-02 | 3.8E-04 | 2.5E-05 | 3.2E-03 | 2.6E-02 | - | - | - |
| Parking Lot | 2.0E-02 | 1.9E-02 | 5.2E-03 | 0.45 | 0.22 | 2.6E-03 | - | - |
| SFR | 1.8E-10 | 0.24 | 0.94 | 3.3E-02 | 3.3E-02 | 2.7E-07 | 7.0E-04 | - |

Of all land uses evaluated, by far the greatest number of data sets existed in the SFR land use; therefore, a deeper evaluation of TN:TP ratios was warranted (Figure 28). Median TN:TP ratios of all SFR watersheds fell beneath the Chaffin et. al. (2014) demarcation, signifying that runoff from SFR watersheds in central and west-central Ohio does not have TN concentrations that provide for unfettered growth of high N-favored HABs. Most watersheds had a median TN:TP within 5.0 of the optimal Redfield ratio, with Blenheim and Indian Springs watersheds being the exceptions (TN:TP ratios of 22.1 and 27.7, respectively). These specific watersheds produce runoff more favorable to toxic, N-loving HABs, and may require individual N-reduction infrastructure for a more balanced TN:TP ratio. Overall, SFR watersheds had a median TN:TP ratio of 17.4, close to balanced algal growth of 16:1, suggesting that runoff reduction may be the optimal goal in HAB reduction from single family residential watersheds.

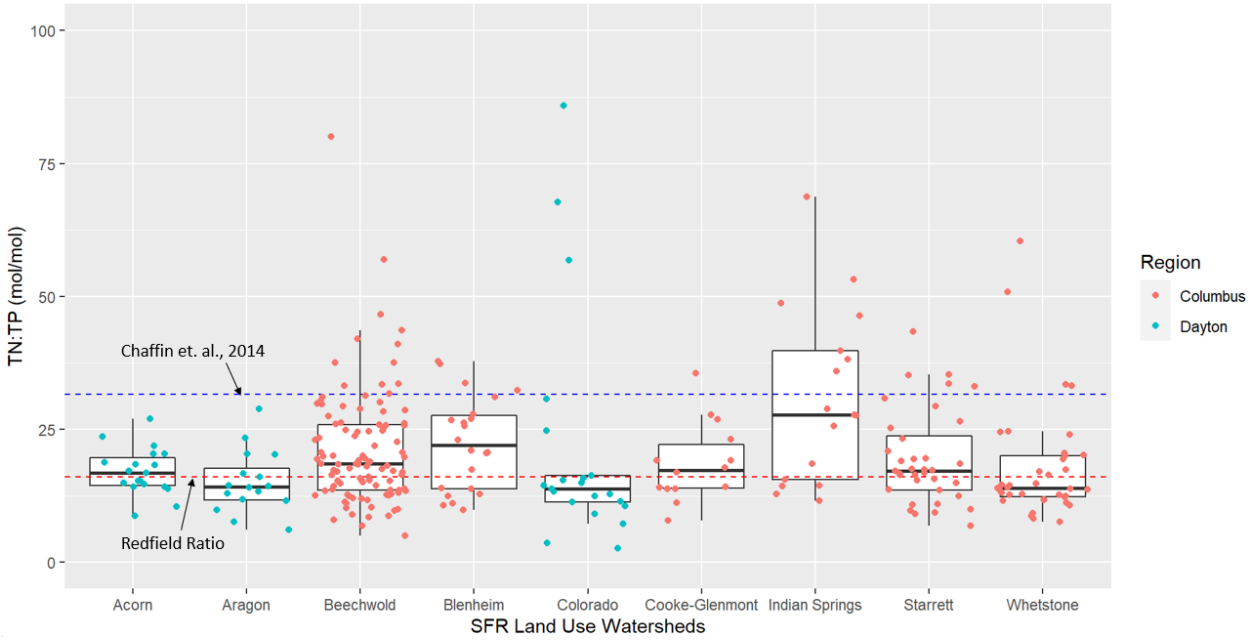


Figure 28: Comparison of TN:TP ratio of all single-family residential (SFR) neighborhoods analyzed. Red signifies watersheds in the Columbus area (Pre-GSI only) and blue represents Dayton-area SFR watersheds.

An exceedance probability plot of TN:TP ratio is presented in Figure 29 for all storm events for each land use. Commercial and MFR land uses were the most likely to produce runoff with N-replete TN:TP ratios, with 51% and 63% percent of storms exceeding this threshold. N-reduction should be a primary focus for these land uses, given their propensity to release elevated concentrations of N. Only 16% of forest runoff events reached that TN:TP ratio, but two land use types were less likely than forests to create N-replete growth conditions. SFR and heavy industrial land, at 12.99% and 8.53% exceedance, were less likely to result in runoff that favors

toxic HABs. In these land uses, selection of SCMs should focus on volume reduction to limit overall pollutant load.

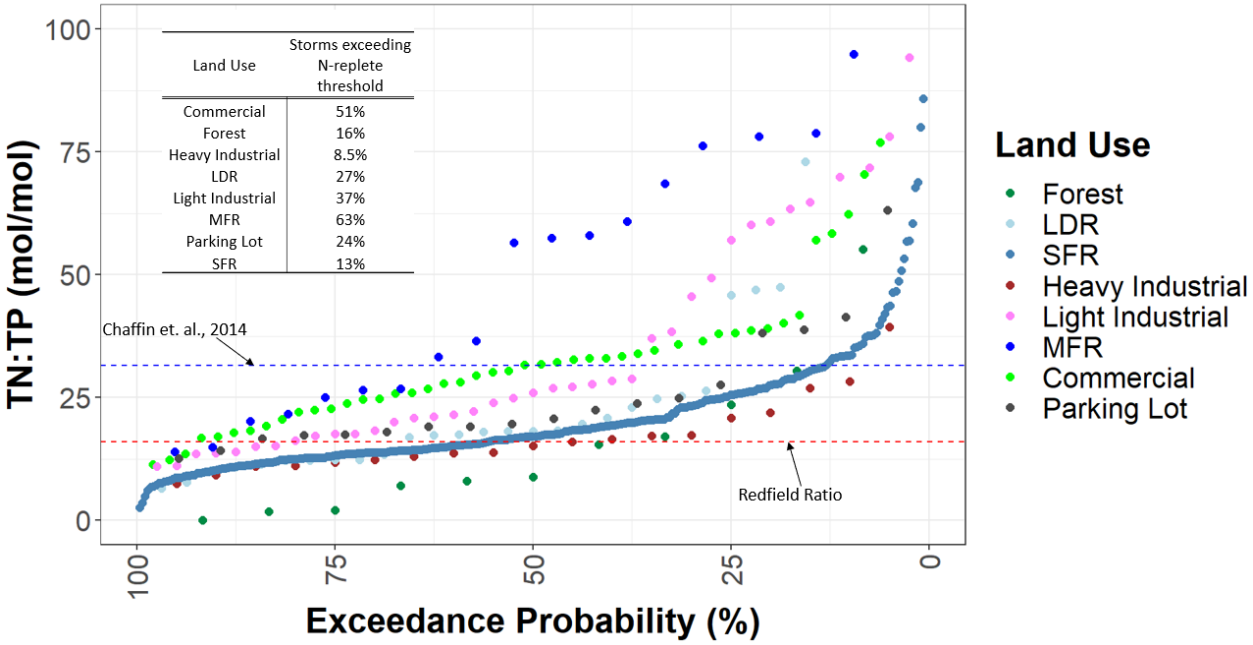


Figure 29: Exceedance probability of TN:TP ratio by land use relative to that to surpass N-replete growth conditions. Included is an inset table showing the value at which each land use crosses the 31.58 TN:TP threshold.

In considering optimal TN:TP ratio in urban runoff, dual conditions of mimicking pre-development conditions and balancing HAB nutrient ratios must be accounted for. As seen in the two forested watersheds analyzed, limited runoff events in natural conditions favor high phosphorus concentrations (and therefore low TN:TP ratios) in comparison to urban land uses. This makes matching pre-development conditions a nuanced discussion when considering the vast differences in runoff hydrology from urban areas. This suggests the implementation of management strategies which (1) reduce runoff volume through infiltration and

evapotranspiration, thereby more closely mimicking pre-development hydrology and (2) focus on reducing N in urban runoff to ameliorate elevated TN:TP ratios. According to Simpson (2022), the average urban watershed in the Dayton region produced 1200% and 500% higher annual loads of TN and TP, respectively, in stormwater runoff than nearby forested watersheds. Due to this difference in pollution generation, having a biologically balanced TN:TP ratio (i.e. Redfield ratio) may be a more realistic benchmark than matching pre-development nutrient load. While this may not eliminate HABs, it would at least reduce the toxicity of any resulting blooms.

If runoff is kept near a 16:1 TN:TP ratio, bulk biomass of N-fixing HABs can be managed while N-reliant toxic blooms can be avoided (Glibert and Burkolder, 2011, Gobler et. al., 2016). Most urban land uses had much higher TN:TP ratios than 16:1, suggesting urban runoff has a greater tendency to encourage toxic algal blooms. SFR, LDR, heavy industrial, and parking lot land uses had N:P ratios within 26% of the Redfield ratio, suggesting runoff from these land uses does not favor either toxic HABs or N-fixing algae, but overall nutrient load reduction is still advised to prevent algal blooms. TN:TP ratios for SFR and heavy industrial land uses were not statistically different than forested land uses, suggesting their runoff is stoichiometrically balanced. That said, the elevated level of imperviousness (particularly for heavy industrial watersheds) could lead to other impacts to water resources such as the "urban stream syndrome" (e.g., erosion, loss of habitat; Fletcher et. al., 2013, Walsh et. al., 2005). Thus, stormwater management strategies in urban areas must balance nutrient concentration reduction in SCMs, nutrient load reduction through runoff volume reduction, *and* provide optimal TN:TP ratio in nutrient-sensitive watersheds.

While runoff from forested watersheds had lower TN:TP ratios than the Redfield ratio, several land uses approached or exceeded the Chaffin et. al. (2014) estimated TN:TP value of N-replete conditions. This number represents the ratio where additional N inputs d not impact algal growth, implying these land uses highly favor toxic HAB varieties like *Microcystis*. Light industrial, commercial, and MFR land uses produced runoff which approached or exceeded TN:TP ratios of 31.58, implying that SCMs which employ N-reducing mechanisms should be prioritized in these land uses. These include internal water storage zones in bioretention (Johnson and Hunt, 2019) and potentially permeable pavement (Braswell et al. 2018) to encourage denitrification, constructed stormwater wetlands (Fletcher et. al., 2013), submerged gravel wetlands (He and Mankin, 2002), and other practices that encourage the reduction of nitrate/nitrite nitrogen. Findings herein also suggest land uses in urban areas that watershed managers should preferentially target for SCM implementation for amelioration of elevated TN:TP ratios.

### 2.3.2 Effects of GSI implementation on urban runoff TN:TP ratio from single family residential watersheds

Median TN and TP concentrations in stormwater runoff, as well as resulting TN:TP ratios, are presented in Figure 30 for all phases of the three Columbus treatment watersheds (pre-GSI, post-GSI, and post-$AI^2$). Summary statistics for TN, TP, and TN:TP, including data for treatment and control watersheds, can be found in Table 9.

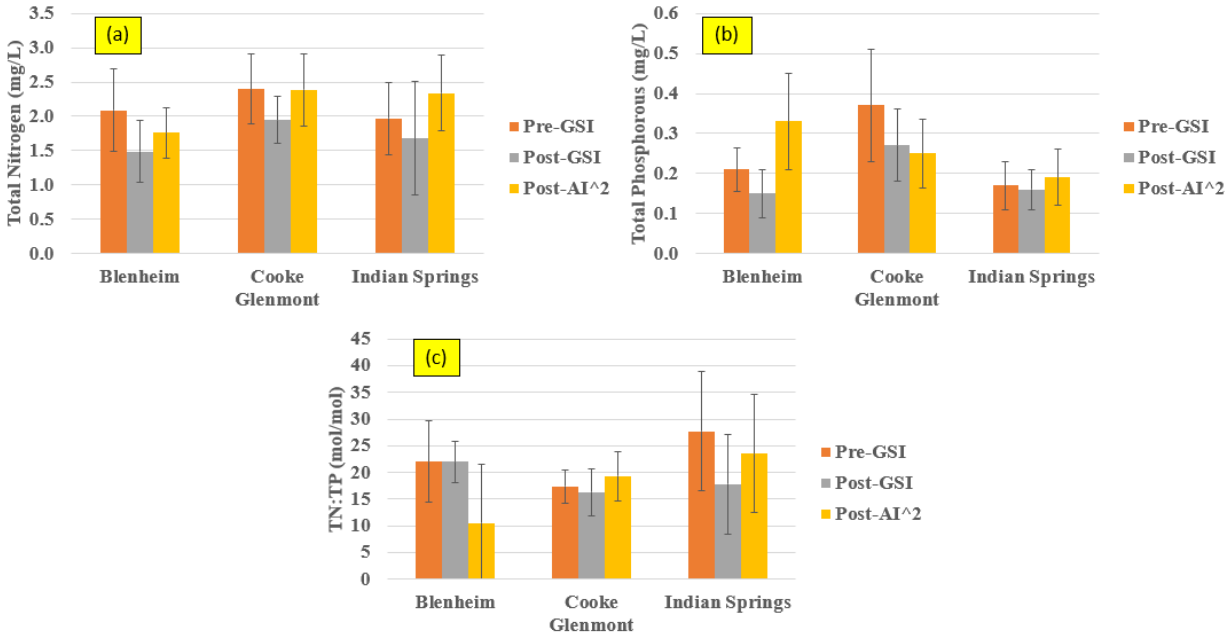


Figure 30: Comparisons of median pollutant concentration for each watershed for (a) total nitrogen (mg/L), (b) total phosphorus (mg/L), and (c) presents TN:TP ratios (mol/mol). Median absolute deviation among storm events is represented in positive and negative error bars.

Table 9: TN, TP, and TN:TP summary statistics for pre-GSI, post-GSI, and post-$AI^2$ for the three treatment watersheds and the control watershed.

| | | Beechwold | Blenheim | | | Cooke-Glenmont | | | Indian Springs | | |
|---|---|---|---|---|---|---|---|---|---|---|---|
| Analysis | Unit | Control | Pre-GSI | Post-GSI | Post-$AI^2$ | Pre-GSI | Post-GSI | Post-$AI^2$ | Pre-GSI | Post-GSI | Post-$AI^2$ |
| TN Mean | mg/L | 2.13 | 2.04 | 1.68 | 1.89 | 2.82 | 2.09 | 2.49 | 2.81 | 1.98 | 2.45 |
| TN Median | mg/L | 1.94 | 2.08 | 1.49 | 1.76 | 2.39 | 1.95 | 2.38 | 1.97 | 1.68 | 2.34 |
| TN MAD | mg/L | 0.48 | 0.60 | 0.45 | 0.36 | 0.51 | 0.34 | 0.52 | 0.53 | 0.83 | 0.55 |
| TP Mean | mg/L | 0.26 | 0.22 | 0.16 | 0.31 | 0.38 | 0.31 | 0.35 | 0.21 | 0.24 | 0.34 |
| TP Median | mg/L | 0.24 | 0.21 | 0.15 | 0.33 | 0.37 | 0.27 | 0.25 | 0.17 | 0.16 | 0.19 |
| TP MAD | mg/L | 0.09 | 0.06 | 0.06 | 0.12 | 0.14 | 0.09 | 0.09 | 0.06 | 0.05 | 0.07 |
| TN:TP Mean | mol/mol | 21.2 | 22.4 | 23.6 | 14.5 | 18.7 | 16.7 | 21.4 | 31.1 | 20.5 | 28.1 |
| TN:TP Median | mol/mol | 18.6 | 22.0 | 22.0 | 10.6 | 17.4 | 16.3 | 19.3 | 27.7 | 17.8 | 23.6 |
| TN:TP MAD | mol/mol | 7.2 | 7.6 | 3.8 | 10.9 | 3.1 | 4.4 | 4.6 | 11.2 | 9.3 | 11.1 |

To determine the impact of watershed-scale GSI on runoff TN:TP ratio, ANCOVA tests were run utilizing the control watershed (Beechwold) as an independent covariate. Non-parametric datasets were logarithmically transformed, and results of normality testing are featured in Table 10. The Post-GSI and Post-$AI^2$ phases were compared to Pre-GSI TN:TP ratios, with year-to-year variation in storm events accounted for by comparison to the control watershed (Table 11). There were no statistically significant ($p>0.05$) differences in TN:TP ratios found between Pre-GSI and other phases for any watershed tested (Figure 31), as median TN:TP ratios were variable across watersheds and did not present consistent patterns between phases.

Table 10: Normality tests for data sets used in ANCOVA analysis

| | Blenheim | | | Cooke-Glenmont | | | Indian Springs | | |
|---|---|---|---|---|---|---|---|---|---|
| | Pre-GSI | Post-GSI | Post-AI$^2$ | Pre-GSI | Post-GSI | Post-AI$^2$ | Pre-GSI | Post-GSI | Post-AI$^2$ |
| Test | Shapiro-Wilk LOG adj | Shapiro-Wilk LOG adj | - - | Shapiro-Wilk LOG adj | Shapiro-Wilk LOG adj | Shapiro-Wilk LOG adj | Shapiro-Wilk - | Shapiro-Wilk - | Shapiro-Wilk LOG adj |
| p-value | 0.203 | 0.745 | N/A | 0.814 | 0.066 | 0.941 | 0.281 | 0.371 | 0.778 |
| Normal? | Normal | Normal | Normal, 2 values | Normal | Normal | Normal | Normal | Normal | Normal |

Table 11: ANCOVA tests conducted on TN:TP ratio between Pre-GSI and Post-GSI, as well as Pre-GSI and Post-AI$^2$ phases for each watershed. Significant ($p<0.05$) differences were not observed between phases in any watershed.

| | | Post-GSI | | | Post-AI$^2$ | | |
|---|---|---|---|---|---|---|---|
| Watershed | Parameter | Statistical Test | p-value | Interpretation | Statistical Test | p-value | Interpretation |
| Blenheim | N:P ratio | ANCOVA-LOG adj | 0.263 | Not significant | ANCOVA-LOG adj | 0.995 | Not significant |
| Cooke-Glenmont | N:P ratio | ANCOVA-LOG adj | 0.31556 | Not significant | ANCOVA-LOG adj | 0.24457 | Not significant |
| Indian Springs | N:P ratio | ANCOVA | 0.168 | Not significant | ANCOVA-LOG adj | 0.854 | Not significant |

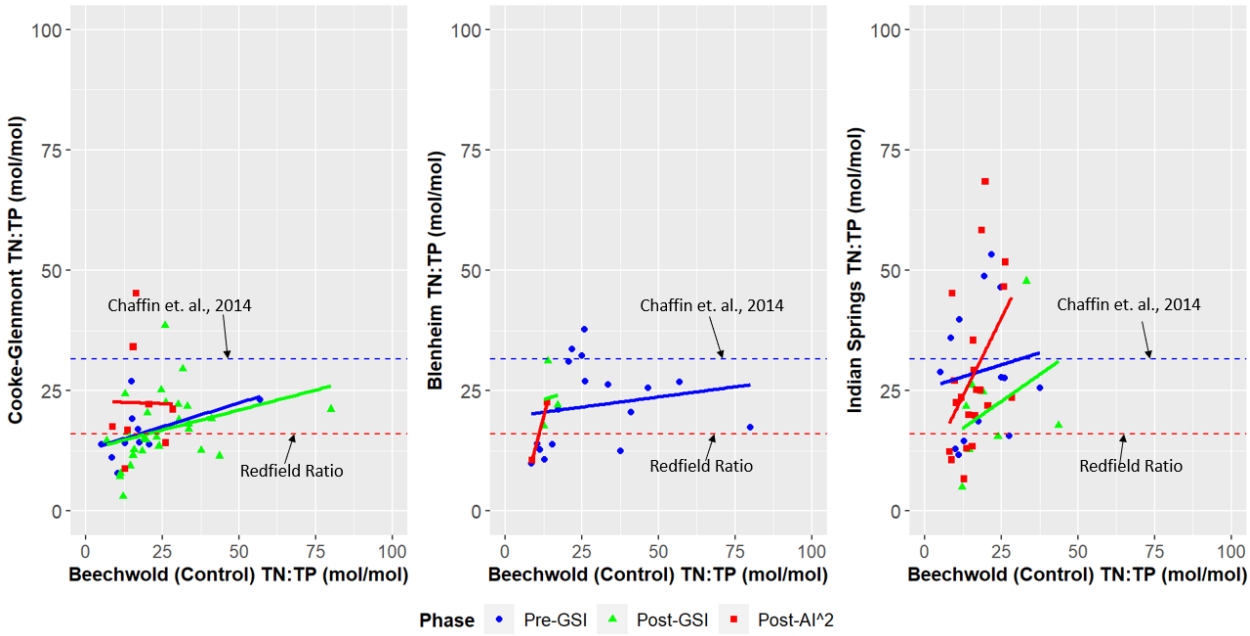


Figure 31: ANCOVA models for TN:TP ratios in watersheds with GSI and $AI^2$ implementation. No significant differences ($p>0.05$) were observed in TN:TP ratios from treatment watersheds relative to the control.

Smith et. al. (under review) confirmed that TN and TP load as well as TN concentration significantly decreased after installation of GSI in the Cooke-Glenmont watershed (Table 12). Substantial (though not significant) nutrient load reduction was also observed in Indian Springs following GSI implementation. Blenheim and Cooke-Glenmont TN:TP ratios were not significantly different from Pre- to Post-GSI despite significant reduction of both pollutants in the case of Cooke-Glenmont. Indian Springs TN:TP ratio decreased from 27.7 to 17.8, as reduction in N outweighed the reduction in TP from pre- to post-GSI.

Median TN and TP concentrations increased in the Post-AI$^2$ phase in all cases except TP at Cooke-Glenmont (e.g., 1.68 to 2.34 mg/L for TN at Indian Springs). Other installed infrastructure resulted in higher runoff volume due to implementation of sump pumps, lateral lining of sanitary sewers, and downspout disconnection. This additional runoff may result in less treatment of stormwater in the GSI (i.e., overflow may become a more dominant pathway), causing watershed outfall pollutant concentrations to increase in the post-AI$^2$ period. In the case of Blenheim, median TP concentration more than doubled between Post-GSI and Post-AI$^2$ phases (0.15 to 0.33 mg/L), suggesting additional infrastructure undermined TP removal provided by the bioretention cells. TN:TP ratio dramatically declined at Blenheim due to P concentrations more than doubling. Increases in runoff TN:TP ratio were observed at Cooke-Glenmont and Indian Springs from Post-GSI to Post-AI$^2$ phases (16.3-19.3 and 17.8-23.6, respectively), but a lower median value was observed in Indian Springs Post-AI$^2$ (23.6) than Pre-GSI (27.7).

Inconsistency between watersheds and no statistically significant variations in TN:TP ratio suggests that watershed-scale implementation of GSI (i.e., both permeable pavement and bioretention) did not consistently affect TN:TP ratio in stormwater runoff from single family residential watersheds. As SFR runoff closely mirrored the Redfield ratio and was not statistically different from surrogates for pre-development conditions (i.e., forest land use), this lack of GSI impact may be considered a beneficial result. That said, nutrient loads from the Columbus watersheds (Smith et al., in review) were still well above those of forests (Table 12), which suggests that greater runoff volume reduction in

the Columbus watersheds is still necessary to approach pre-development nutrient discharge, thereby reducing the potential for HABs in receiving waters.

SFR land use TN:TP ratio closely matched the Redfield ratio, but many other urban land uses (MFR, commercial, light industrial) had much higher TN:TP ratios approaching N-replete growth. Thus, if planning for algal bloom management, these land uses may be optimal for GSI implementation to lower N in relation to P to avoid toxic blooms. Greater GSI implementation than what was undertaken in the three treatment watersheds may be needed to see an effect at the watershed-scale, or the use of alternative SCMs may result in greater modification of TN:TP. That said, TN:TP ratio in urban stormwater needs to be considered as countries around the world grapple with HABs (Yindong et. al., 2021, Tong et. al., 2018, Bade and Likens, 2009, Chiaudani and Vighi, 1974). While many of these water bodies have agriculturally dominated watersheds (e.g., Lake Erie in Ohio), the urban contribution to the nutrient problem cannot be discarded, and wholistic watershed management strategies need to be implemented to ensure that all stakeholders bear the burden of nutrient reduction.

Pollutant load, in kg/ha/yr, from multiple studies which implemented GSI at the watershed scale as well as undeveloped watersheds has been summarized in Table 12. Smith et. al. (under review) found TN and TP load significantly decreased after installation of GSI in the Cooke-Glenmont watershed. Page et. al. (2015) found significant reductions in both TN and TP after GSI installation in North Carolina. However, most reduction was in TN, as the TN:TP ratio dropped from 9.2 to 2.2. Both watersheds from Smith et. al. (in review) presented in this study saw increased TN:TP

ratio (11.7-15.3 for Cooke-Glenmont, 15.3-22.7 for Indian Springs). TN and TP load were reduced in each of these cases, but less N removal relative to P. Results in Table 12 confirm those herein that the effects of GSI on TN:TP ratio are variable, in some cases yielding an increase and in others the opposite. This suggests the need for more research on watershed-scale implementation of GSI and its impacts on TN:TP ratio in light of the worldwide need to reduce HABs.

Table 12: Comparison of TN and TP watershed-scale load for studies of single-family residential watersheds without GSI, single family residential watersheds with GSI, and undeveloped watersheds.

| Study | Infrastructure | Land use | TN (kg/ha/yr) | TP (kg/ha/yr) | TN:TP (mol/mol) |
|---|---|---|---|---|---|
| Page et. al., 2015 | Pre-GSI | Medium-Density Residential | 7.2 | 1.7 | 9.2 |
| Page et. al., 2015 | Post-GSI | Medium-Density Residential | 1.5 | 1.5 | 2.2 |
| Smith et. al., in review | Pre-GSI | Cooke-Glenmont, SFR | 14 | 2.6 | 11.7 |
| Smith et. al., in review | Post-GSI | Cooke-Glenmont, SFR | 8.7 | 1.3 | 15.3 |
| Smith et. al., in review | Pre-GSI | Indian Springs, SFR | 29 | 4.2 | 15.3 |
| Smith et. al., in review | Post-GSI | Indian Springs, SFR | 11 | 1.1 | 22.7 |
| Bedan and Clausen, 2009 | Low Impact Development | SFR | 3.0 | 0.49 | 13.3 |
| Line et. al., 2002 | - | SFR | 59 | 5.7 | 23.0 |
| Line et. al., 2002 | - | Undeveloped | 16 | 1.2 | 27.9 |
| Simpson, 2022 | - | Forest | 0.55 | 0.14 | 8.7 |

## 2.4 Conclusions

Nineteen watershed-scale stormwater quality and quantity data sets from Dayton and Columbus regions were utilized to quantify the TN:TP ratio of various urban land uses and compare them against a surrogate for pre-development conditions (i.e., similar data from two nearby forested watersheds). Furthermore, three treatment watersheds were evaluated in which GSI and other infrastructure retrofits were implemented to understand how they impacted TN:TP modification. Paired watershed statistics were conducted to determine the impact GSI and other watershed improvements had on TN:TP. Conclusions from this research are as follows:

- MFR, commercial, and light industrial land uses had the highest TN:TP ratios, and these land uses should be prioritized for N-reducing SCMs to avoid spurring toxic HAB growth.
- The forested watersheds had the lowest TN:TP ratio studied and the lowest nutrient load, suggesting that typical urban watersheds without SCM implementation are a substantial source of nutrients at TN:TP ratios which contribute to algal blooms.
- SFR, LDR, and heavy industrial land uses all had TN:TP ratios similar to that of the Redfield ratio (TN:TP of 16:1), suggesting that for algal bloom abatement runoff reduction may be most important to prioritize in these watersheds.
- The Post-GSI phase in Columbus generally saw reductions in TN and TP concentrations and loads. The Post-$AI^2$ phase saw increased pollutant loads,

however, as SCMs were overwhelmed by the additional runoff being conveyed to them.

- No significant difference was found in TN:TP ratios in either the Post-GSI or the Post-AI$^2$ phase compared to Pre-GSI. This suggests that large-scale stormwater infrastructure investments in three treatment watersheds had little ability to modify the TN:TP ratio in runoff from SFR watersheds.
- Results from this work can be used to prioritize where to install retrofits of SCMs and to identify particular SCMs for retrofit in an attempt to modify the TN:TP ratio to more closely match the Redfield ratio.

References

American Public Health Association (APHA), American Water Works Association (AWWA), and Water Environment Federation (WEF). (2012). Standard methods for the examination of water and wastewater, Ed. Laura Bridgewater. 22nd ed., Washington, DC.

Bade, D. L., Bouchard, K., & Likens, G. E. (2009). Algal co-limitation by N and P persists after 30 years in Mirror Lake (New Hampshire, USA). SIL Proceedings, 1922-2010, 30(7), 1121–1123.

Barnard, M. A., Chaffin, J. D., Plaas, H. E., Boyer, G. L., Wei, B., Wilhelm, S. W., Rossignol, K. L., Braddy, J. S., Bullerjahn, G. S., Bridgeman, T. B., Davis, T. W., Wei, J., Bu, M., & Paerl, H. W. (2021). Roles of Nutrient Limitation on Western Lake Erie CyanoHAB Toxin Production. Toxins, 13(1), 1–21.

Bedan, E. S., & Clausen, J. C. (2009). Stormwater runoff quality and quantity from traditional and low impact development watersheds. *Journal of the American Water Resources Association*, 45(4), 998–1008.

Bernard, K., Boening-Ulman, K., Tirpak, R. A., Lancaster, E., Jiyoung, L., Mertin, J. F., & Winston, R. J. (2021). Holistic effects of green infrastructure implementation in the Clintonville neighborhood of Columbus Ohio: 2021 interim report. *Volume 1: Hydrology and Water Quality*

Boening-Ulman, K. M., Winston, R. J., Wituszynski, D. M., Smith, J. S., Tirpak, R. A., & Martin, J. F. (2022). Hydrologic impacts of sewershed-scale green infrastructure retrofits : Outcomes of a four-year paired watershed monitoring study. *Journal of Hydrology*, 611 (June), 128014.

Braswell, A. S., Winston, R. J., & Hunt, W. F. (2018). Hydrologic and water quality performance of permeable pavement with internal water storage over a clay soil in Durham, North Carolina. *Journal of Environmental Management*, 224, 277-287.

Chaffin, J. D., Bridgeman, T. B., Bade, D. L., & Mobilian, C. N. (2014). Summer phytoplankton nutrient limitation in Maumee Bay of Lake Erie during high-flow and low-flow years. *Journal of Great Lakes Research*, 40(3), 524–531.

Chiaudani, G., & Vighi, M. (1974). The N:P ratio and tests with Selenastrum to predict eutrophication in lakes. *Water Research*, 8(12), 1063–1069.

Clausen, J. C., & Spooner, J., 1993. Paired watershed study design (No. PB-94-154820/ XAB; EPA-841/F-93/009). Environmental Protection Agency, Washington, DC (United States). Office of Wetlands, Oceans and Watersheds.

Correll, D. L. (1998). (1998) Role of Phosphorus in the Eutrophication of Receiving Waters: A Review. *Journal of Environmental Quality*, 261–266.

Diblasi, C. J., Li, H., Davis, A. P., & Ghosh, U. (2009). Removal and fate of polycyclic aromatic hydrocarbon pollutants in an urban stormwater bioretention facility. *Environmental Science and Technology*, 43(2), 494–502.

Eaton, A. D., Clescerim L. S., Franson, M. A. H., Rice, E. W., & Greenberg, A. E. (Eds.) (2005). *Standard methods for the examination of water & wastewater* (Vol. 21). Ignatius Press, Washington, D.C.

Finkenbine, J.K., Atwater, J.W. and Mavinic, D.S. (2000), Stream Health After Urbanization. *JAWRA Journal of the American Water Resources Association*, 36: 1149-1160

DeBusk, K.M., Hunt, W.F., and Line, D.E. (2011). "Bioretention outflow: Does it mimic nonurban watershed shallow interflow." *Journal of Hydrologic Engineering*. 16(3), 274-279.

Fajardo, V., Brown, B., Young, D., & Nešić, S. (2013). Study of the solubility of iron carbonate in the presence of acetic acid using an EQCM. *NACE - International Corrosion Conference Series*, 2452, 1–20.

Fletcher, T. D., Andrieu, H., & Hamel, P. (2013). Advances in Water Resources Understanding , management and modelling of urban hydrology and its consequences for receiving waters : A state of the art. *Advances in Water Resources*, 51, 261–279.

Glibert, P. M., & Burkholder, J. A. M. (2011). Harmful algal blooms and eutrophication: "strategies" for nutrient uptake and growth outside the Redfield comfort zone. *Chinese Journal of Oceanology and Limnology*, 29(4), 724–738.

Gobler, C. J., Burkholder, J. A. M., Davis, T. W., Harke, M. J., Johengen, T., Stow, C. A., & Van de Waal, D. B. (2016). The dual role of nitrogen supply in controlling the growth and toxicity of cyanobacterial blooms. *Harmful Algae*, 54, 87–97.

He, Q., & Mankin, K. R. (2002). Performance variations of COD and nitrogen removal by vegetated submerged bed wetlands. *Journal of the American Water Resources Association*, 38(6), 1679–1689.

Hobbie, S. E., Finlay, J. C., Janke, B. D., Nidzgorski, D. A., Millet, D. B., & Baker, L. A. (2017). Contrasting nitrogen and phosphorus budgets in urban watersheds and implications for managing urban water pollution. *Proceedings of the National Academy of Sciences of the United States of America*, 114(16), 4177–4182.

Holmes, R. R., Hart, M. L., & Kevern, J. T. (2017). Enhancing the Ability of Pervious Concrete to Remove Heavy Metals from Stormwater. *Journal of Sustainable Water in the Built Environment*, 3(2), 04017004.

Johnson, J. P., & Hunt, W. F. (2019). A retrospective comparison of water quality treatment in a bioretention cell 16 years following initial analysis. *Sustainability* (Switzerland), 11(7).

Kuruppu, U., Rahman, A., & Rahman, M. A. (2019). Permeable pavement as a stormwater best management practice: a review and discussion. *Environmental Earth Sciences*, 78(10), 1–20.

Lee, J. G., Selvakumar, A., Alvi, K., Riverson, J., Zhen, J. X., Shoemaker, L., & Lai, F. hsiung. (2012). A watershed-scale design optimization model for stormwater best management practices. *Environmental Modelling and Software*, 37, 6–18.

Line, D. E., White, N. M., Osmond, D. L., Jennings, G. D., & Mojonnier, C. B. (2002). Line, D. E., & White, N. M. (2007). Effects of Development on Runoff and Pollutant Export. *Water Environment Research*, 79(2), 185–190.

Pollutant Export from Various Land Uses in the Upper Neuse River Basin. *Water Environment Research*, 74(1), 100–108.

Marshall, S., Pettigrove, V., Carew, M., & Hoffmann, A. (2010). Isolating the impact of sediment toxicity in urban streams. *Environmental Pollution*, 158(5), 1716–1725.

May, L., Spears, B. M., Dudley, B. J., & Hatton-Ellis, T. W. (2010). The importance of nitrogen limitation in the restoration of Llangorse Lake, Wales, UK. *Journal of Environmental Monitoring*, 12(1), 338–346.

Ong, S. K., Wang, K., Ling, Y., & Shi, G. (2016). Pervious Concrete Physical Characteristics and Effectiveness in Stormwater Pollution Reduction. April, 57.

Page, J. L., Winston, R. J., Mayes, D. B., Perrin, C. A., & Hunt, W. F. (2015). Retrofitting Residential Streets with Stormwater Control Measures over Sandy Soils for Water Quality Improvement at the Catchment Scale. *Journal of Environmental Engineering*, 141(4), 1–11.

R Core Team (2021). R: A language and environment for statistical computing. R Foundation for Statistical Computing, Vienna, Austria. URL https://www.R-project.org/.

Real Statistics Resource Pack software (Release 7.6). Copyright (2013 – 2021) Charles Zaiontz. www.real-statistics.com.

Reutter, J. M., Ciborowski, J., DePinto, J., Bade, D., Bridgeman, T. B., Culver, D. A., Davis, S., Dayton, E., Kane, D., Mullen, R. W., & Pennuto, C. M. (2011). Lake Erie nutrient loading and harmful algal blooms: Research findings and management implications. June 2011, 1–17.

Simpson, I. M., Winston, R. J., & Brooker, M. R. (2022). Effects of land use, climate, and imperviousness on urban stormwater quality: A meta-analysis. *Science of the Total Environment*, 809, 152206.

Simpson, I. M. (2022). Refining Urban Stormwater Pollution Characterization and Prediction to Better Design, Locate, and Maintain Stormwater Control Measures. Unpublished Dissertation

Smith, J. S., Winston, R. J., Tirpak, R. A., Wituszynski, D. M., Boening, K. M., & Martin, J. F. (2020). The seasonality of nutrients and sediment in residential stormwater runoff: Implications for nutrient-sensitive waters. *Journal of Environmental Management*, 276(September), 111248.

Smith, J. S., Winston, R. J., Wituszynski, D. M., Tirpak, R. A., Boening-Ulman, K. M., Martin, J. F. (Under Review). Effects of Watershed-Scale Green Infrastructure Retrofits on Urban Stormwater Quality: A Paired Watershed Study to Quantify Nutrient and Sediment Removal. *Ecological Engineering*

Tirpak, R. A., Afrooz, A. N., Winston, R. J., Valenca, R., Schiff, K., & Mohanty, S. K. (2021). Conventional and amended bioretention soil media for targeted pollutant treatment: A critical review to guide the state of the practice. *Water Research*, 189, 116648.

Tong, Y., Qiao, Z., Wang, X., Liu, X., Chen, G., Zhang, W., Dong, X., Yan, Z., Han, W., Wang, R., Wang, M., & Lin, Y. (2018). Human activities altered water N:P ratios in the populated regions of China. *Chemosphere*, 210, 1070–1081.

Tong, Y., Wang, M., Peñuelas, J., Liu, X., Paerl, H. W., Elser, J. J., Sardans, J., Couture, R. M., Larssen, T., Hu, H., Dong, X., He, W., Zhang, W., Wang, X., Zhang, Y., Liu, Y., Zeng, S., Kong, X., Janssen, A. B. G., & Lin, Y. (2020). Improvement in municipal wastewater treatment alters lake nitrogen to phosphorus ratios in

populated regions. *Proceedings of the National Academy of Sciences of the United States of America*, 117(21).

United States Environmental Protection Agency (USEPA). (1993). *Methods for determination of inorganic substances in environmental samples.* Office of Research and Development, U.S. Environmental Protection Agency, Washington, D.C.

United States Environmental Protection Agency (USEPA). (1994). *Determination of trace elements in waters and wastes by inductively coupled plasma-mass spectrometry* (Rev. 5.4). Office of Research and Development, U.S. Environmental Protection Agency, Washington, D.C.

Walsh, C. J., Roy, A. H., Feminella, J. W., Cottingham, P. D., Groffman, P. M., & Morgan, R. P. (2005). The urban stream syndrome: current knowledge and the search for a cure. *Journal of the North American Benthological Society*, (24)3, 706-723

Yindong, T., Xiwen, X., Miao, Q., Jingjing, S., Yiyan, Z., Wei, Z., Mengzhu, W., Xuejun, W., & Yang, Z. (2021). Lake warming intensifies the seasonal pattern of internal nutrient cycling in the eutrophic lake and potential impacts on algal blooms. *Water Research*, 188.

# Bibliography


Ahmaruzzaman, M. (2010). A review on the utilization of fly ash. Progress in Energy and Combustion Science, 36(3), 327–363.

American Public Health Association (APHA), American Water Works Association (AWWA), and Water Environment Federation (WEF). (2012). Standard methods for the examination of water and wastewater, Ed. Laura Bridgewater. 22nd ed., Washington, DC.

Bade, D. L., Bouchard, K., & Likens, G. E. (2009). Algal co-limitation by N and P persists after 30 years in Mirror Lake (New Hampshire, USA). SIL Proceedings, 1922-2010, 30(7), 1121–1123.

Barnard, M. A., Chaffin, J. D., Plaas, H. E., Boyer, G. L., Wei, B., Wilhelm, S. W., Rossignol, K. L., Braddy, J. S., Bullerjahn, G. S., Bridgeman, T. B., Davis, T. W., Wei, J., Bu, M., & Paerl, H. W. (2021). Roles of Nutrient Limitation on Western Lake Erie CyanoHAB Toxin Production. Toxins, 13(1), 1–21.

Bedan, E. S., & Clausen, J. C. (2009). Stormwater runoff quality and quantity from traditional and low impact development watersheds. *Journal of the American Water Resources Association*, 45(4), 998–1008.

Bernard, K., Boening-Ulman, K., Tirpak, R. A., Lancaster, E., Jiyoung, L., Mertin, J. F., & Winston, R. J. (2021). Holistic effects of green infrastructure implementation in the Clintonville neighborhood of Columbus Ohio: 2021 interim report. *Volume 1: Hydrology and Water Quality*

Beulah, M., & Prahallada, M. C. (2012). Effect of replacement of cement by metakalion on the properties of high performance concrete subjected to hydrochloric acid attack. *International Journal of Engineering Research and Applications*, 2(6), 033-038.

Boening-Ulman, K. M., Winston, R. J., Wituszynski, D. M., Smith, J. S., Tirpak, R. A., & Martin, J. F. (2022). Hydrologic impacts of sewershed-scale green infrastructure retrofits : Outcomes of a four-year paired watershed monitoring study. *Journal of Hydrology*, 611 (June), 128014.

Braswell, A. S., Winston, R. J., & Hunt, W. F. (2018). Hydrologic and water quality performance of permeable pavement with internal water storage over a clay soil in Durham, North Carolina. *Journal of Environmental Management*, 224, 277-287.

Bullard, J. W., Jennings, H. M., Livingston, R. A., Nonat, A., Scherer, G. W., Schweitzer, J. S., Scrivener, K. L., & Thomas, J. J. (2011). Mechanisms of cement hydration. Cement and Concrete Research, 41(12), 1208–1223.

Burris, Lisa E., and Maria CG Juenger. "Milling as a pretreatment method for increasing the reactivity of natural zeolites for use as supplementary cementitious materials." Cement and Concrete Composites 65 (2016): 163-170.

Chaffin, J. D., Bridgeman, T. B., Bade, D. L., & Mobilian, C. N. (2014). Summer phytoplankton nutrient limitation in Maumee Bay of Lake Erie during high-flow and low-flow years. *Journal of Great Lakes Research*, 40(3), 524–531.

Chen, Q., Yao, Y., Li, X., Lu, J., Zhou, J., & Huang, Z. (2018). Comparison of heavy metal removals from aqueous solutions by chemical precipitation and characteristics of precipitates. *Journal of Water Process Engineering*, 26 (October), 289–300.

Chiaudani, G., & Vighi, M. (1974). The N:P ratio and tests with Selenastrum to predict eutrophication in lakes. *Water Research*, 8(12), 1063–1069.

Clausen, J. C., & Spooner, J., 1993. Paired watershed study design (No. PB-94-154820/ XAB; EPA-841/F-93/009). Environmental Protection Agency, Washington, DC (United States). Office of Wetlands, Oceans and Watersheds.

Correll, D. L. (1998). (1998) Role of Phosphorus in the Eutrophication of Receiving Waters: A Review. *Journal of Environmental Quality*, 261–266.

Crittenden, J. C., Trussell, R. R., Hand, D. W., Howe, K. J., & Tchobanoglous, G. (2012). *MWH's water treatment: principles and design*. John Wiley & Sons.

Czuma, N., Baran, P., Franus, W., Zabierowski, P., & Zarębska, K. (2019). Synthesis of zeolites from fly ash with the use of modified two-step hydrothermal method and preliminary SO 2 sorption tests. *Adsorption Science and Technology*, 37(1–2), 61–76.

de Repentigny, C., Courcelles, B., & Zagury, G. J. (2018). Spent MgO-carbon refractory bricks as a material for permeable reactive barriers to treat a nickel- and cobalt-contaminated groundwater. *Environmental Science and Pollution Research*, 25(23), 23205–23214.

DeBusk, K.M., Hunt, W.F., and Line, D.E. (2011). "Bioretention outflow: Does it mimic nonurban watershed shallow interflow." *Journal of Hydrologic Engineering*. 16(3), 274-279.

Diblasi, C. J., Li, H., Davis, A. P., & Ghosh, U. (2009). Removal and fate of polycyclic aromatic hydrocarbon pollutants in an urban stormwater bioretention facility. *Environmental Science and Technology*, 43(2), 494–502.

Eaton, A. D., Clescerim L. S., Franson, M. A. H., Rice, E. W., & Greenberg, A. E. (Eds.) (2005). *Standard methods for the examination of water & wastewater* (Vol. 21). Ignatius Press, Washington, D.C.

Ekolu, S. O., & Bitandi, L. K. (2018). Prediction of Longevities of ZVI and Pervious Concrete Reactive Barriers Using the Transport Simulation Model. *Journal of Environmental Engineering*, 144(9), 04018074.

Ekolu, S. O., Azene, F. Z., & Diop, S. (2014, July). A concrete reactive barrier for acid mine drainage treatment. In *Proceedings of the Institution of Civil Engineers-Water Management* (Vol. 167, No. 7, pp. 373-380). Thomas Telford Ltd.

Finkenbine, J.K., Atwater, J.W. and Mavinic, D.S. (2000), Stream Health After Urbanization. *JAWRA Journal of the American Water Resources Association*, 36: 1149-1160

Fletcher, T. D., Andrieu, H., & Hamel, P. (2013). Advances in Water Resources Understanding , management and modelling of urban hydrology and its consequences for receiving waters : A state of the art. *Advances in Water Resources*, 51, 261–279.

Gavaskar, A. R. (1999). Design and construction techniques for permeable reactive barriers. *Journal of Hazardous Materials*, 68(1–2), 41–71.

Glibert, P. M., & Burkholder, J. A. M. (2011). Harmful algal blooms and eutrophication: "strategies" for nutrient uptake and growth outside the Redfield comfort zone. *Chinese Journal of Oceanology and Limnology*, 29(4), 724–738.

Gobler, C. J., Burkholder, J. A. M., Davis, T. W., Harke, M. J., Johengen, T., Stow, C. A., & Van de Waal, D. B. (2016). The dual role of nitrogen supply in controlling the growth and toxicity of cyanobacterial blooms. *Harmful Algae*, 54, 87–97.

Gustafsson J (2011) Visual MINTEQ ver. 3.0 KTH Department ofLand andWater Resources Engineering, Stockholm, Sweden Based on de Allison JD, Brown DS, Novo-Gradac KJ, MINTEQA2 ver 4, 1991

Gutberlet, T., Hilbig, H., & Beddoe, R. E. (2015). Acid attack on hydrated cement - Effect of mineral acids on the degradation process. *Cement and Concrete Research*, 74, 35–43.

Hale, B., Evans, L., & Lambert, R. (2012). Effects of cement or lime on Cd, Co, Cu, Ni, Pb, Sb and Zn mobility in field-contaminated and aged soils. *Journal of Hazardous Materials*, 199–200, 119–127.

Haselbach, L., Poor, C., & Tilson, J. (2014). Dissolved zinc and copper retention from stormwater runoff in ordinary portland cement pervious concrete. *Construction and Building Materials*, 53, 652–657.

He, Q., & Mankin, K. R. (2002). Performance variations of COD and nitrogen removal by vegetated submerged bed wetlands. *Journal of the American Water Resources Association*, 38(6), 1679–1689.

Hobbie, S. E., Finlay, J. C., Janke, B. D., Nidzgorski, D. A., Millet, D. B., & Baker, L. A. (2017). Contrasting nitrogen and phosphorus budgets in urban watersheds and implications for managing urban water pollution. *Proceedings of the National Academy of Sciences of the United States of America*, 114(16), 4177–4182.

Holmes, R. R., Hart, M. L., & Kevern, J. T. (2017). Enhancing the Ability of Pervious Concrete to Remove Heavy Metals from Stormwater. *Journal of Sustainable Water in the Built Environment*, 3(2), 04017004.

Holmes, R. R., Hart, M. L., & Kevern, J. T. (2017). Enhancing the Ability of Pervious Concrete to Remove Heavy Metals from Stormwater. Journal of Sustainable Water in the Built Environment, 3(2), 04017004.

Holmes, R. R., Hart, M. L., & Kevern, J. T. (2017). Heavy metal removal capacity of individual components of permeable reactive concrete. Journal of Contaminant Hydrology, 196, 52–61.

Holmes, R. R., Hart, M. L., & Kevern, J. T. (2018). Removal and Breakthrough of Lead, Cadmium, and Zinc in Permeable Reactive Concrete. *Environmental Engineering Science*, 35(5), 408–419.

Johnson, D. B., & Hallberg, K. B. (2005). Acid mine drainage remediation options: A review. *Science of the Total Environment*, 338(1-2 SPEC. ISS.), 3–14.

Johnson, J. P., & Hunt, W. F. (2019). A retrospective comparison of water quality treatment in a bioretention cell 16 years following initial analysis. *Sustainability* (Switzerland), 11(7).

Khatib, J. M., Mangat, P. S., & Wright, L. (2016). Mechanical and physical properties of concrete containing FGD waste. *Magazine of concrete Research*, 68(11), 550-560.

Knox, A. S., Paller, M. H., & Dixon, K. L. (2012). A Permeable Active Amendment Concrete (PAAC) for Contaminant Remediation and Erosion Control (ER-2134). June, 1–116.

Kuruppu, U., Rahman, A., & Rahman, M. A. (2019). Permeable pavement as a stormwater best management practice: a review and discussion. *Environmental Earth Sciences*, 78(10), 1–20.

Larsson, M., Nosrati, A., Kaur, S., Wagner, J., Baus, U., & Nydén, M. (2018). Copper removal from acid mine drainage-polluted water using glutaraldehyde-polyethyleneimine modified diatomaceous earth particles. *Heliyon*, 4(2), e00520.

Lee, J. G., Selvakumar, A., Alvi, K., Riverson, J., Zhen, J. X., Shoemaker, L., & Lai, F. hsiung. (2012). A watershed-scale design optimization model for stormwater best management practices. *Environmental Modelling and Software*, 37, 6–18.

Li, W., Ni, P., & Yi, Y. (2019). Comparison of reactive magnesia, quick lime, and ordinary Portland cement for stabilization/solidification of heavy metal-contaminated soils. *Science of the Total Environment*, 671, 741–753.

Li, Y., Xu, Z., Ma, H., & Hursthouse, A. S. (2019). Removal of Manganese(II) from Acid Mine Wastewater: A Review of the Challenges and Opportunities with Special Emphasis on Mn-Oxidizing Bacteria and Microalgae. *Water* **2019**, 11, 2493.

Line, D. E., White, N. M., Osmond, D. L., Jennings, G. D., & Mojonnier, C. B. (2002). Line, D. E., & White, N. M. (2007). Effects of Development on Runoff and Pollutant Export. *Water Environment Research*, 79(2), 185–190.

Liu, J., & Li, Y. (2020). Runoff purification effects of permeable concrete modified by diatomite and zeolite powder. *Advances in Materials Science and Engineering*, *2020*.

Marchon, D., & Flatt, R. J. (2016). Mechanisms of cement hydration. In *Science and Technology of Concrete Admixtures*. Elsevier Ltd.

Marshall, S., Pettigrove, V., Carew, M., & Hoffmann, A. (2010). Isolating the impact of sediment toxicity in urban streams. *Environmental Pollution*, 158(5), 1716–1725.

May, L., Spears, B. M., Dudley, B. J., & Hatton-Ellis, T. W. (2010). The importance of nitrogen limitation in the restoration of Llangorse Lake, Wales, UK. *Journal of Environmental Monitoring*, 12(1), 338–346.

Monhemius, A. J. (1977). Precipitation Diagrams for Metal Hydroxides, Sulphides, Arsenates and Phosphates. *Transactions of the Institution of Mining and Metallurgy, Section C: Mineral Processing and Extractive Metallurgy*, 86 (December 1977).

Muthu, M., Chandrasekharapuram Ramakrishnan, K., Santhanam, M., Rangarajan, M., & Kumar, M. (2019). Heavy Metal Removal and Leaching from Pervious Concrete Filter: Influence of Operating Water Head and Reduced Graphene Oxide Addition. *Journal of Environmental Engineering*, 145(9), 04019049.

Naidu, G., Ryu, S., Thiruvenkatachari, R., Choi, Y., Jeong, S., & Vigneswaran, S. (2019). A critical review on remediation, reuse, and resource recovery from acid mine drainage. *Environmental Pollution*, 247, 1110–1124.

O'Reilly, K. M. (2020). Investigating the Impacts of Acid Mine Drainage on Ecosystem Functioning Using a Leaf Litter Decomposition Analysis [Unpublished Undergraduate Thesis] The Ohio State University

Ok, Y. S., Yang, J. E., Zhang, Y. S., Kim, S. J., & Chung, D. Y. (2007). Heavy metal adsorption by a formulated zeolite-Portland cement mixture. *Journal of Hazardous Materials*, 147(1–2), 91–96.

Ong, S. K., Wang, K., Ling, Y., & Shi, G. (2016). Pervious Concrete Physical Characteristics and Effectiveness in Stormwater Pollution Reduction. April, 57.

Ong, S. K., Wang, K., Ling, Y., & Shi, G. (2016). Pervious Concrete Physical Characteristics and Effectiveness in Stormwater Pollution Reduction. April, 57.

Page, J. L., Winston, R. J., Mayes, D. B., Perrin, C. A., & Hunt, W. F. (2015). Retrofitting Residential Streets with Stormwater Control Measures over Sandy Soils for Water Quality Improvement at the Catchment Scale. *Journal of Environmental Engineering*, 141(4), 1–11.

Pernicová, R. (2014). Analysis of Formation and Testing of Efflorescence on Concrete Elements. Advanced Materials Research, 1025–1026, 641–644.

Pickering, W. F. (1983). Extraction of copper, lead, zinc or cadmium ions sorbed on calcium carbonate. *Water, Air, and Soil Pollution*, 20(3), 299-309.

Pollutant Export from Various Land Uses in the Upper Neuse River Basin. *Water Environment Research*, 74(1), 100–108.

R Core Team (2021). R: A language and environment for statistical computing. R Foundation for Statistical Computing, Vienna, Austria. URL https://www.R-project.org/.

Real Statistics Resource Pack software (Release 7.6). Copyright (2013 – 2021) Charles Zaiontz. www.real-statistics.com.

Reutter, J. M., Ciborowski, J., DePinto, J., Bade, D., Bridgeman, T. B., Culver, D. A., Davis, S., Dayton, E., Kane, D., Mullen, R. W., & Pennuto, C. M. (2011). Lake Erie nutrient loading and harmful algal blooms: Research findings and management implications. June 2011, 1–17.

Saboo, N., Shivhare, S., Kori, K. K., & Chandrappa, A. K. (2019). Effect of fly ash and metakaolin on pervious concrete properties. *Construction and Building Materials*, 223, 322–328.

Scrivener, K., Ouzia, A., Juilland, P., & Kunhi Mohamed, A. (2019). Advances in understanding cement hydration mechanisms. *Cement and Concrete Research*, 124(June), 105823.

Sdiri, A., & Bouaziz, S. (2014). Re-evaluation of several heavy metals removal by natural limestones. *Frontiers of Chemical Science and Engineering*, 8(4), 418–432.

Sdiri, A., Higashi, T., Jamoussi, F., & Bouaziz, S. (2012). Effects of impurities on the removal of heavy metals by natural limestones in aqueous systems. *Journal of Environmental Management*, 93(1), 245–253.

Senhadji, Y., Escadeillas, G., Mouli, M., Khelafi, H., & Benosman. (2014). Influence of natural pozzolan, silica fume and limestone fine on strength, acid resistance and microstructure of mortar. *Powder Technology*, 254, 314–323.

Shabalala, A. (2020). Efficacies of Pervious Concrete and Zero-Valent Iron as Reactive Media for Treating Acid Mine Drainage. *Mine Water Solutions, 14th IMWA Congress, Christchuch, New Zealand (9-13 November 2020)*, 83–87.

Shabalala, A. N., & Ekolu, S. O. (2019). Quality of water recovered by treating acid mine drainage using pervious concrete adsorbent. *Water SA*, 45(4), 638–647.

Shabalala, A. N., Ekolu, S. O., & Diop, S. (2014). Permeable reactive barriers for acid mine drainage treatment: a review. *Construction Materials and Structures*, 1416–1426.

Shively, W., Bishop, P., Gress, D., & Brown, T. (1986). Leaching tests of heavy metals stabilized with Portland cement. *Journal of the Water Pollution Control Federation*, 58(3), 234–241.

Simpson, I. M. (2022). Refining Urban Stormwater Pollution Characterization and Prediction to Better Design, Locate, and Maintain Stormwater Control Measures. Unpublished Dissertation

Simpson, I. M., Winston, R. J., & Brooker, M. R. (2022). Effects of land use, climate, and imperviousness on urban stormwater quality: A meta-analysis. *Science of the Total Environment*, 809, 152206.

Skousen, G., Ziemkiewicz, P. F., & Mcdonald, L. M. (2019). The Extractive Industries and Society Acid mine drainage formation , control and treatment : Approaches and strategies. 6(October 2018), 241–249.

Skousen, J., Zipper, C. E., Rose, A., Ziemkiewicz, P. F., Nairn, R., McDonald, L. M., & Kleinmann, R. L. (2017). Review of Passive Systems for Acid Mine Drainage Treatment. In *Mine Water and the Environment* (Vol. 36, Issue 1, pp. 133–153). Springer Verlag.

Smith, J. S., Winston, R. J., Tirpak, R. A., Wituszynski, D. M., Boening, K. M., & Martin, J. F. (2020). The seasonality of nutrients and sediment in residential stormwater runoff: Implications for nutrient-sensitive waters. *Journal of Environmental Management*, 276(September), 111248.

Smith, J. S., Winston, R. J., Wituszynski, D. M., Tirpak, R. A., Boening-Ulman, K. M., Martin, J. F. (Under Review). Effects of Watershed-Scale Green Infrastructure Retrofits on Urban Stormwater Quality: A Paired Watershed Study to Quantify Nutrient and Sediment Removal. *Ecological Engineering*

Stanley, H. (2020). *The Role of Beaver Ponds in Aquatic Ecosystems Impacted by Acid Mine Drainage* [Unpublished Honors Undergraduate Thesis] The Ohio State University

Stehouwer, R. C., Sutton, P., Fowler, R. K., & Dick, W. A. (1995). *Minespoil amendment with dry flue gas desulfurization by-products: Element solubility and mobility* (Vol. 24, No. 1, pp. 165-174). American Society of Agronomy, Crop Science Society of America, and Soil Science Society of America.

Tasić, Ž. Z., Bogdanović, G. D., & Antonijević, M. M. (2019). Application of natural zeolite in wastewater treatment: A review. *Journal of Mining and Metallurgy A: Mining*, 55(1), 67–79.

Tennis, P. D., & Jennings, H. M. (2000). Model for two types of calcium silicate hydrate in the microstructure of Portland cement pastes. *Cement and Concrete Research*, 30(6), 855–863.

Teymouri, E., Mousavi, S. F., Karami, H., Farzin, S., & Hosseini Kheirabad, M. (2020). Municipal Wastewater pretreatment using porous concrete containing fine-grained mineral adsorbents. Journal of Water Process Engineering, 36(May), 101346.

Thisani, S. K., Kallon, D. V. Von, & Byrne, P. (2021). Effects of contact time and flow configuration on the acid mine drainage remediation capabilities of pervious concrete. *Sustainability (Switzerland)*, 13(19).

Thornton, I. (1996). Impacts of mining on the environment; some local, regional and global issues. *Applied Geochemistry*, 11(1–2), 355–361.

Tirpak, R. A., Afrooz, A. N., Winston, R. J., Valenca, R., Schiff, K., & Mohanty, S. K. (2021). Conventional and amended bioretention soil media for targeted pollutant treatment: A critical review to guide the state of the practice. *Water Research*, 189, 116648.

Tong, Y., Qiao, Z., Wang, X., Liu, X., Chen, G., Zhang, W., Dong, X., Yan, Z., Han, W., Wang, R., Wang, M., & Lin, Y. (2018). Human activities altered water N:P ratios in the populated regions of China. *Chemosphere*, 210, 1070–1081.

Tong, Y., Wang, M., Peñuelas, J., Liu, X., Paerl, H. W., Elser, J. J., Sardans, J., Couture, R. M., Larssen, T., Hu, H., Dong, X., He, W., Zhang, W., Wang, X., Zhang, Y., Liu, Y., Zeng, S., Kong, X., Janssen, A. B. G., & Lin, Y. (2020). Improvement in municipal wastewater treatment alters lake nitrogen to phosphorus ratios in populated regions. *Proceedings of the National Academy of Sciences of the United States of America*, 117(21).

Tremblay, G.A., Hogan, C.M.: Mine Environment Neutral Drainage (MEND) Manual 5.4.2d: Prevention and Control. Canada Centre for Mineral and Energy Technology, Natural Resources Canada, Ottawa, 2001.

Uma Maguesvari, M., & Sundararajan, T. (2017). Influence of fly ash and fine aggregates on the characteristics of pervious concrete. *International Journal of Applied Engineering Research*, 12(8), 1598–1609.

United States Environmental Protection Agency (USEPA). (1993). *Methods for determination of inorganic substances in environmental samples.* Office of Research and Development, U.S. Environmental Protection Agency, Washington, D.C.

United States Environmental Protection Agency (USEPA). (1994). *Determination of trace elements in waters and wastes by inductively coupled plasma-mass spectrometry* (Rev. 5.4). Office of Research and Development, U.S. Environmental Protection Agency, Washington, D.C.

USEPA. 2009. National Recommended water Quality Criteria, Office of Water, Office of Science and Technology (4304T), Washington, DC.

Walsh, C. J., Roy, A. H., Feminella, J. W., Cottingham, P. D., Groffman, P. M., & Morgan, R. P. (2005). The urban stream syndrome: current knowledge and the search for a cure. *Journal of the North American Benthological Society*, (24)3, 706-723

Wang, D., Shi, C., Farzadnia, N., Shi, Z., & Jia, H. (2018). A review on effects of limestone powder on the properties of concrete. *Construction and Building Materials*, 192, 153–166.

Watters, G. T., Menker, T., & O'Dee, S. H. (2005). A comparison of terrestrial snail faunas between strip-mined land and relatively undisturbed land in Ohio, USA - An evaluation of recovery potential and changing faunal assemblages. *Biological Conservation*, 126(2), 166–174.Wright, L., & Khatib, J. M. (2016). Sustainability of desulphurised (FGD) waste in construction. In *Sustainability of Construction Materials* (Second Edi). Elsevier Ltd.

Yindong, T., Xiwen, X., Miao, Q., Jingjing, S., Yiyan, Z., Wei, Z., Mengzhu, W., Xuejun, W., & Yang, Z. (2021). Lake warming intensifies the seasonal pattern of internal nutrient cycling in the eutrophic lake and potential impacts on algal blooms. *Water Research*, 188.

Appendix A

Table 13: Comparison of concrete cube weights when soaked in water for 1 minute or 30 minutes.

| Mix | Soak | 1 min | 30 min | Average Gain | % Gain |
|---|---|---|---|---|---|
| Fly Ash A | Acid | 0.311 | 0.314 | 0.003 | 1.085887 |
| | | 0.307 | 0.311 | | |
| | | 0.303 | 0.306 | | |
| | Limewater | 0.32 | 0.32 | 0.001 | 0.40965 |
| | | 0.328 | 0.33 | | |
| | | 0.323 | 0.325 | | |
| Fly Ash D | Acid | 0.304 | 0.305 | 0.001 | 0.438625 |
| | | 0.308 | 0.309 | | |
| | | 0.302 | 0.304 | | |
| | Limewater | 0.316 | 0.317 | 0.000 | -0.10888 |
| | | 0.31 | 0.309 | | |
| | | 0.312 | 0.311 | | |
| Zeolite | Acid | 0.292 | 0.293 | 0.000 | -0.00322 |
| | | 0.284 | 0.283 | | |
| | | 0.284 | 0.284 | | |
| | Limewater | 0.29 | 0.289 | 0.000 | -0.00195 |
| | | 0.297 | 0.297 | | |
| | | 0.295 | 0.296 | | |
| OPC | Limewater | 0.314 | 0.315 | 0.001 | 0.212653 |
| | | 0.313 | 0.314 | | |
| | | 0.315 | 0.315 | | |

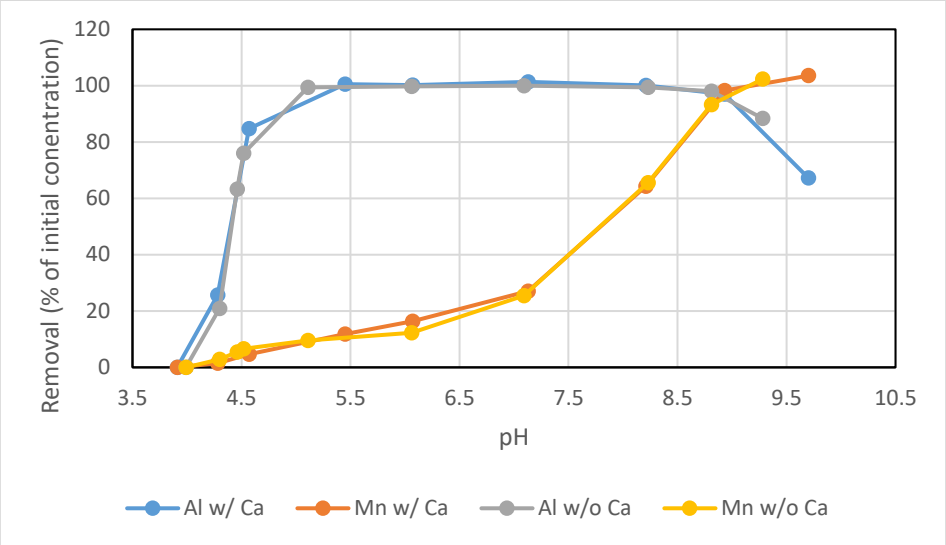


Figure 32: Synthetic AMD pH-controlled solutions, one with 0.4 mmol of Ca added and one without. Percent removal of Al and Mn is compared over pH.